ELECTRICITY GENERATION WITH ORGANIC MATTER AND AMMONIUM REMOVAL FROM SWINE WASTEWATER VIA MICROBIAL FUEL CELLS

A DISSERTATION
SUBMITTED TO THE FACULTY OF THE GRADUATE SCHOOL
OF THE UNIVERSITY OF MINNESOTA
BY

Hongjian Lin

IN PARTIAL FULFILLMENT OF THE REQUIREMENTS
FOR THE DEGREE OF
DOCTOR OF PHILOSOPHY

Adviser: Dr. Jun Zhu

November 2013

Acknowledgements

I thank my advisor Dr. Jun Zhu, Professor in the Department of Bioproducts and Biosystems Engineering at University of Minnesota, for his guidance, support and encouragement during my graduate study. I was also allowed by him to decide and then to pursue a specific research question, which gave me the freedom to develop my own expertise of knowledge.

I thank other graduate advisory committee members for their willingness to be on the committee: Dr. Bo Hu, Assistant Professor in the Department of Bioproducts and Biosystems Engineering; Dr. Kevin Janni, Professor in the Department of Bioproducts and Biosystems Engineering; and Dr. Timothy LaPara, Associate Professor in the Department of Civil Engineering. They were always available for serving on the committee and for providing guidance and research facilities.

I would like to express my appreciation to my colleagues Dr. Xiao Wu, Dr. Wanying Yao, lab technician Mr. Curtis Miller, Professor Ping Wang and undergrad assistant Chad Nelson as well as to my friends Mr. Jeff Ulrich and Dr. Senyu Chen. I could not have had the experiments done without their great help during my study.

Finally, I would like to extend my appreciation to my parents Dexiang Dai and Shuping Chen, my grandparents, and my younger sister Jie Lin, because they show consistent love and support to me.

Abstract

Livestock industry generates a large amount of manure and wastewater. Minnesota, the third largest hog producing state in the US, produces 7 million pigs per year and meanwhile generates 11 million tons of dry manure. Wastewater from swine farms contains high concentrations of organic matters, nitrogen and phosphorus. A poor management and treatment of the wastewater would cause severe environmental issues to soil, water, and air, such as eutrophication, impairment in drinking water quality, and the odor issue. So an appropriate treatment of the swine wastewater is an urgent and crucial issue to sustain the industry.

Microbial fuel cell (MFC) is an emerging technology that shows a potential use in swine wastewater treatment. The reactor realizes biological oxidation at anode for organic matters, and electrochemical reduction at cathode. It is sustainable because it converts waste to electricity, recovers nutrients, and reduces the cost for wastewater treatment. The overall goal of this study is to develop effective MFCs for treating synthetic and swine wastewater to generate electrical energy and, at the same time, to achieve efficient removal of COD and total ammonium nitrogen.

The first step was to choose suitable bacterial consortia to inoculate single-chamber air-cathode MFCs. Activated (AC) and anaerobic (AN) sludge showed faster enrichment of MFC anodic biofilm by 2 to 3 d than river sediment (RS), while AN-MFC presented highest VFA degradation rate, indicating that the bacteria in AN sludge were better adapted to MFC anodes due to the similar anaerobic environment and volatile fatty acid

concentrations in a swine manure anaerobic digester. However, RS-MFC anode surface was covered with well-developed layers of biomass (bacterial cells and extracellular polymeric substances) and had a much larger power output (195 μW or 98 mW m^{-2}) than AC- and AN-MFC after one month operation. For mature MFCs that were under long-time operation, a transient application of negative voltages (-3 V) improved the cathode activity and maximum power output by 37%, due to the bactericidal effect of the electrode potential higher than +1.5 V *vs.* standard hydrogen electrode (SHE).

The second step was to model the single-chamber MFCs based on the assumption that the anode attached bacterial monolayer serves as biocatalysts for MFC exoelectrogenesis. By modifying the Freter model and combining it with Butler-Volmer equation, this model adequately describes the processes of electricity generation, substrate utilization, and suspended and attached biomass growth, in both batch and continuous operational mode. The results showed that the activation overpotential of the anode substantial reduced during the anode enrichment process, which was a result of increased exchange current density due to the increased biocatalyst. It was also found that electricity generation reduced sludge generation. Smaller external resistors were suggested to use to improve the organic matter removal and to reduce sludge generation, while an external resistor close to the internal resistor should be used to obtain the maximum power generation.

The third step of this study modeled the kinetic data of swine wastewater characteristics in MFCs, including conductivity, COD, volatile fatty acids (VFAs), total ammoniacal nitrogen (TAN), nitrite, nitrate, and phosphate concentrations. The removals of VFA and TAN had the half-life times of 4.99 and 7.84 d, respectively. Among the removed TAN,

13.6% was recovered from the evaporated air outside of MFC cathode, indicating its potential use for ammonium recovery from animal wastewater. The mechanism for phosphate removal was principally the salt precipitation from cathode, and needed improvement as the removal was far from completion. MFC with an external resistor of 2.2 kΩ and fed with raw swine wastewater generated relatively small power (28.2 μW), energy efficiency (0.37%) and Coulombic efficiency (0.15%). The main reason for the impaired performance was the inhibitory effects associated with TAN on Pt activity and VFA on anodic biofilm activity. Diluted swine wastewater, with a dilution factor of 2 or higher, dramatically improved the power generation as the inhibitory effect was reduced. Smaller external resistor in the circuit promoted the organic matter degradation and shortened the required reaction time in batch mode.

The fourth step was to reduce the inhibitory effect of swine wastewater in electricity generation by selective removal of ammonium and VFAs. This study showed that sorption using natural zeolite was an effective way for ammonium mitigation in swine wastewater. The kinetic process of the ammonium sorption on zeolite was best described by the pseudo-second-order model, and the resulting TAN sorption capacity at equilibrium was 11.6 mg/g. The isotherm data were best fitted by the Langmuir model, and the maximum TAN sorption capacity was 34.2 mg/g. The thermodynamic parameters indicated the spontaneity (ΔG° = -6.65 kJ/mol by the Langmuir model) and exothermic nature (ΔH° = -22.3 kJ/mol) of ammonium sorption on zeolite. Addition of GAC in zeolite decreased ammonium diffusion to zeolite particles, but it enhanced the maximum zeolite sorption capacity and COD (mainly VFAs) removal. Zeolite and GAC were

effective in the selective adsorption of ammonia and VFAs in swine wastewater and consequently improved the power generation by over 80%, energy efficiency by up to 78%, and Coulombic efficiency by up to 37% of microbial fuel cells.

The final step was to optimize air-cathode and MFC configuration for ammonium removal. The 5% PTFE-treated cathode had a leaking problem, while the other cathodes, including 20% PTFE+GDLs, 5% PTFE+GDLs, and 20% PTFE, did not have the problem of leaking, and the last one performed best both in power generation and ammonia removal. Tests in MFCs A and C revealed that the half-life time of the total ammonium was proportional to electrical current, which was a strong evident demonstrating that the oxygen reduction reaction at cathode promoted ammonia volatilization by elevating pH nearby. On average, an increase of 1 mA in electrical current would reduce the half-life time by 2.8 d and 0.85 d for MFC A and C, respectively. Modifying regular MFCs to membrane contactor mode improved ammonia removal, because the surface area of hydrophobic membrane was increased. This improvement was indicated by the substantially reduced half-life time from the best case of 2.54 d of the best performed regular MFCs to only 0.67 d. The modification also allowed ammonia recovery from wastewater, and 78% of the removed ammonia was captured in sulfuric acid solution. This study demonstrated a novel way of ammonium recovery from wastewater by MFCs based on membrane contactor mode, and better performance is still expected through optimizing the gas-diffusion materials and reactor configuration.

Table of Contents

List of Tables

List of Figures

Chapter 1. General Introduction

1.1 Swine industry and environmental concerns

Livestock industry is an essential part of the agricultural sector, and this industry generates a large amount of manure: between 133 and 300 million tons per year on a dry basis in the United States according to an estimation made in 2005 [1]. Livestock industry is also under expansion during the last decade evidenced by the increasing number of animal farms and inventories (Table 1-1) and the increasing scale of animal production based on concentrated animal feeding operations (CAFOs). Among the different animal categories, the swine industry is an important component. In Minnesota alone, the third largest hog producing state in the US, there are over 7 million pigs per year going to the market, which produces 11 million tons of dry manure annually [2]. The scale of hog operation is also increasing at a high rate due to its economies of scale, from 2,589 heads per farm in 1998 to 7,930 head per farm in 2009 in the US [3]. As the expanding amount of waste needs to be mitigated or treated before disposal, the environmental concerns due to the waste (manure and wastewater) are magnified by the larger hog production and larger operation.

Table 1-1. Farms and animal number (in million heads) inventories of major categories of livestock and poultry in US in 1997, 2002, and 2007 [a]

	Cattle and calves		Milk cows		Hogs		Layers		Broilers and other meat-type chickens	
Year	Farms	Number	Farms	Number	Farms	Number	Farms	Number	Farms	Number
1997	1,188,659	99.91	125,041	9.14	124,889	61.19	91,625	314.14	35,500	1,214
2002	1,018,359	95.50	91,989	9.10	78,895	60.41	98,315	334.44	37,937	1,389
2007	963,669	96.35	69,890	9.27	75,442	67.79	145,615	349.77	32,668	1,603

[a] Data are compiled from USDA statistics [4, 5].

Waste from swine farms is mainly in the form of pig wastewater or slurry, a mixture of feces, urine, and washing water, containing high concentrations of nitrogen and phosphorus. A poor management and treatment of the waste would thus cause severe environmental issues to soil, water, and air [6]. An excessive disposal of swine slurry within localized areas may result in overloading organic materials, heavy metals (Cu and Zn) and nutrients (P and N) in soil that may leach to ground or surface water, and consequently impair drinking water or cause eutrophication. According to N-based or P-based standards, only 49% or 27% of large swine farms (>1,000 animal units) found enough land to apply their manure [1].

Besides the pollution caused by manure disposal, the hog production, manure storage, and even treatment unit [7] may release air pollutants such as volatile fatty acids and ammonia. Greenhouse gases (GHGs, methane and carbon dioxide) emission, if not captured, may intensify the global warming to certain degrees [8]. So an appropriate management and treatment of the swine waste is an urgent and crucial issue to sustain the industry.

1.2 Swine wastewater treatment

The amount of swine wastewater (or slurry depending on total solids) generation and its composition depend on practices such as feeding, animal housing, waste collection and storage method. Generally speaking, pig waste has a total solids ranging between 2% and 8% when mechanically collected, and has a reduced total solids of 0.5% to 2% (more diluted) when washed and collected using water[9]. Swine wastewater thus has

varying amount of five-day biochemical oxygen demand (BOD_5, between10000 and 50000 mg/L), total N (3000 to 5200 mg-N/L), NH_4-N (1820-3330 mg-N/L), phosphorus (660-920 mg/L), and pathogens [10]. Treatment of swine wastewater aims to reduce or eliminate those pollutants, and potentially reuse the huge amount of nutrients available (Table 1-2) in manure and wastewater.

Table 1-2. Manure nutrients generated (in thousand tons) by livestock industry in US in 1997 [a]

Animal category	All animals As excreted [b]		Confined animals [d] As excreted [b]		Confined animals [d] Recoverable [c]		Potential CAFOs [d] As excreted [b]		Potential CAFOs [d] Recoverable [c]	
	N	P	N	P	N	P	N	P	N	P
Fattened cattle	506	155	491	151	177	115	424	130	152	99
Milk cows	908	163	731	131	288	111	194	35	62	24
Other beef and dairy	3,002	960	201	59	59	49	-	-	-	-
Swine	**543**	**161**	**524**	**155**	**124**	**126**	**300**	**89**	**71**	**72**
Poultry	895	302	895	302	523	251	428	148	252	123
All	5,854	1,742	2,843	798	1,172	652	1,512	449	549	325

[a] Data are compiled and calculated from the reference [11].
[b] *As excreted* manure is the total manure excreted by animals without further handling.
[c] Recoverable means the manure nutrients available for application, which estimates for confined animals or potential CAFOs after adjusting for expected losses of nutrients during collection, transfer, storage, and treatment. However, it is not clear which treatment methods are assumed to use in that study.
[d] Definitions of Confined Animals and Potential CAFOS are not defined in the study, but they may resemble that of AFOs and CAFOs, respectively.

Depending on different ultimate uses or disposal of pig waste, various treatment technologies are available despite the fact that these technologies do not completely meet the treatment requirement. As sufficient cropland is not always available for direct disposal, and excessive disposal would result in nutrient leaching and runoff, other treatment technologies are developed, including solid-liquid separation, composting, aeration, anaerobic digestion, aerobic treatment, activated-sludge process, sequencing

batch reactor, biofiltration and artificial wetland [6, 12]. Anaerobic digestion is the most commonly used one. It decomposes organic matters by complex microbial consortia responsible for hydrolytic, acidogenic, acetogenic, and methanogenic stages. It also generates methane as an energy product [12]. Disadvantages of this treatment only include the following: uneconomical when total solids is low, the effluent needs further treatment for nutrient removal, and not stable when characteristics of influent wastewater or operational parameters change. Aerobic or activated-sludge processes achieve substantial chemical oxygen demand (COD) and ammonium removal, but they increase the GHGs emission and keep a high operational cost.

Microbial fuel cell (MFC, also known as a type of bioelectrochemical reactor) is an emerging technology that shows a potential use in swine wastewater treatment. It basically fulfills biological oxidation at anode for organic carbon, and electrochemical or biological reduction at cathode [13, 14]. Microbial consortia at anode are versatile to organic substrates such as glucose, volatile fatty acids, glycerol, and even cellulose. It is sustainable because it converts waste to electricity, and reduces the cost for wastewater treatment. The literature review section will discuss its advantages and challenges for swine wastewater treatment in detail.

1.3 Objectives

The overall goal of this study is to develop effective MFCs for treating synthetic and swine wastewater to generate electrical energy and, at the same time, to achieve efficient removal of COD and total ammonium nitrogen. Specific objectives for this study are as

follows:

1. To develop lab-scale single-chamber MFCs. MFCs will be inoculated with bacterial sludge/sediment of different origins and subject to electric stimulation (+2 V). The hypotheses are that inocula of different origins will enrich electrode biofilm with different microbial community so that the capabilities of electricity generation differ among the differently inoculated MFCs, and that electric stimulation generating hydrogen will provide additional electron donors for denitrifying bacteria, thus accelerating inoculation and improving denitrification thereafter. Electric stimulation will also be applied to long-term operated MFCs to test its impact on electricity generation. Impact of inoculum type and electric stimulation on the microbial community, biofilm structure, internal resistances, and organic substrate removal will be compared.

2. To model the electrochemical and biological properties (activation overpotential and exchange current density) of MFC. Current models in the literature do not provide tools to simulate or predict the change of overpotentials and other electrochemical properties on the assumption that the anodic biofilm catalyzes organic oxidation. The hypothesis here assumes that inclusion of activation overpotential and exchange current density in a model will be more effective to model the performance of MFCs with regard to electricity generation and organic matter removal.

3. To construct MFCs coupled with internal or external zeolite/granular activated

carbon (GAC) packed beds. Too high ammonia level has been demonstrated inhibitory to electricity generation [15], and volatile fatty acids (VFAs) inhibitory to anaerobic digestion. With a hypothesis that zeolite/GAC packed bed reduces ammonium/VFAs concentration in swine wastewater to an acceptable level for MFC, experiments will be conducted to test the isotherms and kinetics of zeolite for ammonium sorption and GAC for VFAs sorption. Ideal doses that sufficiently absorb ammonium/VFAs will be determined. Major performing indicators for the coupled reactor include power generation, COD, total nitrogen, and ammonium removals.

4. To modify air-cathode of MFCs for ammonium removal. The hypotheses are that there is a certain level of hydrophobic treatment on cathode that allows best ammonia volatilization, and that the electricity generation in MFCs promotes ammonia volatilization. Experiments of optimizing the level of hydrophobic treatment on cathode and increasing the cathode surface area will be conducted in order to improve the ammonium removal efficiency in MFCs.

Chapter 2. Literature Review

2.1 Microbial fuel cells

2.1.1 Basic principles

Microbial fuel cell is an attached-growth process with electrodes as the active sites for redox reactions, highlighted with the electron transfer to anode by exoelectrogens. The exoelectrogens, or named as anode-respiring microorganisms and electrochemically active microorganisms, have wide applications in metal recycling, bioelectrochemical reactors, and other environmental remediation techniques [16]. Multiple varieties of microbes are confirmed as exoelectrogens in MFCs and microbial electrolysis cells (MECs, a similar device to MFCs but requiring a small external voltage application) studies, including α, β, γ and δ proteobacteria, firmicutes, acidobacteria, and actinobacteria [17]. *Shewanella* spp., *Geobacter* spp. and *Geospirillum* spp. are among the most extensively studied [18].

The feature of exoelectrogens is that they are able to externally transfer electrons from themselves to a solid anode, an external electron acceptor, automatically or with the assistance of mediator molecules [19]. The recent finding that exoelectrogens function well without external addition of electron shuttles realizes the operation of MFC in a more economical way, and it has substantially promoted recent studies. Researchers have identified three mechanisms for extracellular electron transfer between bacteria and anode: electron shuttles, direct contact, and nanowires [20-22] (Figure 2-1).

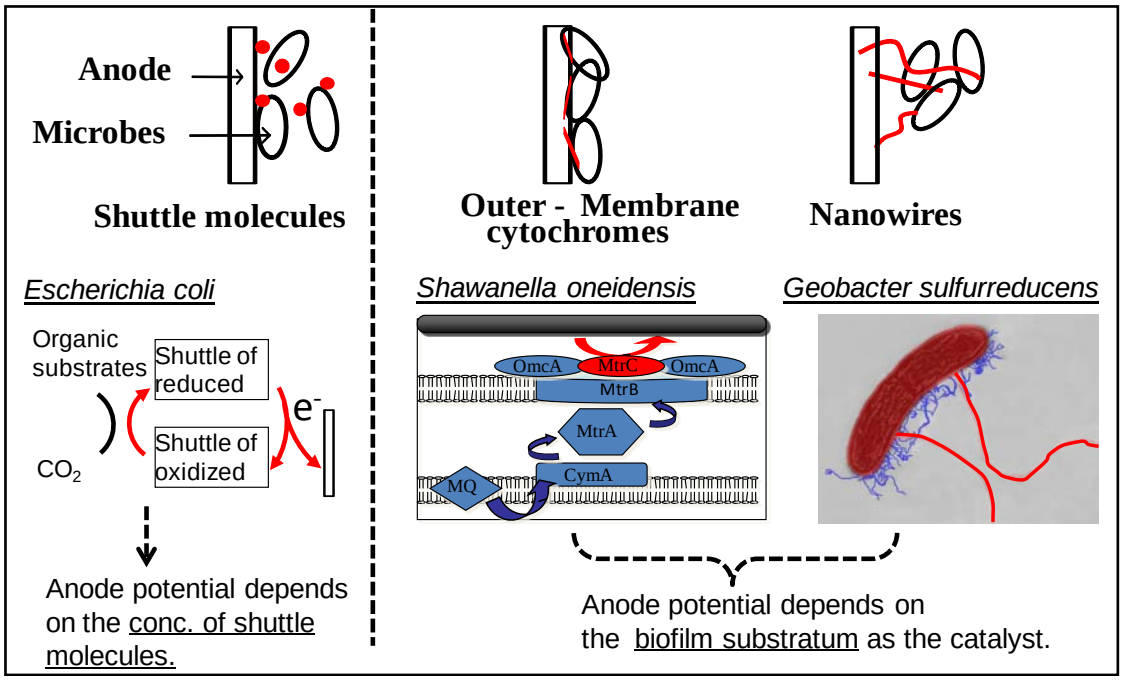

Figure 2-1. Illustration of mechanisms for electron transfer from bacteria to anode.

In an MFC, electrons are released by exoelectrogens from organic electron donor and accepted by the anode; meanwhile, electrons to cathode are further accepted by oxygen gas, nitrate (for MFC), or other terminal electron acceptors [16]. The difference of electrode potentials generates electromotive force (E_{emf}) in MFC, and the electricity can be harvested by external resistors. The following equations describe unbalanced anodic and cathodic reactions for MFCs using oxygen gas an oxidant:

$$\text{Organic substrate} + H_2O + \text{anode} \xrightarrow{\text{exoelectrogenic bacteria}} CO_2 + (\text{anode-electron})^- + 2H^+$$

$$(\text{Cathode-electron})^- + \tfrac{1}{2}\, O_2 + 2H^+ \xrightarrow{\text{catalysts/biocatalysts}} H_2O + \text{cathode}$$

Compared to conventional wastewater treatment methods such as anaerobic digestion, activated sludge method or sequencing batch reactor, MFC reactors have the following important advantages: high versatility for different types of organic matters of varying

concentrations; less requirement for valuable electron donor addition; overcoming fermentation barriers and achieving substantially improved energy recovery; high energy recovery; improved organic removal by bacteria growth and by electricity generation; improved removal of ammonium and phosphate; and achieving low COD values in effluent.

2.1.2 Mechanisms for exoelectrogenesis

The free electrons released by organic matter oxidation could be donated to terminal electron acceptors within bacteria through electron transport chains [18], but these electrons can also be transferred outward of cell membranes, as what happens in MFCs and other bioelectrochemical systems. Three mechanisms for extracellular electron transfer process between bacteria and anode are identified: electron shuttles, direct contact, and nanowires (Figure 2-1).

Electron shuttles

A wide range of chemicals could work as electron shuttles, or mediator molecules, such as potassium ferricyanide, neutral red, and thionine [23]. These molecules are soluble and diffusible in water. When they are present in medium, they intermediately accept electrons from bacteria and transport them outward of cells. The reduced mediators reach anode by random, allowing the release of electrons to anode. The oxidized mediators are then diffused back and function in the next cycle of electron transfer. In the early studies, researchers supplement shuttle molecules in medium to enhance its electrochemical activity. But recently, some metabolic products of exoelectrogens were

proved as mediators, such as psyocyanin by *Pseudomonas* and quinone by *Lactococcus lactis* [19]. Some of these molecules are also suspected of functioning in quorum-sensing as signal molecules or autoinducers [24]. More common cases are that these metabolic products belong to certain intermediates of biosynthesis, e.g., riboflavin as precursor for biosynthesis of quinine [25] or flavin mononucleotides [19].

Marsili et al. [25] studied the biofilm and medium of *Shewanella oneidensis* MR-1 and *Shewanella sp.* MR-4 to understand the process involved in electron transfer of these two strains. When cells of the mid-exponential phase were inoculated in an anode chamber, current (3-6 μA) was immediately generated, and reached a plateau value of 32-45 μA in 72 h. The medium was then replaced by fresh anaerobic medium supplemented with carbon source. The replacement reduced the current by 73%. This indicated that the electron transfer process was interrupted by the removal of shuttle molecules or by the removal of planktonic cells. The medium was again replaced with the original medium but without planktonic cells which were removed by centrifugation. The current also immediately recovered to the original value. Subsequent analysis confirmed that riboflavin, a redox-active molecule secreted by these two strains, played as the mediator.

Direct contact

Direct contact as a mechanism of electron transfer is based on the fact that certain enzymes (most commonly, c-type cytochromes) imbedded in outer cell membranes are part of electron transport chains for conventional redox reactions. When bacteria grow

on anode to form biofilm, these enzymes could play as interfaces between bacteria and anode. A difference between direct contact and the shuttle molecules is that the former relies on diffusive transport of molecules, while the latter does not [26], although *c*-type cytochromes behave as a form of fixed redox mediators as well. Gram-positive bacteria was thought to lack outer membrane electron transport proteins, and several of these bacteria therefore required electron shuttles due to this infeasibility of direct contact [19].

Bond and Lovley [23] designed an MFC using anode as the sole electron acceptor. They examined pure *Geobacter sulfurreducens* in the MFC system operating with 5 mM acetate and a 500 Ω of external resistor. It was found that an appreciable amount of current (up to 0.80 mA) and power (up to 0.09 mW) were generated in the reactor. On the contrary, pure *Escherichia coli* run in the similar configuration with glucose and a suitable carbon source was not observed with electricity generation. The medium in the *G. sulfurreducens* MFC was totally replaced by nutrients (P or N)-deficient buffer with only acetate (5 mM), the current recovered to the stable level as in the original medium immediately after the completion of the replacement, which was distinct from one of the results in the study by Marsili et al. [25]. The medium replacement removed both plankton biomass and any soluble contents in the original medium. Therefore, this spontaneous current restoration indicates that the electron transfer between anode and microorganisms is probably done by the cells which were already attached to the anode and still remained on it during the medium replacement. Scanning electron microscopic (SEM) photo confirmed that there was a layer of microbial cells attached to the surface

of the anode. The attachment was neither precisely even nor one-layer. Some part of it demonstrated “tower” architecture.

Assuming proteins playing a role in electron transfer, their analysis found an electron transport rate from microorganisms to anode of 0.21-1.2 μmol of electrons/mg of protein/min. The authors thought this result was comparable to previous ones with values of 1 to 3μmol of electrons/mg of protein/min for *G. sulfurreducens*. Electron transfer to the graphite anode in this case (or Fe(III) oxides in natural systems) was more limited than to soluble electron acceptors (e.g., Fe(III) citrates).

Nanowires

Nanowires in this context mean conductive filamentous or pilus-like appendages (50-150 nm in diameter, and tens of μm in length) produced by bacteria, behaving as conduct wires to transfer electrons outwards [27]. Certain metal-reducing bacteria, such as some of *Shewanella spp.* and *Geobacter spp.*, are able to produce nanowires in certain conditions. Their presence is also realized by bacteria such as *Synechocystis spp.* and *Pelotomaculum thermopropionicum*. Nanowires appear more frequently in electron acceptor-limiting environment, e.g., with low concentration of oxygen gas or fumarate. They are very fragile structures; interrupts such as agitation will break them into pieces [27]. Cytochromes MtrC and OmcA may function as intermediate electron carriers to nanowires or suspected of nanowires themselves.

El-Naggar et al. [28] isolated nanowires from *S. oneidensis*, and measured their capability for electron transfer through nanofabricated electrodes. Two electrodes were

connected to a nanowire followed by current-voltage sweep. Current was measured to linearly increase with the increasing voltage. Sweep was repeated after the nanowire was cut, and that current response was consequently not observed. This experiment showed that the electrodes were connected only by nanowires, and the resistivity of nanowires was estimated as $1\Omega \cdot cm$, transferring 10^9 electrons per s at 100 mV in equivalent.

2.1.3 MFC inoculation

Multiple varieties of genetic groups of microbes are confirmed as exoelectrogens in MFC or MEC studies, including α, β, γ and δ proteobacteria, firmicutes, acidobacteria, actinobacteria [17], and even yeasts [29]. Some exoelectrogens are Fe (III)-reducing bacteria which are able to express ferric reductase to reduce ferric ion (Fe^{3+}), hydrous ferric oxides, or solid ferric oxides to ferrous ion (Fe^{2+}) in anaerobic conditions. They could be *Shewanella* spp., *Geobacter* spp., *Geospirillum* spp., *Geovibrio* spp., and some hyperthermophilic *Archaea* [18]. Not all these Fe (III) reducers are exoelectrogens able to transfer electrons to extracellular anode; neither vice versa. Mechanism for the exoelectrogenic process could therefore be complex due to this biodiversity, and is still under investigation.

There is no direct evidence showing that a pure culture of microorganism enhances the performance of MFCs, and reactors are mostly inoculated by undefined cultures derived from domestic WW, anaerobic sludge, activated sludge, and soil bacteria, marine sediment, and other MFC anodic effluent/suspended bacteria. On the other hand, MFC inoculated by multiple sludge, e.g., a mixed consortium of wetland sediment and

anaerobic sludge, outperforms other MFCs with a single sludge inoculation, indicated by a substantially (nearly 1/8) smaller internal resistance and higher (doubled) power density [30]. A study based on MFC mode compared the effects of different inocula, i.e., anaerobic sludge, MFC anode solution, and MFC anode biofilm, on the acclimation time and the plateau value of the generated voltage/power [31]. The acclimation time for all of these inocula was about 50 h including a lag period of 20 h, while the plateau values were about 90, 140, and 205 mV, respectively. Compared to anaerobic sludge, a five-fold increase in the maximum power density of 40 mW/m^2 was achieved by inoculating a new anode through scraping and applying MFC anode biofilm. Similarly, these inoculation techniques can be applied to MEC to achieve good performance [32], because these two modes of operation have shared species of exoelectrogens in anode biofilm, e.g., *Geobacter* spp. and *Pelobacter propionicus* [33]. The substrate also has a selective effect on bacteria species even when the same inoculation technique is used [33]. For example, *Geobacter* spp. tend to flourish when acetate is used and buffered with CO_2 [34].

The impact of substrate concentration on biofilm formation and electron transfer rate of MFC was investigated. Nielsen et al. [26] added lactate solution in MFC every other week in an experiment lasting over one year to evaluate the short- and long-term effects of lactate solution (0.23 mM in anode chamber). When the reactor was ready, an addition of lactate solution almost immediately enticed the current going up to a peak value. With the consumption of lactate, the current decreased to a level as before the supplementation. That means the lactate addition as a substrate stimulated electricity

generation temporarily, but in the long run, it did not modify much the electrochemically active biomass that was responsible for current generation. The medium was modified by the long time operation and lactate addition. For example, the initial pH was 7.4-7.9; while after operations, pH was 5.9-6.2 for the un-supplemented reactors, and 5.0-5.1 for the lactate-added ones. This can be explained by the fact that the oxidation of carbon sources acidifies solution. The average cumulative current efficiency of the supplemented MFC ranged between 45% and 65% during 372- and 482-day operation. By varying lactate concentration, a Coulombic efficiency of 25% was achieved for 3.8 mM, and 58% for 0.12 mM. Therefore, the lactate addition did not necessarily encourage electron transfer or growth of current-generating bacteria, since the major part of the substrate went to other products when its concentration was increased. Three of MFC reactors were not added with exogenous lactate as an electron donor, and they continuously generated electricity of 0.07 mA through the year of experiment. Bacteria on the anode chamber of these MFCs may feed on electron donors in sandy sediments in the reactor during the experiment.

Phosphate buffer solution (PBS) usually encourages better performance during a steady state operation of MFCs, and there are several ways by which it benefits bioelectrochemical systems. First, increased buffer concentration reduces electrolyte limitation [35], as it was evidenced to decrease the percentage of electrolyte resistance in total internal resistance from 78% to 47% when phosphate buffer was increased from 50 mM to 200 mM. Second, it reduces diffusion resistance of proton from anode to bulk solution, as the conjugate bases of PBS, e.g., $NaHPO_4^-$ and HPO_4^{2-} (Figure 2-2),

combine with proton generated in anodic oxidation. A current density of 9.3 A/m^2 was achieved at 100 mM buffer. Although this value is still much lower than the theoretical maximum, it doubled from the value of the 50 mM of buffer [36]. Third, due to conjugated bases, it helps to maintain a suitable pH range locally around anode which is easily to go as low as 4 if it's not buffered. However, a higher (>25 mM) PBS is not beneficial for MFC startup, as it prolongs startup time and decreases maximal voltage [37].

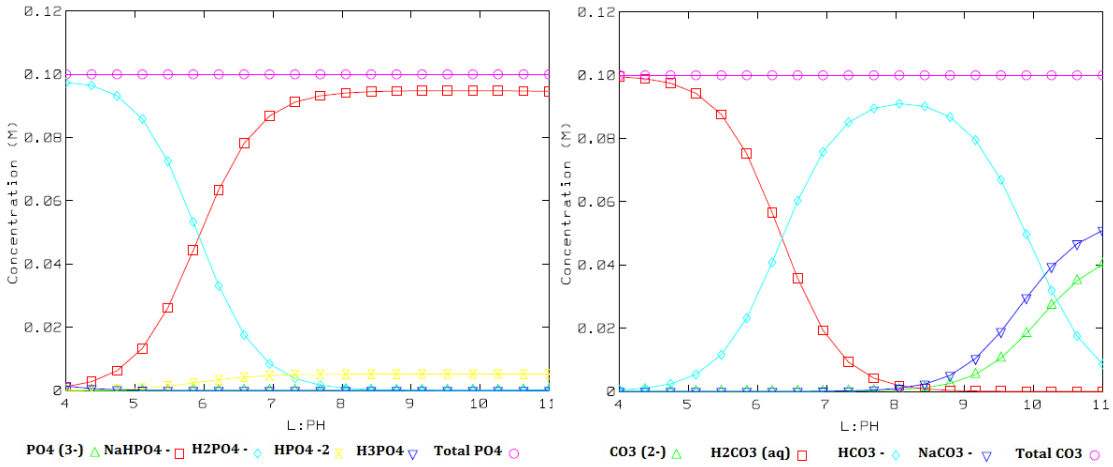

Figure 2-2. Titration curves of phosphate buffer and bicarbonate buffer. The pH range is 4-11 for phosphate buffer (left) and bicarbonate buffer (right) solutions (100 mM), and the acetate is 20 mM. The plots were generated by MINEQL+ chemical equilibrium modeling software.

Applying a positive potential on anode was also observed to facilitate two-chambered and potassium ferricyanide-mediated MFC startup [38]. The positively poised MFC had a constant anode potential of 200 mV *vs.* the Ag/AgCl reference electrode, and this accelerated the complete startup period from 59 d to 35 d. Open circuit voltage and maximum power output were also significantly improved, by 20% (day 24) and 155%, respectively. These differences disappeared after day 59, when both the poised and the

control MFCs finished the startup. The authors attributed this acceleration to the shortened acclimation of anodic respiring bacteria, which was likely a result of a higher driving force for substrate oxidation (*ΔE1* in Figure 2-3) when positively poised. Two other studies [39, 40] also demonstrated the beneficial effect of a positively poised potential/applied voltage, although too high a potential would deteriorate the microbial synthesis of terminal electron donors and terminate the electron transfer. The startup time of MFC, inoculated by previous MFC effluent, was not much impacted by negatively poised anode potentials of -400 mV, -200 mV and 0 mV *vs.* the Ag/AgCl reference electrode [41].

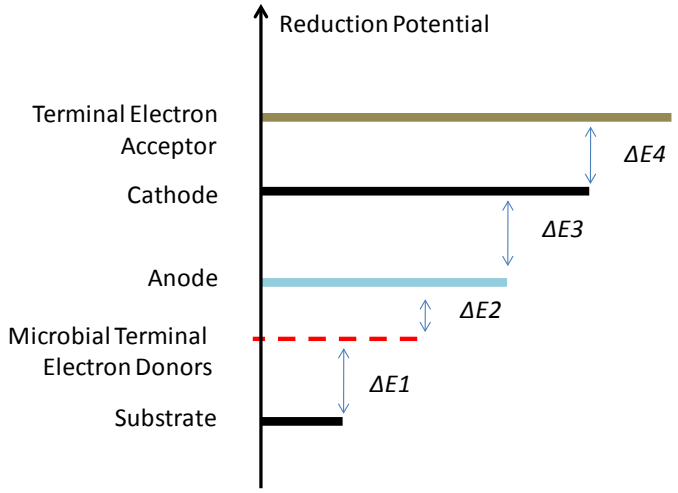

Figure 2-3. Schematic of electron transfer steps in MFC. *ΔEs* indicate the change in reduction potentials in each step between terminal electron donors to terminal electron acceptors.

2.1.4 Anodic biofilm

Biofilm formation on anode surface is essential to exoelectrogenesis. The structure and property of a biofilm are usually examined with destructive methods at the end of

incubation or operation [23, 26], such as protein quantification, microscopic techniques, and community analysis. McLean et al. [42] developed a nondestructive method of real-time fluorescent microscopic imaging to investigate the morphology of *S. oneidensis* MR-1 on an anode surface of a continuous-flow MFC. When MFC experienced an exponential stage and reached steady state after about 40-80 h, the current was 0.15 μA and 0.3 μA for external resistors of 100 Ω and 1 MΩ, respectively. Fluorescent microscopic images and SEM images of the two MFC reactors showed distinctions in biofilm structure established in the steady state at 80 h. The higher resistance (1 MΩ) corresponded to the lower current (0.15 μA), and stimulated the biofilm growth to about 50 μm, while the lower resistance corresponded to only 5 μm thick. In order to determine the ability of electron transfer of a single *S. oneidensis* cell under the two different loads, cell number and current density were quantified. The results showed that the specific electron transfer rate was enhanced to 200 fA/cell (at 15 h) at the lower external resistor. On the other hand, the 1 MΩ circuit yielded a rate of 80 fA/cell. The transfer rate was reduced to 63 and 39 fA/cell at steady state at 75 h, respectively. However, causal relationship between the electron transfer rate of a cell and the load was not readily obvious in this study. For example, it could be the inner layer of a biofilm responsible for exoelectrogenesis, while microbes of outer layer only take part in the organic degradation.

Studies on a newly constructed G. *sulfurreducens* Δ1501 mutant [43] demonstrated that a lack of extracellular polysaccharide limited cell aggregates with each other and to anode (poised to 0.24 V *vs.* NHE which is 0.04 V *vs.* Ag/AgCl). This inhibited the

growth of biofilm on Fe (III)-coated surface, which dramatically decreased the reduction of the insoluble Fe (III). After 7 days of cultivation, the concentration of the reduction product, Fe (II), was 5 mM in solution, much less than 50 mM generated by the wild strains. However, adding 5 μM of mediator or shuttle molecules, anthraquinone-2, 6-disulfonate, restored its ability of ferric reduction indicating that it was the deprivation of the electron transfer outward to a surface (or anode) but not a defect of outer membranes that disrupted ferric reduction. Further analysis showed that the extracellular matrix of the mutant contained 60% less polysaccharide and almost had an elimination of *c*-type cytochromes, e.g., OmcZ. When the wild strain was treated with Congo red that inhibited the activity of extracellular polysaccharide, it showed the similarly impaired function as the mutant.

The functionality of biofilm in MEC for hydrogen production was impacted by many factors, e.g., pH, substrate concentration and applied voltage, even though it had already stably accumulated on anode [44]. Effects of some of these factors (pH and substrate concentration) were well reflected by the anode potential. An anode potential of lower than -360 mV (*vs.* Ag/AgCl) corresponded to hydrogen generation. A reasonably higher pH in the range of 6-7, and a higher substrate concentration in the range of 100-600 mg/L stimulated the drop of anode potential to around -400 mV. Different from the two factors discussed, when the applied voltage was increased from 200 to 1000 mV, the anode potential almost kept constant but with a slight trend of increase, while the cathode potential gradually decreased.

2.1.5 Related functionality for wastewater treatment

Micro-environments of MFC reactors, not only as a result of chemical gradient, surface condition and shear, but also different locations or components of this type of bioreactors, vary a lot. This heterogeneity provides opportunities for treating various contaminants of wastewater at different locations of MFCs. Different reactor configurations and operations, such as batch reactor, CSTR, packed-bed reactor, and upflow anaerobic sludge blanket, can be applied to MFCs, which further creates its application in wastewater treatment. So the overall effectiveness of the reactors for animal or food processing wastewater depends on which reactor configuration is used and how the reactor components work with respect to its own functionality. This section discusses the functionalities which relate to wastewater treatment.

Assimilation and biomass growth

Plankton biomass in a reactor usually forms the attached biomass after certain periods of operation, either on supporting surfaces or granules. The attached biomass, or the biofilm, increases solid retention time and reduces biomass washout, and leads to higher overall biomass concentration in the reactor and more efficient organic matter removal. The MFC anode and cathode also provide ideal supporting surfaces for biofilm formation [45, 46], so electrodes facilitate COD and nutrients removal. Enhancing biomass growth by better MFC configuration, e.g., increasing electrode surface area and using packed-bed materials, may improve attached biomass growth and reduce the hydraulic retention time.

Redox reactions

Anode-respiring bacteria that feed on organic matters oxidize substrates and donate electrons to anode, and the cathode accepts electrons. The electron motive force extracts portion of the released energy in the substrate oxidation in the form of electrical energy. Therefore, two important and interrelated functionalities are present during this process: organic matter removal and electricity generation. There is a lot of literatures on electricity generation, but scare on organic matter (or substrates in Table 2-1) removal as a result of redox reaction.

Table 2-1. Common organic feedstock for MFC and their chemical properties

Substrate	**Molecular weight**	**Formula**	**pKa**	**COD equivalent**	**Degree of reduction**
Acetic acid	60	CH_3COOH	4.76	1.07	4
Glucose	180	$C_6H_{12}O_6$	12.28	1.07	4
Glycerol	92	$C_3H_8O_3$	NA	1.22	4.67

	Typical COD mg/L	**Typical pH**	**Alkalinity mg-$CaCO_3$/L**	**Reference**
Domestic WW	204-481	6.5-7.5	50-200	[47]
Swine WW	12000-17000	7.3	114	[48, 49]
Brewery WW	30000-70000	5-6	NA	[50, 51]
Biodiesel WW	1160, up to 170000	5.5-10	NA	[52, 53]

Ammonia volatilization

Ammonium is the major form of nitrogen compounds in animal wastewater. It exists in equilibrium between ammonia, the unprotonated form, and the ammonium, the protonated form. The oxygen reduction reaction (ORR) at the air-cathode side of MFCs consumes protons and generates hydroxide. As a result, the elevated pH drives the ammonium ion to form ammonia which can be transferred outside through the gas-

diffusion layers of the air-cathode, and so the total ammoniacal nitrogen (TAN) can be removed from wastewater.

Nitrification and denitrification

Another way of removing ammonium is through the nitrification followed by denitrification. The nitrification is fulfilled by chemoautotrophic nitrifying bacteria at aerobic condition in two separate reactions: ammonia is oxidized in the first step to nitrite by ammonia-oxidizing bacteria with the assistance of ammonia monooxygenase enzyme, and nitrite is further oxidized in the second step to nitrate by nitrite-oxidizing bacteria employing nitrite oxidoreductase.

The growth of nitrifying bacteria is slow since the energy release of the redox couple of nitrite/nitrate is small, so an additional step of nitrifying bacteria enrichment in mineral salt medium in aerobic cathode compartment or on air-cathode is needed. However, it was also observed that nitrifying bacteria naturally grew and functioned on air-cathode [54] or on electrodes in medium with or without organic substrates [55, 56].

Denitrifying bacteria can use nitrate as electron acceptor in the absence of oxygen and result in gaseous nitrogen-containing chemicals such as N_2, NO, and N_2O. These bacteria are either heterotrophs or autotrophs. Among them, hydrogenotrophic denitrifiers are especially of interest because the electron donor hydrogen is ubiquitous and they are more efficient in nitrate removal than bacteria rely on other organic electron donors [57]. So bio-electro reactors, which generate hydrogen gas during water electrolysis at electrolytic mode, was devised to provide hydrogen gas for

hydrogenotrophic denitrifiers and to simultaneously remove nitrate. As this type of reactors consumes external electrical energy, it is not as sustainable as a reactor that can provide electrons from wasted organics. As a potentiostat-poised graphite cathode was able to provide electrons to *Geobacter metallireducens* for partial denitrification [58], bio-cathode (biofilm as the catalyst) of MFCs was further conceptualized for nitrate removal [59]. So two-chamber MFC with granular graphite as the bio-cathode support was devised, and this MFC was proved effective to provide electrons to the denitrifying biofilm and reduced nitrate at a rate of 146 g NO_3-N m^{-3} d^{-1} [60]. By combining the nitrification and denitrification processes (by obligate denitrifiers) in the same aerated cathode chamber, ammonium removal was accomplished in MFCs [61, 62].

Salt precipitation

In a two-chamber MFC with both anode and cathode operated at anaerobic condition, the pulverized $FePO_4$, or the grinded digested sewage sludge which naturally contained $FePO_4$, was added in cathode chamber to serve as electron acceptor [63]. This ferric reduction mobilized the $FePO_4$ particles and resulted in ortho-phosphate species, which was then precipitated as struvite crystals as a fertilizer ($MgNH_4PO_4 \cdot 6H_2O$) from the cathode effluent after Mg^{2+} and NH_4^+ addition. However, immobilized phosphate has not been proved to be present in a form of $FePO_4$ in animal wastewater, so this mobilization capability of MFCs may not find its direct use.

Another study observed natural struvite precipitation on air-cathode when swine wastewater was used as the substrate [64]. It was proposed that it was the elevated pH at

the vicinity of cathode caused by ORR that reduced struvite solubility and promoted crystallization and precipitation. This principle was earlier proved working in electrolytic cells [65], but the electrolysis process required external power supplies which were not needed in MFCs.

2.1.6 Reactor design and performance

Performance of MFC or other bioelectrochemical systems greatly depends on their reactor material and design, or so called “architecture” [13]. Important considerations in the literature for improving MFC performance include choices of chamber and membrane design, anode, cathode, and catalyst materials. Plain carbon cloth is one of the most suitable for anode, and air cathode made from wet-proofed carbon cloth with Pt coating is currently the most used cathode material for MFC [66]. General requirement on electrode materials include the following [67]: microbial adhesive, catalytic, high specific surface area, electrically conductive, noncorrosive, and scalable.

Performance of different reactors is examined through comparing a set of terms relating to efficiency (Table 2-2). When reactors are used for wastewater treatment, other efficiency and rate terms are further needed for comparing performance. COD, ammonium nitrogen (or ammonia nitrogen for the same meaning) or total nitrogen removals, and their removal rates, which will be latterly defined when mentioned, are necessary when describing their efficacy for wastewater treatment.

Table 2-2. A set of definitions used for comparing MFC performance

Term	Symbol	Standard unit
External voltage	U_{ext}	V
Open circuit voltage	OCV	V
Current density	i	A/m^2
Power density	P	W/m^2
Coulombic recovery	r_{ce}	Electron recovered/Electron in substrate
Internal resistance	R_{int}	Ω
Activation overpotential	η_{act}	V
Concentration overpotential	η_{conc}	V

During the MFC operation, organic matters in wastewater provide carbon source for microbial growth, and also electron donors for exoelectrogens. The circuit harvests electric energy by external resistors, so a Coulombic recovery (r_{ce}), the ratio of the charge (in coulombs) recovered to the charge that is ideally released by the degradation of organic matters. The Coulombic recovery can be as high as 80% for defined electron donors (e.g., acetate), and varies between 5% and 50% for complex substrates measured by COD or BOD_5 in wastewater [68, 69]. The power generated on the resistor, sometimes normalized to electrode areas, denotes the performance of MFC as a power supply [70, 71]. Single-chamber MFC with air-cathode usually works better than two-chamber reactors in power density, but its columbic efficiency is lower mainly because oxygen diffuses to reactor medium.

MFC can also serve as a device for COD and nutrient removal for wastewater treatment purposes as previous discussed, and this paragraph summarizes some of the studies. An oxic/anoxic-cathode MFC achieved 98% COD removal with the influent COD of 950 mg/L operated in continuous mode [46]. An air-cathode MFC in continuous mode [72] removed 15-20% and 30% of COD in domestic wastewater with initial COD of 450

mg/L, under the organic loading rate of 175 g/L-day and 1.75g/L-day, respectively. Another single-chamber MFC [73] in continuous mode tested lower organic loading rate of 0.41 g/L-day for influent COD of 240 mg/L, and the achieved COD removal in effluent was about 60%. Samples of 10-fold diluted swine wastewater were subject to two-chamber MFCs, and 86% COD and 83% ammonium nitrogen removals were achieved in 30 to 50 h operation [74]. Volatile fatty acids (especially acetate) in swine wastewater are more preferred substrate for exoelectrogenic bacteria, and their removal is more efficient. For example, 422 mg/L of volatile acids was totally removed by MFC, while only 84% of soluble COD (initially 8270 mg/L) was removed in 260 h operation [75]. Compared with synthetic substrate such as acetate and glucose, application in real wastewater showed lower power density (5-25 W/m^3, or 70-300 mW/m^2, [69]), lower columbic efficiency (5%-40%), and lower COD removal.

2.1.7 Analysis techniques

Voltammetry scan

MEC reactor is intrinsically a bioelectrochemical system where mature electrochemical techniques can be applied to evaluate experimental materials and reactors, and also to predict performance of MEC reactors. Fundamental ideas for voltammetry are the electrode kinetics and mass transport: when the concentration gradient of a reactant is maintained, the reaction rate of electron transfer with respect to potential is proportional to the exponential of an applied voltage, controlled by the Butler-Volmer equation; when concentration gradient of a reactant is unbalanced due to a high applied voltage, the

current begins to decrease with respect to potential, a process modeled by the Cottrell equation [76]. The current density of these two processes is electrode kinetic- (or activation overpotential) limited and mass transport- (or concentration overpotential) limited, respectively. Voltammetry scan in MFC and MEC is usually applied to the region of kinetic-limited [77] but sometimes to the whole curve [78, 79].

Linear sweeping voltammetry (LSV) and cyclic voltammetry (CV) are techniques employed to investigate phenomenon of electrolysis, and they have been used to test and screen electrode materials and catalysts [77, 80-82], and to characterize biofilm samples [78]. Both techniques use a three-electrode setup: a working electrode (to be tested), a reference electrode and an auxiliary (or a counter) electrode. In LSV, the voltage varies over a range at a constant rate (e.g., -1 or -2 mV/s) in one direction and the electrode is tested in a phosphate buffer, e.g., in a 2 mM phosphate buffer. The first scan usually does not provide accurate information due to discharge and polarization of the electrode, and only the subsequent results are used to interpret characteristics of a material [83]. When the applied voltage reaches an onset value (V_e) overcoming the energy of the Fermi-level as well as the overpotential of the electrode, a current is generated. Therefore, V_e values partly represent the performance of electrode materials [77, 81, 82]. Since the working current of MECs is usually much higher than 0, other more reasonable current values (e.g., -3.2 log A/cm^2) can be chosen to standardize the onset potentials of electrodes coated with different catalysts (Figure 2-4 from [80]). LSV results show that after several cycles of MEC operation, the onset potentials of catalysts

were altered and indicated increases of overpotential throughout the period of operation [80].

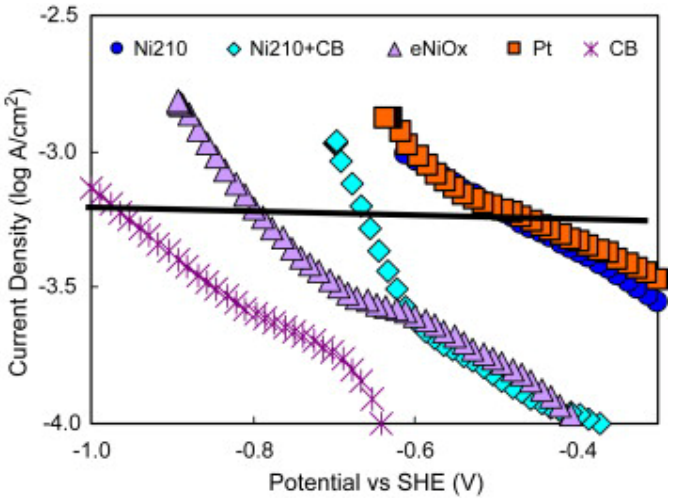

Figure 2-4. An example of linear sweep voltammetry result for comparing different catalysts. The y-axis is logarithm of current density. The figure is adopted from the reference [80].

CV uses an experiment setup similar to LSV, but differs in the scan by using forward and backward sweep sequentially [78, 84]. However, even when the CV curve is obtained, only the positive wave is usually used due to less background electrolysis [78]. Electrochemical activity was assumed to be evidenced by current peaks of a CV curve in a biofilm sample from an MFC reactor. In comparison, a biomass-free electrode and a biomass sample from an anaerobic reactor showed no peak indicating electrochemical activity (Figure 2-5 from [78]). The peak current was used to compare electrochemical activity of biofilm formed on an anode at different pH. Results showed a significant higher peak current of biofilm enriched and tested under an alkaline condition (pH=9) [79]. CV has been intensively applied in evaluating MFC electrodes but not yet in MEC electrodes.

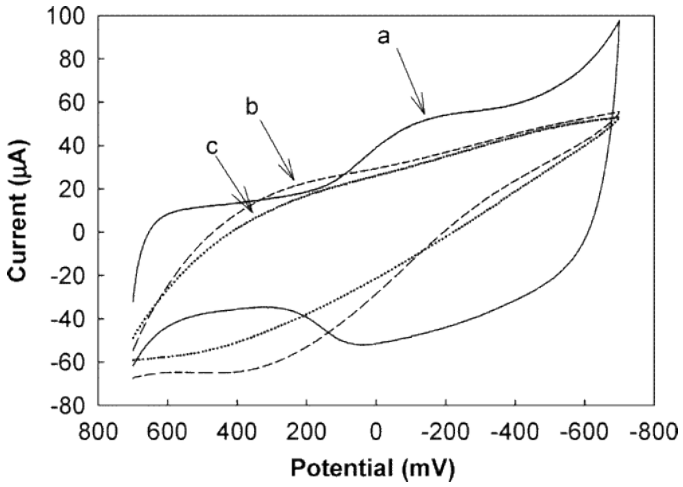

Figure 2-5. An example of using cyclic voltammetry result for comparing electrochemical activity. The figure is adopted from the reference [78].

Electrochemical impedance spectroscopy

Electrochemical impedance spectroscopy (EIS) is a useful tool to evaluate resistance of an individual electrode and the internal resistance (R_{int}) of MFC and MEC. The internal resistance here means the sum of polarization resistances of electrodes (anodic, R_p^a; and cathodic, R_p^c) and the ohmic/solution resistances (R_s, consisting of ohmic resistances of electrodes, solution, or membrane). Internal resistance in MEC plays an important role in its performance, especially in columbic recovery [85], thus a better understanding is helpful to optimize a reactor.

EIS is measured in a two- and three-electrode setup for a full fuel cell and an electrode, respectively. As an example of three-electrode setup, a potentiostat linked to a frequency response analyzer is connected to a reference electrode which is placed in the solution of the chamber used. The frequency response analyzer outputs an AC signal of small amplitude, e.g., 10 mV, as well as the varying frequencies. The resulting impedance is

recorded and presented in the form of Nyquist plots (or complex plane plots) or Bode plots (Figure 2-6) to be analyzed and fitted for resistances [67] through a one-time constant model [86]. Through this application, a dramatic reduction of anodic internal resistance was found in an MFC where *Shewanella oneidensis* MR-1 was added. It was concluded that the substrate oxidation by these bacteria occurred on the anode, which reduced the polarization resistance according to the mixed potential theory [86]. Similarly, Wang et al. [38] compared the distribution of internal resistance of two different MFCs using EIS, and found that the charge transfer resistance, which constituted the majority of the internal resistance, differed much from each other, 80 Ω *vs.* 185 Ω. Another study used the EIS method to evaluate impact of bulk pH on the anode impedance, and found that pH 9 was more favorable than neutral or acidic condition due to a much reduced anodic polarization resistance [79]. This result can be explained by an early study evaluating the effect of proton transport inside the MFC biofilm on anodic current density. It concluded that a higher bulk pH value expedited the transportation of the protonated conjugate base in the buffer system [36]. EIS was suggested to study microbial metabolism on electrodes, effect of electron mediators, monitoring of biofilm development on electrode, and the diffusion process [87].

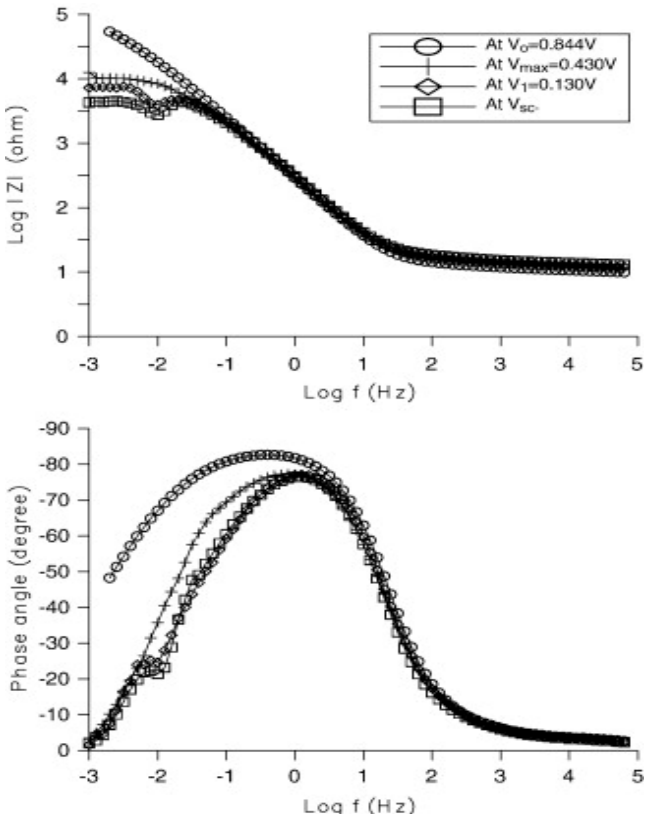

Figure 2-6. An example of using electrochemical impedance spectroscopy to identify internal resistance. The figure is adopted from the reference [86].

Tafel plot

The Tafel equation, modeling activation overpotential against the logarithm of current density, is yielded from the Butley-Volmer equation at high overpotential regions [67, 88]. The corresponding semi-logarithmic plot of the current density against the overpotential is called a Tafel plot (Figure 2-7). The slope of the linear part of the curve, termed as the Tafel slope (or b), is an important experimental parameter for interpreting reaction mechanism; log (i_0), determined by extrapolation of the linear curve to zero overpotential, provides information about the rate of redox on electrodes at equilibrium. A larger log (i_0) and a smaller slope are preferred for electrode and catalyst materials of

an MEC reactor. The plot is usually obtained by scanning electrode at an overpotential range within several hundreds of mV (relative to open-circuit potential) at a small scan rate of 0.1 mV/s [67], but not necessarily.

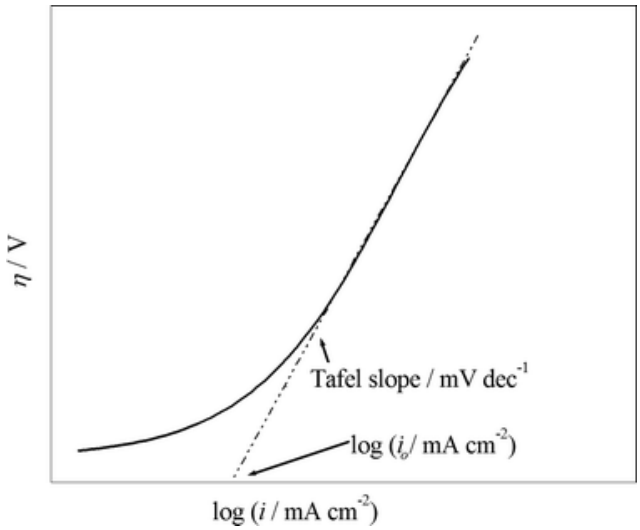

Figure 2-7. An example of a Tafel plot for determining the exchange current density of an electrode. The figure is adopted from the reference [88].

Other electrochemical techniques

Other electrochemical techniques for performance evaluation of MEC are similar to those for MFC and enzymatic fuel cells (EMC), including fuel cell/electrode polarization techniques, current interruption, differential pulse voltammetry, chronoamperometry, chronopotentiometry, V- (E- and I-) t curves, and rotating-disk electrode and rotating ring disk electrode. These techniques have been summarized and well discussed for facilitating MFC and EMC studies [88]. Non-electrochemical techniques can be applied or combined with electrochemical techniques to better understand various aspects of MEC reactors, such as denaturing gradient gel electrophoresis [88], scanning electron microscopy [89], fluorescence in situ

hybridization [78], polymerase chain reaction [90], and single-strand conformation polymorphism [44].

2.2 Nitrogen removal

Swine wastewater contains high total nitrogen level. The inorganic nitrogen is mainly ammonium, which varies from several hundred mg/L NH_4-N to almost three thousand [91]. Based on the fact that nitrate and nitrite are much easier to remove than ammonium, a process that oxidizes ammonium (mainly nitrification; or anammox in rare cases) in swine wastewater is generally necessary as a pretreatment. Electrochemical-related processes for denitrification are also briefly discussed.

2.2.1 Ammonium removal

Swine wastewater contains a major portion of total nitrogen in the form of ammonium, but conventional anaerobic digestion alone does not effectively reduce ammonium concentration. Various pretreatment or post-treatment processes have been developed for ammonium removal but are not cost effective, such as air stripping and aeration. Diverse microbial physiology pathways also demonstrate their roles in ammonium removal, mainly by oxidation (nitrification/denitrification) and the others by assimilative metabolism. The partial nitrification, where ammonia oxidizing bacteria accumulate nitrite at the presence of oxygen, has been tested as a pretreatment for anammox for swine wastewater [91, 92]. Ammonium conversion to nitrite was about 60%, and the total nitrogen removal could achieve 55% or higher [92]. In most studies, however, nitrification provides intermediates (NO_2^- and NO_3^-) for denitrification, which is

discussed in the *Nitrate Removal* section.

Zeolite sorption

Zeolite, a natural alumino-silicate mineral, is found to be an effective and selective sorbent for ammonium in wastewater [93-95]. The adsorption is a result of its building block, a tetrahedron structure, where a silicon or aluminum atom is located at the center and four atoms of oxygen outside. The substitution of Si^{4+} by Al^{3+} leaves the structure a negative charge, and thus allows cation sorption and exchange with external medium. The ammonium sorption performance depends on factors such as chemical components of zeolite, modification used, initial ammonium concentration, presence of other competing cations, the amount of zeolite added, reactor types, pH, temperature, and reaction time. Due to variations of these conditions, the ammonium (maximum) absorption capacity of natural zeolite ranges between 2.7 and 30.6 mg/g-zeolite.

In a sorption study based on batch operation of stirred shakers, 4.5 mg/g of sorption capacity was achieved in 24 h reaction for synthetic wastewater containing 500 mg/L ammonium nitrogen [96]. The zeolite particle was 1 to 4 mm mesh size, and the loading was 1 g for 10 mL solution. The Langmuir model fitting showed sorption maximum up to 10.84 mg/g. Their column study (100 g zeolite in 245 mL column) showed that 0.1 N HCl solution was much more efficient in ammonium desorption than deionized water, but desorption study in Na- or K-containing buffer solution, which impacts sorption processes, was not carried out yet. Biological aerated filter packed with zeolite as media consistently achieved 80% to 100% ammonium removal for initial concentrations

between 22 and 57 mg NH_4-N/L [97]. As the study neither set control groups without aeration nor monitored nitrite or nitrate concentrations, it was not clear if the zeolite adsorption or nitrification procedure removed the majority of ammonium.

A study based on high NH_4-N (4500 mg/L) swine wastewater also revealed a 46% ammonium removal within 24 h with zeolite load of 5 g/25 mL [98]. Using a closed-loop fixed bed reactor, the ammonium removal was further improved to 55%. When the swine wastewater was diluted to 560 mg NH_4-N/L (by 1/8), the same configuration adsorbed 96% of ammonium; however, the dilution wasted a significant amount of tap water and was not sustainable. Another study used powdered zeolite as sorbents in sequencing batch reactor [99]. By changing the first operation of anoxic filling to aeration mixing, the reactor removed 82% (a 12% more) of total nitrogen in a hydraulic retention time of 1.5 d. All the above results show a possibility of using zeolite as sorbents to reduce ammonium nitrogen and avoid ammonia inhibition in swine wastewater, and the quick sorption process (adsorption and release) is likely to be coupled with microbial fuel cells for better treatment performance.

Microbial fuel cells for ammonium removal

There are some studies using MFC for ammonium removal. A study compared air-cathode MFC and a two-chamber MFC for their ammonium removal performance and mechanism [100]. The air-cathode MFC removed 60% ammonium in 5 d at an initial concentration of 188 mg NH_4-N/L, while nitrite and nitrate did not accumulate (<1.5 mg/L) in this period. A control group with an abiotic cathode and non-buffered solution

had a comparable ammonium removal, so it suggested that localized ammonium vitalization due to pH increase substantially contributed to ammonium removal. In two-chamber MFC, ammonium was removed mainly by a physical way of air sparging. A lack of direct ammonium oxidation on anode was proved by cyclic voltammetry test in another study, where a direct oxidation would only happen after a long period acclimation in solution containing ammonium [56]. This study did not detect microbial species responsible for anammox, but biological nitrification was likely to be occurring on cathode due to the presence of nitrifiers there.

The mechanism of simultaneous nitrification and denitrification, combined with the concept of "loop configuration," was applicable in MFC [61]. Under this configuration, ammonium containing wastewater was directed to anode chamber to oxidize organic substrates, then conveyed to aerobic nitrification stage in a fix bed reactor, and finally directed to cathode chamber for denitrification. Although a low COD/N ratios (about 4) it had, this loop system still achieved denitrification rate of 0.41 kg NO_3-N $m^{-3}d^{-1}$ (up to about 70% nitrogen removal of the initial concentration of 80 mg NH_4-N/L), and 2.0 kg COD $m^{-3}d^{-1}$ (100% removal). The same group later tried another configuration that realized simultaneous nitrification and denitrification in cathode chamber [101]. This design improved total nitrogen removal to 94% for an initial ammonium of 52 mg NH_4-N/L. An ammonium nitrogen concentration between 500 to 1000 mg NH_4-N/L started to inhibit MFC electricity generation [15]. The half-maximum effective concentration was close to optimum ammonium concentration, indicating a careful control on NH_4 level would be desirable.

2.2.2 Nitrate removal

Abiotic electrolytic process

The abiotic electrolytic process for nitrate reduction assumes that no biological phenomenon is involved at electrodes. Nitrate ions are reduced to nitrite and finally to nitrogen gas in a stepwise way on the abiotic cathode surface mostly made from metals [102]. While anodic reaction forms oxygen gas, cathode reduces nitrate to nitrogen gas, and the pH is maintained by phosphate or carbonate/bicarbonate buffer solution. Nitrite and ammonium may accumulate a little bit which limits the denitrification efficiency, so additives such as sodium chloride are used to overcome their formation. The reason is that chloride is partially oxidized to hypochlorite which is a strong oxidant to react with nitrite and ammonium. An increased current improves the nitrate removal rate but the energy input accordingly increases [103].

Biotic electrolytic process

A main difference of the biotic from the abiotic electrolytic process is that the presence of denitrifying microorganisms, either autotrophs or heterotrophs on cathode surface plays a role in nitrate removal [104]. These ubiquitously present bacteria are able to use hydrogen gas generated in water electrolysis as electron donor to provide reducing power for hydrogenotrophs [105, 106], or to directly accept electrons from cathode [57, 107]. Autotrophic denitrifiers also use inorganic carbon source (carbon dioxide and bicarbonate) for assimilative metabolism. Heterotrophs get their carbon source and reducing power from organic substrates such as methanol, ethanol and acetate.

In the electrolytic process the absence of oxygen gas (anaerobic condition) is usually a necessity, but there are some studies finding oxic nitrification/denitrification happens in stirrer tank reactors [108] and sequencing batch reactors [109]. There is no report in the literatures studying oxic denitrification combined with electrolytic process, as oxygen is considered competing with bio-electrolytic denitrification process. The only study [110]until now that might have used electrolytic mode for aerobic biotic denitrification applied very small external voltages (0.2 and 0.4 V). This small voltage should not overcome the overpotential for oxygen evolution, and the reactor used ion exchange membrane, so cathode condition was still considered anaerobic.

Microbial fuel cell process

Microbial fuel cells have been studied for denitrification since the recent demonstration of biologically cathodic nitrate reduction in MFCs. A basic rationale is that the redox potential (+0.74 V) of nitrate/nitrogen gas couple is quite close to that of the oxygen reduction (+0.82 V). A two-chamber MFC, using graphite-Mn(IV) as anode, graphite-Fe(III) as cathode, and porcelain membrane as a separator for chambers, was test for its performance for nitrate reduction [110, 111]. The result showed a maximum removal rate of 0.084 mg NO_3-N cm^{-2} d^{-1} (chamber volume was not given) at an initial nitrate nitrogen concentration of about 70 mg/L and a low external resistor of 10 Ω. A low columbic efficiency of 7% implied that a higher nitrogen removal may be achieved by improving the utilization of anodic substrate. Another two-chamber MFC using granular graphite and cation exchange membrane revealed that microbial growth and methane production accounted for up to 30% and 40% of columbic loss [112], respectively. On

the cathode part $NH4^+$ and $NO2^-$ were below detection limit, while the discharge of N_2O was significant at higher poised cathode potentials (> 0 V).

Single-chamber MFC with air-cathode, which allows oxygen diffusion to reactor camber, was also tested for denitrification [113]. A distinction was observed between this reactor and two-chamber anoxic reactors: cathodic bacteria did not directly accept electrons from the cathode to reduce nitrate. Microbial community analysis revealed the presence of microbial species related with denitrification on electrode biofilm and bulk solution. As denitrifiers are mostly facultative aerobes, it is not surprising that they grow at air-cathode MFC reactors. This study consistently achieved more than 85% nitrate removal in 8 h for the initial nitrate concentration up to 120 mg NO_3-N/L (or 8 mM nitrate), and the remaining nitrate was about 7 mg NO_3-N/L which seemed to be constant even after 60 h. The high ratio of COD to nitrate ratio was considered as a driving force for rapid nitrate removal in this study.

2.2.3 Challenges in application

From the literature review on nitrogen removal, it can be concluded that modification of MFC is still necessary for better performance due to the following associated issues: the Coulombic efficiency of anode substrate is lower (e.g., due to methane production), indicating a possibility of better use of the anodic substrate; the remaining nitrogen in single-chamber MFC is still detectable, and needs more efficient removal; there are no MFC reactors used to treat wastewater of high nitrogen strength, and ammonium inhibition tends to slow down the nitrogen removal processes. In summary, further

studies are needed to improve Coulombic efficiency and COD removal, to reduce or eliminate inhibitory effect of swine wastewater to electricity generation, and to further improve NH_4-N removal by choosing better air-cathode and increasing cathode surface area.

2.3 Modeling microbial fuel cell

Mathematical models, categorized to dynamic and stationary ones [67], provide a useful way to understand MFC reactors for their product generations and wastewater treatment efficiency (e.g., COD and nitrogen removals). Effective models, no matter they are mechanistic, empirical, or grey-box type, may also provide an approach to estimate some important biological and electrochemical parameters for comparing different reactors. Due to numerous processes involved, this type of system is usually complex, but preceding models of biological and electrochemical processes share some similarity with MFC. For example, basic governing equations such as Ohm's law and Butler-Volmer equation (for quantifying activation overpotential) are also useful in MFC modeling and will be discussed earlier. The concentration overpotential can be derived from Nernst equation [114-117], expressed as follows:

$$\eta_{conc} = \frac{RT}{nF} ln(\prod \frac{S_b}{S_{surface}}) \quad (2\text{-}1)$$

where R is the ideal gas constant (8.314 J/K-mol), T is the temperature (K), n is the molar number of chargers transferred every mole of substrate, F is Faraday's constant (96,485 C/mol), S_b is the bulk concentration of reagents, and $S_{surface}$ is the concentration of reagents on the electrode surface.

For a half reaction such as $ox + n\ e^- \rightarrow red$, Nernst equation quantifies the electrode potential as follows:

$$E = E^0 - \frac{RT}{nF} ln(\prod \frac{a_{red}^{v1}}{a_{ox}^{v2}}) \quad (2\text{-}2)$$

where E is the electrode potential(V), E^0 is the standard redox potential (all species involved in reaction are at unit activity), $\prod \frac{a_{red}^{v1}}{a_{ox}^{v2}}$ is the reaction quotient (the ratio of activities of the reduced to the oxidized is raised to their stoichiometric coefficients of $v1, v2$), and, a_{red} and a_{ox} are the activities of reduced and oxidized states, respectively.

Based on the above governing equations and integrated with other anaerobic or exoelectrogenic processes, several mathematical models have been developed to describe MFC or a simple aspect of the reactor. The first microbial fuel cell model [118] simply focused on the output current in terms of substrate and mediator concentrations as well as external loadings (resistors). An anode biofilm-based dynamic and multi-dimensional model was recently proposed for the first time for MFC. This model was able to predict the biofilm and suspended biomass growth. Their later model [45] incorporated Anaerobic Digestion Model No.1, and resulted in a good agreement with experimental data of COD removal and current generation. For the purpose of predicting general bioelectrochemical behaviors with simpler and adequate models, other studies based on ordinary differential equations rather than partial differential equations were also carried out [119, 120]. However, there is no model developed from the fact that the anodic biomass serves as catalyst for substrate oxidation, and growth of the biomass reduces activation overpotential and increases exchange current density.

Chapter 3. Improved Performance of Microbial Fuel Cells Enriched with Natural Microbial Inocula and Treated by Electrical Current

3.1 Introduction

A microbial fuel cell (MFC) is a device harvesting electrical energy from organic substrates in liquid environment with anodic biomass serving as catalysts [14]. An MFC fulfills biological oxidation at anodes for organic substrate, and electrochemical or biological reduction at cathodes for oxygen or other electron acceptors. The catalytic microorganisms at anodes are capable of handling organic substrates such as glucose, volatile fatty acids, glycerol, and even cellulose [121, 122], and can thus be used in degrading organic substrates in various types of wastewater.

Studies on MFC anodic biofilm formation are undergoing in order to improve electricity generation capability and organic substrate degradation rate for practical application of MFCs. The catalyzing effect of anodic biofilm can be largely dependent on inoculum types [123, 124] due to the difference of inocula in the dominant mechanism for anodic exo-cellular electron transfer [125] and in the biofilm morphology and uniformity [126]. Compared with pure culture inoculation for anodic biofilm, mixed microbial consortia are more beneficial as they promote microbial versatility in substrate utilization and avoid medium sterilization. The consortia could originate from natural or artificial aquatic environments [30, 121, 127, 128]. However, a direct comparison of MFC performance in both electricity generation and substrate utilization under the same reactor design and operating conditions has not been carried out to select effective

inoculum.

A moderate electrical stimulation is another factor that has an impact on anodic biofilm formation and its morphology. The effects of the electrical stimulation through a voltage (±2 V) around the value of water electrolysis, either transient or permanent application, have been studied in other research areas [107, 129, 130]. Distinct mechanisms and effects could occur depending on the current intensity and treatment time as well as on the characteristics investigated. The application of electrical stimulation in MFCs, in a way of regulating the anodic potential, has been demonstrated to accelerate anodic microbial growth and to bolster anodic electrochemical activity [38, 41]. To the contrary, the effect of direct voltage stimulation, rather than just poising anodic potential, has not been fully assessed for MFC [39, 131]. It is clear that a large applied voltage damages catalytic effect of biofilms [39]; however, it is unclear whether and how the stimulation would accelerate anodic biofilm formation and thereafter improve the MFC performance, not to mention its interacted effects with different inoculum sources. The effect of the applied voltage on MFC electrodes on which mature biofilms have already developed need also be investigated, as it was observed that accumulated biofilm reduced the electrode activity [132].

This study used single-chamber and membrane-less air-cathode MFCs as model reactors to evaluate different inoculum sources for anode inoculation. MFC performance of different treatments was evaluated and compared in terms of MFC characteristics, including lag phase period, maximum growth rate, internal resistance, maximum power generation, and substrate utilization. A direct current (DC) external voltage (+2 V, or an

equivalent electrical current of 0.18 mA cm^{-2}) was applied during MFC inoculation, and evaluated for its impact on MFC performance. When MFCs developed mature anodic biofilms after 3-month operation, a series of DC voltages (±0.5, ±1, ±2, and ±3 V) were applied to two of the reactors to evaluate MFC responses.

3.2 Materials and methods

3.2.1 Inoculum types and media

The bacteria present in various sludge/sediments including river sediment (RS), activated sludge (AC), and anaerobic sludge (AN) were used as inoculum sources. The river sediment was obtained from the river bed of Le Sueur River in St. Clair, MN. The activated sludge was obtained from the City of Waseca Wastewater Treatment Plant, and the anaerobic sludge was obtained from a swine manure lagoon at the University of Minnesota Southern Research and Outreach Center in Waseca, MN. The covered lagoon digester was modified from a concrete manure storage tank, with a circular structure, 35 m (115 ft) in internal diameter, and 4.27 m (14 ft) in depth. A dome-shaped cover, made of vinyl coated fabric material of 0.35 mm thick was placed on top of the tank. The collected inocula of sediment and sludge were sieved through a 1 mm mesh to remove sand, gravels, and plant residues, and stored at 4°C in refrigerator prior to use.

Sodium acetate and butyrate were dissolved in distilled water to prepare a medium with 20 mM acetate and butyrate, resulting in a total chemical oxygen demand (COD) of 4200 mg L^{-1} for the initial medium. A 50 mmol L^{-1} phosphate buffer solution (PBS; 18 mmol L^{-1} of monosodium phosphate and 32 mmol L^{-1} of disodium phosphate) was

added to the substrate solution. Other nutrients were also supplemented to enhance bacterial growth (g L^{-1}): 0.31 NH_4Cl, 0.13 KCl, and mineral and vitamin solutions as reported elsewhere [133].

3.2.2 Microbial fuel cell construction and operation

Single-chamber air-cathode MFC reactors (Figure 3-1), with a total volume of 150 mL, were fabricated from clear/extruded acrylic tubes (5 cm in internal diameter and 7.6 cm in length), covered with 0.25 cm thick acrylic endplates at the anode side. The anode was made using plain carbon cloth, and the air-cathode was made of 0.5 mg cm^{-2} Pt-containing (10% in carbon black) carbon cloth treated with Nafion (sulfonated tetrafluoroethylene based fluoropolymer-copolymer, allowing for cation transport). Polytetrafluoroethylene (PTFE) was applied as a gas diffusion backing layer at the air-facing side of cathode [66]. The surface area per reactor volume was 13 m^2 m^{-3} for both electrodes. A 2.2 kΩ resistor was connected in the circuit as an external load.

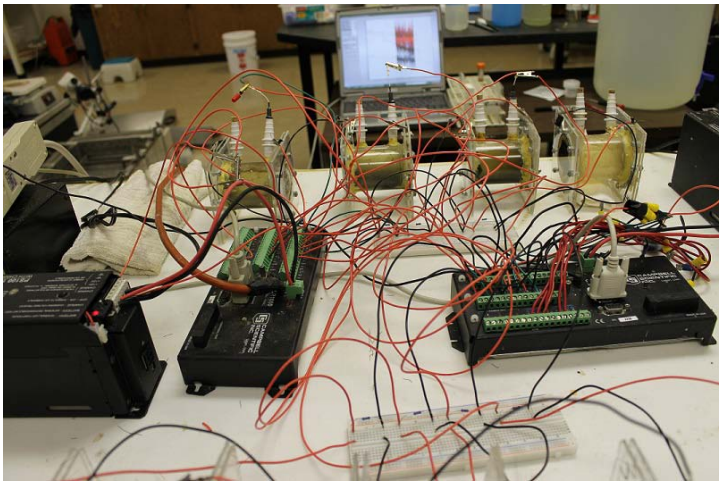

Figure 3-1. Photos of MFC reactors used in the study.

River sediment, activated sludge, and anaerobic sludge were separately used as inocula in reactors with a sludge volume of 10% of the total reactor. MFCs with different inocula were treated with or without current stimulation during the startup period. Reactors were first filled with a mixed solution of the inoculum and medium, and then air-tightly sealed to maintain anaerobic condition at the anode end. They were kept undisturbed to avoid perturbation on anodic microbial attachment and growth. Direct current stimulation was applied to the reactors: an external voltage of +2 V (an equivalent current of 0.18 mA cm^{-2}; resulting an anodic potential of about 1500 mV and cathodic potential of about -500 mV *vs.* SHE) was intermittently applied for 1 h in every 8 h for 3 d. The plus sign indicates that the positive terminal of the power supply was connected to the anodes. The experiment was carried out with two replicates for 12 MFC reactors.

When MFCs were operated for 3 months, they were further tested for performance responses to electrical stimulation by a series of direct voltages (±0.5, ±1, ±2, and ±3 V). Each one of these voltage stimulations was applied for 1 h. Polarization curves and electrode potentials were obtained when MFCs recovered from the stimulation, usually 12 h after removal of the voltages.

3.2.3 Data acquisition system

The voltage (V_{ext}) evolution across resistors was measured by voltage probes and recorded by a CR 1000 data logger (Campbell Scientific, Inc., Logan, UT). The anodic and cathodic potentials were monitored against standard Ag/AgCl electrodes (MF-2072, BASi, Inc., West Lafayette, IN). The data logger supporting software, LoggerNet

Version 3.4, was installed in a personal computer and used to monitor and collect the electrode potential and voltage data.

3.2.4 Liquid analysis

The volatile suspended solids (VSS) of inocula were determined based on the procedures in AHPA Standard Methods [134]. The reason for choosing VSS of the samples as an indicator was that it approximately represented the amount of living biomass which may potentially contribute to inoculation. Well-mixed samples (5 mL) were filtered through a pre-weighed GF/C fiberglass filter (Fisherbrand G4, Fisher Scientific, Pittsburgh, PA) and oven dried to a constant weight at 105 °C. The dried filter was ignited at 550 °C in a muffle furnace for 40 min for VSS determination. The chemical oxygen demand (COD) and volatile acids of liquid samples were analyzed using a spectrophotometer (Hach DR 2800, Hach Company, Loveland, CO), pH a pHTestr10 pH meter (Oakton Instruments, Vernon Hills, IL), and conductivity an HI 8700 conductivity meter (Hannah Instruments, Woonsocket, RI).

Calibration curve for VSS determination in synthetic medium was developed based on OD600 readings from spectrophotometer. For each test, about 5 mL of well mixed liquid sample was obtained from effluent, and tested in Hach DR 2800 for OD600 after selecting the wavelength of 600 nm. Distilled water was used as a blank to zero the reading. Liquid samples with known VSS concentrations were used for calibration, and the calibration curve and equation were shown in Figure 3-2.

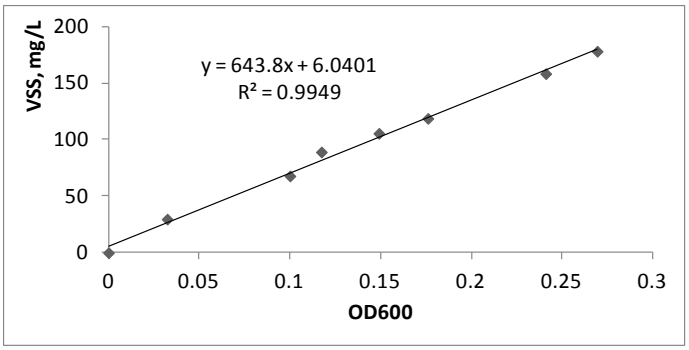

Figure 3-2. Calibration curve for VSS determination by OD600.

3.2.5 Gas chromatography

The volatile fatty acid profile, e.g., acetate and butyrate concentrations, was quantified using a gas chromatograph (GC; CP-3800, Varian Inc., Palo Alto, CA) equipped with a flame ionization detector. A fused-silica capillary column (HP-FFAP, 30 m×0.25 mm×0.25 μm) was used. The injector and detector temperatures were set at 220°C and 250°C, respectively. The temperature in the oven was kept at 60°C for 2 min, ascended to 140°C at 8°C min^{-1}, and then kept constant at 140°C for another 6 min. Helium with a flow rate of 25 mL min^{-1} was used as the carrier gas.

Chemical equilibriums for gas chromatography

The degree of dissociation of volatile fatty acids (VFAs) depends on pH conditions of the effluent. For example, when the effluent pH is higher than the acidity dissociation constant (p*Ka*) of a volatile fatty acid by 1 pH unit, 93% of the total fatty acid exists in the form of anions which are not ready to vaporize even when temperature increases. As in most cases pH values of effluents of bioelectrochemical reactors are around neutral or higher, an acidification of effluent is necessary before using GC to determine the

concentrations of fatty acid anions, e.g., acetate and butyrate. Addition of formic acid can accomplish this work. Modeling the chemical equilibrium using software Mineql+ can approximately estimate how much formic acid should be added. The following paragraphs explain the procedures to use the software for modeling the complex chemical system. A general conclusion of the modeling is that 0.5 M of formic acid addition is sufficient to shift 97% anions to their acids in all the three cases. To guarantee a sufficient acidification a final formic concentration at least of 1.0 M is recommended as some of it may be evaporated in GC injector and column at a temperature higher than 100 ℃. Another study [135] used 1.5 M of formic acid addition. The effect of temperature on the formic acid addition is beyond the scope of this study. In the modeling, the p*Ka* values of some of VFAs are as follows:

Formic	⟷	H^+ + Formate	p*Ka* = 3.745	(3-1)
Acetic	⟷	H^+ + Acetate	p*Ka* = 4.757	(3-2)
Butyric	⟷	H^+ + Butyrate	p*Ka* = 4.830	(3-3)
iso-Butyric	⟷	H^+ + *iso*-Butyrate	p*Ka* = 4.880	(3-4)

Case 1*: 20 mM of NaAc and 20 mM of NaBtyr, titrated by formic acid*

Choose the cations and anions present in an effluent, and do a thermo-scan to obtain the p*Ka* and *Delta H* values. Insert one when there is no term by default in the software by choosing the components, e.g., choosing H and Butanot for inserting HButanot, and edit the p*Ka* value under the column Log K (Figure 3-3).

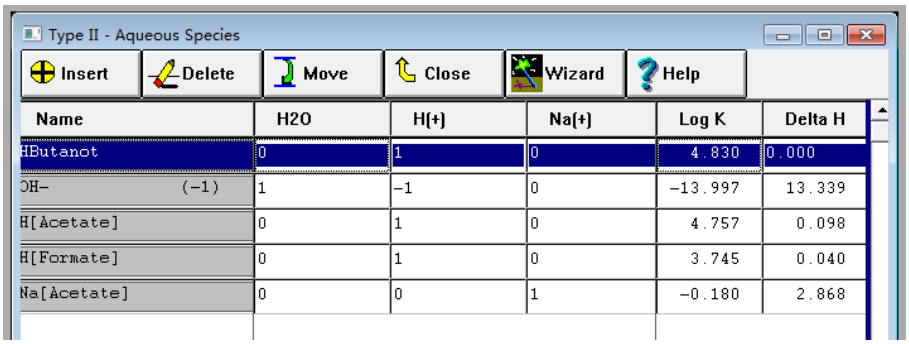

Figure 3-3. Result after "thermo-scan" of the existing ions.

Under Wizard, fill in the following information for Totals and pH. Since a titration will be done by increasing formic acid, the pH value should be calculated by Mineql+ based on electroneutrality (equivalent to charge balance), shown in Figure 3-4. Click "Close" and set MultiRun parameters as in Figure 3-5. Then click "Run" to calculate results.

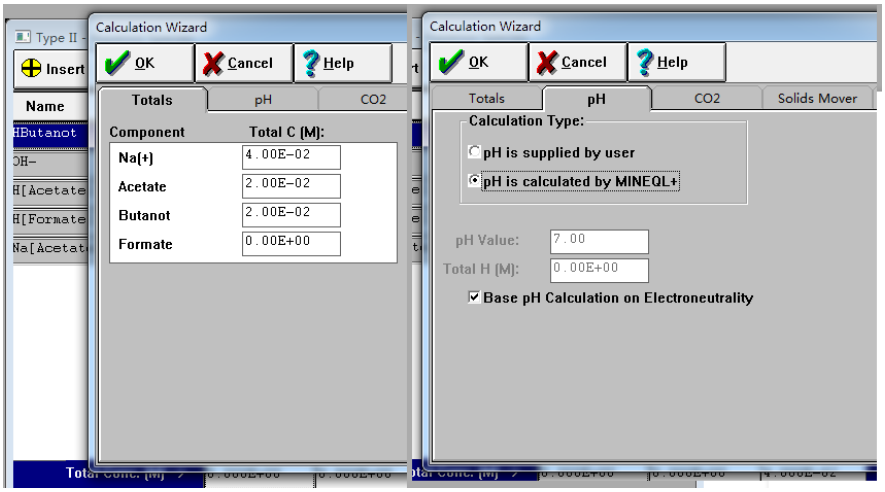

Figure 3-4. Input Totals and pH.

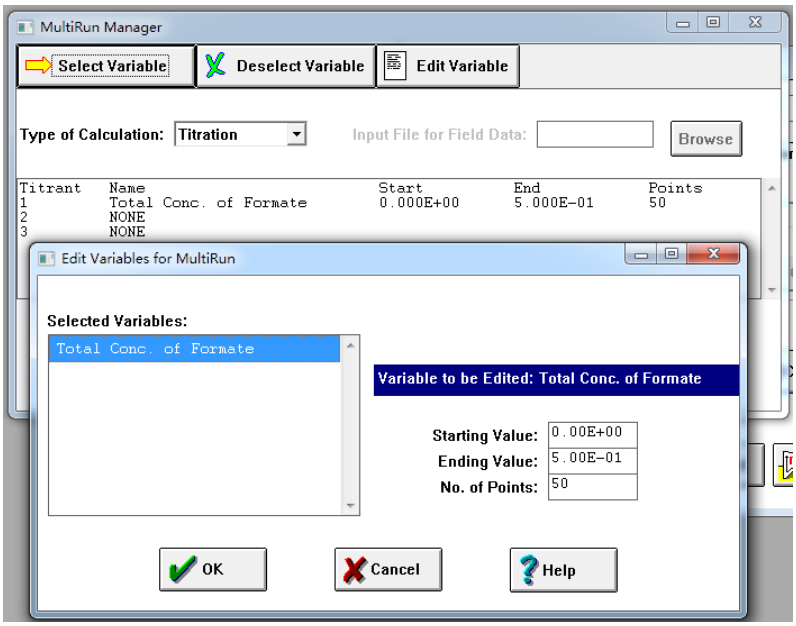

Figure 3-5. Parameter setting for formic acid titration.

The titration result can be obtained by clicking “Graph IT” icon. As it can be seen from Figure 3-6, addition of formic acid is effective to shift the dissociation to the other side, forming corresponding acids. The concentration profiles of each component at 0.2 M of the total formate can be obtained by obtaining a special report of a summary of all species (at Run 21), attached in Figure 3-7. For both acetate and butyrate, 0.0196 mM of the corresponding acids are present, which is 98% of the total fatty acid cations. Further addition only increases the acids by a little amount. For example, at Run 31 (0.3 M of total formic anion), the acetic is increased to 0.0197 mM and butyric to 0.0198 mM. Similarly, modeling of titration using other acids can also be obtained; but formic acid is one of the most suitable, as the common inorganic acids (e.g., HCl, H_2SO_4, HNO_3, and H_3PO_4) will bring about damages to capillary GC column due to their accumulation in the front part of a column to impair the stationary phase.

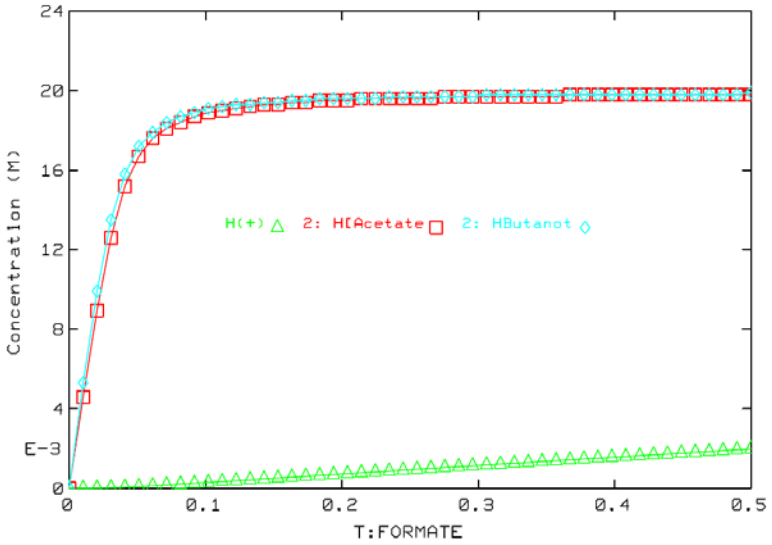

Figure 3-6. Titration result.

MINEQL+ Ver 4.61 Page 1
Data Extracted from : 20AcBt.mdo
SINGLE RUN SUMMARY

This report compiles the output data (concentration, Log C, Log K) for all species within a single run.

MINEQL+ Ver 4.61 Page 2
Data Extracted from : 20AcBt.mdo
Run: 23

ID	Species		Conc.	Log C	Log K
Type I - COMPONENTS					
2	H2O		1.000E+00	0.000	0.000
3	H(+)		8.280E-04	-3.082	0.000
45	Na(+)		4.000E-02	-1.398	0.000
86	Acetate		4.130E-04	-3.384	0.000
87	Butanot		3.510E-04	-3.455	0.000
95	Formate		4.010E-02	-1.397	0.000
Type II - COMPLEXES					
500004	HButanot		1.960E-02	-1.707	4.830
3800	OH-	(-1)	1.220E-11	-10.915	-14.000
45900	H[Acetate]		1.960E-02	-1.708	4.760
47500	H[Formate]		1.840E-01	-0.734	3.750
141200	Na[Acetate]		1.090E-05	-4.962	-0.180
Type III - FIXED ENTITIES					
3801	H2O (Solution)				0.000
Type VI - SPECIES NOT CONSIDERED					
175310	pH	(+1)	8.280E+03	3.918	7.000
Other Species					
900003	Activity of H+		8.280E-04	-3.082	0.000

Figure 3-7. A summary of species at Run 21 in formic titration.

***Case 2**: 60 mM of NaAc and 60 mM of NaBtyr, titrated by formic acid*

By clicking "Aqueous Complexes" under Menu -> Model -> Tableau, the content of NaAc and NaBtyr can be reset to 60 mM under Wizard. An output at 0.5 M formic addition is obtained in Figure 3-8.

MINEQL+ Ver 4.61 Page 1
Data Extracted from : 60AcBt.mdo
SINGLE RUN SUMMARY

This report compiles the output data (concentration, Log C, Log K) for all species within a single run.

MINEQL+ Ver 4.61 Page 2
Data Extracted from : 60AcBt.mdo
Run: 51

ID	Species		Conc.	Log C	Log K
Type I - COMPONENTS					
2	H2O		1.000E+00	0.000	0.000
3	H(+)		5.870E-04	-3.231	0.000
45	Na(+)		1.200E-01	-0.921	0.000
86	Acetate		1.730E-03	-2.761	0.000
87	Butanot		1.470E-03	-2.831	0.000
95	Formate		1.170E-01	-0.931	0.000
Type II - COMPLEXES					
500004	HButanot		5.850E-02	-1.233	4.830
3800	OH-	(-1)	1.710E-11	-10.766	-14.000
45900	H[Acetate]		5.810E-02	-1.236	4.760
47500	H[Formate]		3.830E-01	-0.417	3.750
141200	Na[Acetate]		1.370E-04	-3.863	-0.180
Type III - FIXED ENTITIES					
3801	H2O (Solution)				0.000
Type VI - SPECIES NOT CONSIDERED					
175310	pH	(+1)	5.870E+03	3.769	7.000
Other Species					
900003	Activity of H+		5.870E-04	-3.231	0.000

Figure 3-8. A summary of species at Run 51 in formic titration for 60 mM NaAc and NaBtyr.

***Case 3**: 20 mM of NaAc and 20 mM of NaBtyr, with phosphate buffer solution (18 mM NaH_2PO_4 and 32 mM Na_2HPO_4) titrated by formic acid*

By clicking "Select Components" under Model, PO_4^{3-} is added to the system. An output

at 0.5 M formic addition is obtained in Figure 3-9.

MINEQL+ Ver 4.61 Page 1
Data Extracted from : 20AcBt50PBS.mdo
SINGLE RUN SUMMARY

This report compiles the output data (concentration, Log C, Log K) for all species within a single run.

MINEQL+ Ver 4.61 Page 2
Data Extracted from : 20AcBt50PBS.mdo
Run: 51

ID	Species		Conc.	Log C	Log K
Type I - COMPONENTS					
2	H2O		1.000E+00	0.000	0.000
3	H(+)		9.690E-04	-3.014	0.000
45	Na(+)		1.220E-01	-0.914	0.000
54	PO4(3-)		1.250E-15	-14.902	0.000
86	Acetate		3.540E-04	-3.451	0.000
87	Butanot		3.010E-04	-3.522	0.000
95	Formate		7.830E-02	-1.106	0.000
Type II - COMPLEXES					
500005	HButanot		1.970E-02	-1.706	4.830
3800	OH-	(-1)	1.040E-11	-10.983	-14.000
38704	NaHPO4-	(-1)	4.120E-06	-5.385	13.450
41000	H2PO4-	(-1)	4.400E-02	-1.357	19.570
41100	HPO4-2	(-2)	2.880E-06	-5.541	12.380
41200	H3PO4		6.000E-03	-2.222	21.720
45900	H[Acetate]		1.960E-02	-1.707	4.760
47500	H[Formate]		4.220E-01	-0.375	3.750
141200	Na[Acetate]		2.850E-05	-4.545	-0.180
Type III - FIXED ENTITIES					
3801	H2O (Solution)				0.000
Type VI - SPECIES NOT CONSIDERED					
175310	pH	(+1)	9.690E+03	3.986	7.000
Other Species					
900003	Activity of H+		9.690E-04	-3.014	0.000

Figure 3-9. A summary of species at Run 51 in formic titration for 20 mM NaAc and NaBtyr, and 50 mM PBS.

Calibration for gas chromatography

The regression problem was to obtain a model for predicting the volatile fatty acid concentration by peak area of gas chromatography. Simple linear regression via ordinary least squares (OLS) estimation was applied to establish this kind of calibration model through the use of a regression software *Arc*. The procedure for a model of acetic acid

concentration was used as an example.

Residual sum of squares function is defined as RSS $(h_0, h_1) = \sum_{i=1}^{n} (y_i - (\hat{h}_0 + \hat{h}_1 * x_i))^2$. Based on definition of RSS, OLS method minimizes RSS (h_0, h_1) by choosing appropriate (h_0, h_1), and the resulted (h_0, h_1) is estimation of coefficients $(\hat{\eta}_0, \hat{\eta}_1)$. When these two parameters are estimated, both the predictor (applied in this study) and estimator (of mean function) at a given x value can be calculated from $\hat{\eta}_0 + \hat{\eta}_1 * x_i$to be the same value; however, variances of these two estimations are different as that of the former is larger than the latter. Meanwhile, an R^2, coefficient of determination, is obtained to represent the proportion of the total sample variability that can be explained by linear relationship between the regressor and predictor. In this case of a simple linear regression, R^2 is also equivalent to the square of the correlation coefficient $(\hat{\rho}(x, y) = \frac{\widehat{Cov}(x,y)}{\widehat{sd}(x)\widehat{sd}(y)})$.

Before carrying out a regression analysis, it is helpful to evaluate data condition [136], e.g., to examine if there is an influential point by Cook's distance $(D_i = \frac{1}{k\,\widehat{sd}^2}\sum_{j=1}^{n}(\hat{y}_{(i),j} - \hat{y}_j)^2$; if $D_i > 0.5$, it is valuable to look into the case), and to examine potential outliers by the method of checking every case. For the case of calibrating acetic acid concentration against peak area, there is no influential point or outlier indicated, as shown in Figure 3-10.

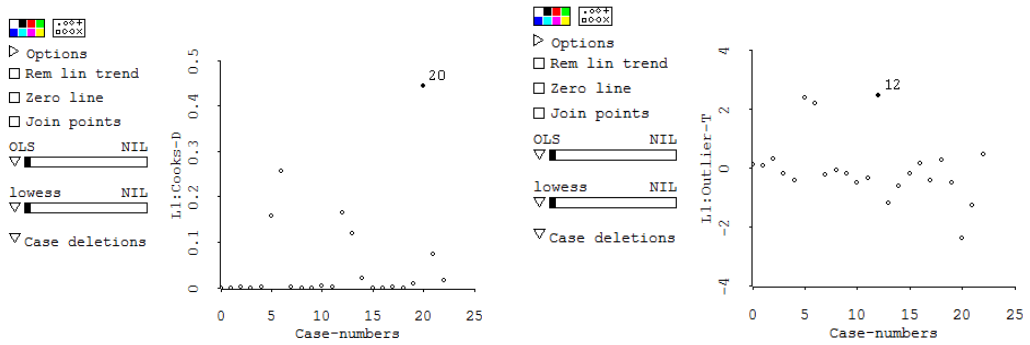

Figure 3-10. Cook's distances (left-hand side) and outlier-T values (right-hand side) of every case. The outlier p-value for case 12 is 0.57 which is larger than 0.05, thus not significant.

The linear model is thus y=0.03254x-0.1711 according to the result of OLS regression displayed in Figure 3-11. The R^2 of 0.9902 indicates that 99.02% of the total variability can be explained by the linear relationship between acetic acid concentration and peak area. Similar, a calibration model was obtained for butyric acid against peak area after removing three cases of outliers (points 5, 6 and 13), generating a model of y=0.01120x-0.1703 with R^2 of 0.9954. For higher concentration data set, acetic acid has y=0.03308x-0.0637 with R^2 of 0.9927; butyric acid has y=0.01115x+1.4785 with R^2 of 0.9886.

```
Data set = GCCalibforLow, Name of Fit = L1
Normal Regression
Kernel mean function = Identity
Response      = Concentration
Terms         = (AcetPeakArea)
Coefficient Estimates
Label          Estimate        Std. Error    t-value    p-value
Constant      -0.171084        0.326099       -0.525     0.6053
AcetPeakArea   0.0325362       0.000703707    46.235     0.0000

R Squared:               0.990272
Sigma hat:               0.941273
Number of cases:              23
Degrees of freedom:           21

Summary Analysis of Variance Table
Source         df       SS            MS           F    p-value
Regression      1     1894.         1894.     2137.71    0.0000
Residual       21   18.6059      0.885996
Plot: [Plot1]GCCalibforLow:V:L1:Outlier-T H:Case-numbers
Plot: [Plot2]GCCalibforLow:V:Concentration H:AcetPeakArea

Data set = GCCalibforLow, Summary Statistics
Variable       N Average     Std Dev     Minimum      Median     Maximum
AcetPeakArea  23  370.07      285.18         1.8       326.3       830.5
Concentration 23   11.87       9.324           0         10.         25.

Data set = GCCalibforLow, Sample Correlations
AcetPeakArea   1.0000  0.9951
Concentration  0.9951  1.0000
              AcetPea Concent
```

Figure 3-11. OLS calibration results for acetic acid concentration against peak area.

Calibration curves

In summary, a final concentration of 1.0 M formic acid addition is recommended to acidify effluents of bioelectrochemical reactors. The corresponding calibration curves for low or high concentrations of acetic acid and butyric acid (y in mM, x in μV*Min) are listed as follows:

Equal or lower than 20 mM:

Acetic:	y=0.03254x-0.1711	$R^2 = 0.9902$	(3-5)
Butyric:	y=0.01120x-0.1703	$R^2 = 0.9954$	(3-6)

Higher than 20 mM:

Acetic: $y= 0.03308x-0.0637$ $R^2 = 0.9927$ (3-7)
Butyric: $y=0.01115x+1.4785$ $R^2 = 0.9886$ (3-8)

3.2.6 Scanning electron microscope

After 1 month operation, anodic carbon cloth of 2 mm by 2 mm was cut from the anodes for scanning electron microscope (SEM) evaluation using Hitachi variable pressure SEM (S3500N, Hitachi, Japan). The samples were fixed for about 12 h at 4°C in a solution containing 2.5% paraformaldehyde and 1.5% glutaraldehyde buffered in 0.1 mol L^{-1} cocadylate. The samples were then gently washed three times (15 min for each wash) with 0.1 mol L^{-1} cocadylate buffer, followed by dehydration for 30 min for each step in a series of ethanol/water solutions of increasing concentrations (25%, 50%, 70%, 85%, 95%, 100%, and 100%, v/v). The dehydrated samples were mounted and dried in a critical point carbon dioxide dryer, and sputter coated with gold for SEM observation. The accelerating voltage was set at 5 to 10 kV at high vacuum and the magnification varied between ×70 and ×12k.

3.2.7 Cyclic voltammetry

MFC cathodes, cut into 2 cm by 2 cm piece, were characterized by cyclic voltammetry (CV) using CHI 760C electrochemical workstation (CH Instruments, Inc., Austin, TX). CV was started from -0.4 to +0.8 V *vs.* Ag/AgCl at a scan rate of 20 mV s^{-1}, and went back to -0.4 V *vs.* Ag/AgCl. During the test, the three electrodes (counter, reference, and working electrodes) were placed in 40 mmol L^{-1} acetate medium buffered with 50 mmol L^{-1} PBS.

3.2.8 Calculation

Lag phase period

The lag phase period (in d) was the elapsed time during which the external voltage (V_{ext}) did not show an apparent increase, and was determined by examining the first derivative of V_{ext} against time: the lag phase was terminated when the first derivative of V_{ext} was continuously greater than 0. After this period, V_{ext} started to increase following a sigmoid shape.

Polarization curves and transient analysis

When MFCs were operated for at least 2 months, the polarization curves of the MFC reactors were obtained by stepwise varying R_{ext} from 20 kΩ to 560 Ω. The voltage across the resistor was measured when a stable reading was available after about 15 to 30 min or longer. The rationale for this method is that the voltage output (V_{ext}) and the current ($I = \frac{V_{ext}}{R_{ext}}$) follow a linear relationship in the region of Ohmic loss [88]:

$$V_{ext} = V_b - IR_{int} \quad (3\text{-}9)$$

where V_b is the extrapolated intercept of voltage output. The slope of the fitted line is the internal resistance, and the expression for the maximum power output can be deduced as follows [35]:

$$P_{max} = {V_b}^2/(4\,R_{int}) \quad (3\text{-}10)$$

Another method was implemented in this study for measuring internal resistance and

MFC capacitance in the region where the charge transfer loss, or activation overpotential, was the dominant resistance [137]. This method modeled the current profile at 1 s intervals when the external resistance was abruptly changed from 20.75 kΩ to 33 kΩ.

3.2.9 Statistical analysis

ANOVA and post hoc tests (*LSD*) were used for multiple comparisons all at a significance level of $\alpha = 0.05$.

3.3 Results and discussion

3.3.1 Microbial fuel cell enrichment

The 12 MFC reactors were inoculated with three different inocula (RS, river sediment; AC, activated sludge; and AN, anaerobic sludge) with or without an electrical current stimulation (0 mA or 0.18 mA/cm^2). The VSS and TSS properties of the inocula were shown in Table 3-1. Acetate and butyrate, each with an initial concentration of 20 mmol L^{-1}, were chosen as organic substrate in media, mainly because of their wide availability as fermentation byproducts and degradable substrates for exoelectrogenic bacteria. The RS-MFC showed a significant different lag phase period from those of the other two MFCs (AC- and AN-MFCs; $p < 0.05$). As the organic substrates and nutrients in the media for all reactors were initially the same, this delay could be attributed to the low availability of bacteria in the river sediment. The VSS analysis (Table 3-1) confirmed that RS contained VSS of only 3.2 g L^{-1}, which was much lower than those of AC and AN (22.4 and 12.1 g L^{-1}, respectively), and the VSS had a strong negative Pearson

correlation with the lag phase periods (r = -0.86). Another reason for the rapid enrichment of AN sludge can be the similar anaerobic environment between the MFC anodes and the anaerobic digester, and the similar volatile fatty acid concentrations in the MFC media and in swine manure influent which was the medium for the anaerobic digester where the sludge was obtained. Furthermore, RS had a much higher TSS (e.g., fine soil particles), which meant that RS also absorbed comparably more bacteria on soil particle surface and made more gradual bacteria desorption to medium [123].

Table 3-1. Sludge characteristics and MFC lag phase periods

Inocula	**VSS** $\mathbf{g\ L^{-1}}$	**TSS** $\mathbf{g\ L^{-1}}$	**λ** **d**
River sediment	3.2	30.2	6.2
Activated sludge	22.4	30.3	3.8
Anaerobic sludge	12.1	20.1	4.0

For all the inoculum sources, the electrical current stimulation markedly impaired the MFC startup, evidenced by the fact that voltage output did not increase until the removal of the current stimulation and the prolonged lag phase periods. Although the applied voltage poised a positive anodic potential (about 1500 mV *vs.* SHE) which might help bacterial growth (but when its value was low, e.g., +400 mV *vs.* SHE [38]), it also generated a current density of 0.18 mA cm^{-2} which might have a bactericidal effect [138]. The presence of this effect was indicated by the decreased substrate utilization rate in this study, and could be a result of the electrochemical dimerization of intracellular coenzyme A induced by electrode potentials higher than 0.94 V *vs.* SHE [139]. Another possible reason is that the electrolysis in phosphate buffer solution (average conductivity

of 8.7 mS cm^{-1}) that could promote the formation of hydrogen peroxides (H_2O_2) and radicals (·OH and $\cdot O_2$) on electrodes [140]. However, the potassium permanganate ($KMnO_4$) titration of the effluent immediately after 1 h treatment of the +2 V DC did not detect hydrogen peroxide, suggesting the absence of the hydrogen peroxide or a level lower than the detection limit of 20 mg L^{-1}.

3.3.2 Biofilm examination

After the MFC reactors were operated for one month, samples of carbon cloths were cut from anodes and subject to SEM examination. Biofilms, which were considered biological catalysts for acetate or butyrate oxidation, were clearly shown on the surface of all enriched anodes (Figure 3-12), while the anodes before inoculation showed neither bacteria nor extracellular matrix attached to the surface. Bacterial cells of short-rod shape, mostly with a diameter of 0.2 to 0.5 μm and a length of 0.7 to 1.0 μm, were surrounded by filamentous materials and extracellular polymeric substances (EPS, mainly composed of proteins, polysaccharides, and humic substances) packed together. The anode surface, filamentous materials and EPS were the immediate environments of the bacteria in biofilm, and these environments could serve as electron acceptors for anodic respiring bacteria [141].

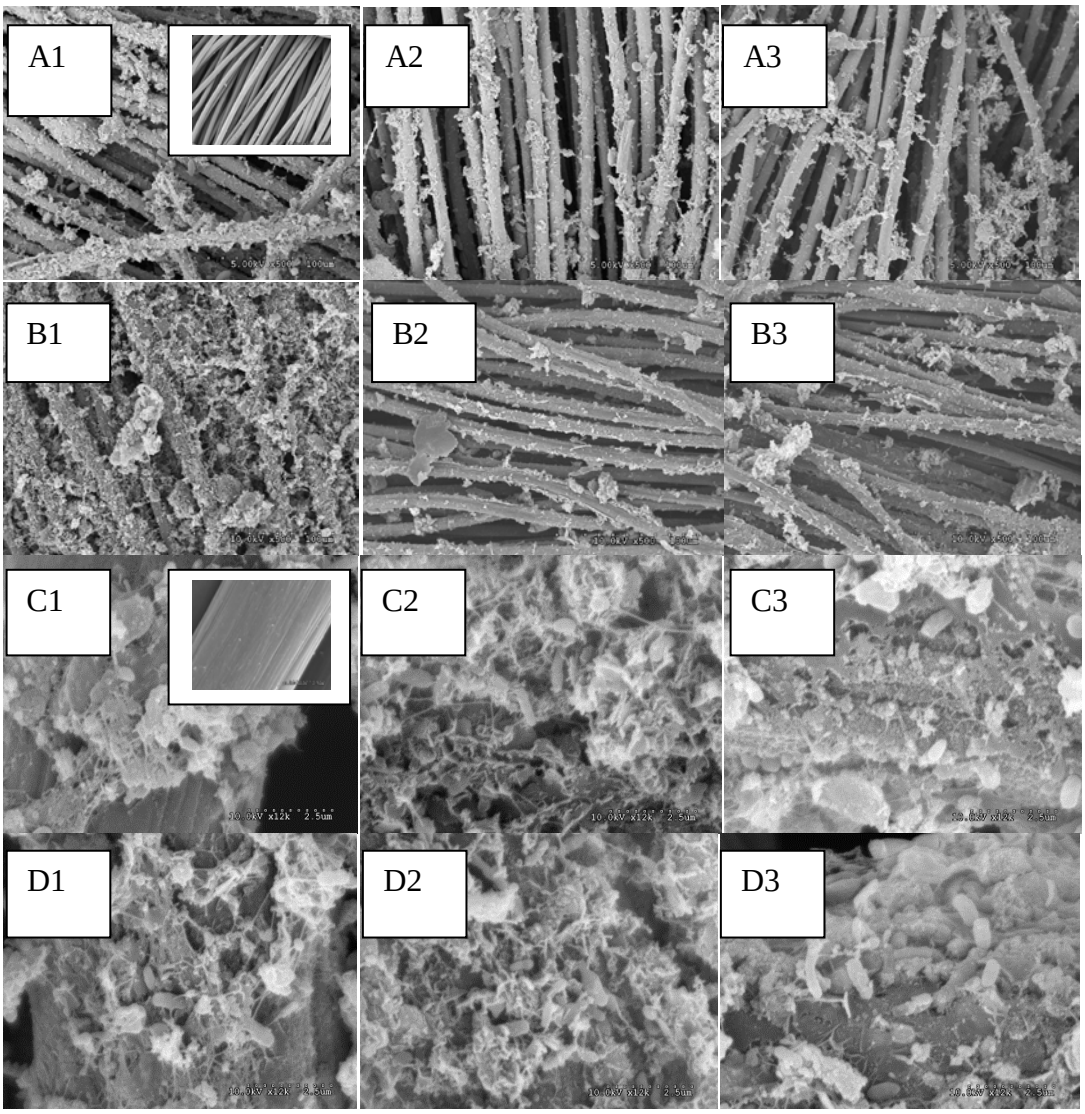

Figure 3-12. SEM images of the MFC anodes. Anodes were enriched with river sediment (denoted as 1), activated sludge (denoted as 2), and anaerobic sludge (denoted as 3) at different electrical current stimulation (A and C represent the ones without stimulation during startup period; B and D with +2 V stimulation). Images A and B were taken at magnification ratio of 500, and C and D at 12k. Insets in A1 and C1 were the un-inoculated anodes inserted for comparison.

The RS-MFC anode surface was almost completely and homogeneously covered by layers of biomass, while the one enriched with AC contained the sparsest biomass. Compared with river sediment, MFC anodes enriched with activated sludge and anaerobic sludge had more large granules attached to them, but were more

heterogeneously covered. This finding was in agreement with a previous study using wetland sediment as an inoculum source, a natural consortium similar to RS here, which resulted in a thicker biofilm than that of other inocula [30]. The better biofilm coverage indicated the increased amount of bio-catalyst (quantified by the attached biomass concentration *w*) and enhanced the anodic exchange current density ($j_{oAU}w$). So the increased exchange current density then reduced the activation overpotential ($\eta_{act,A}$, accounting partly to the MFC internal resistance) on anode according to the Butler-Volmer equation [120]:

$$I = j_{oAU} w A e^{\frac{\alpha_A F \eta_{act,A}}{RT}} \quad (3\text{-}11)$$

where I is the electric current, j_{oAU} is the unit exchange current density of exoelectrogenic biomass, *w* is the attached biomass concentration on anode surface, and α_A is the transfer coefficient of the anodic reaction.

Electrical stimulation distributed biomass on carbon fibers in a more homogeneous way, and also increased the amount of biomass attached to carbon wires. Some tubular fungal cells (a diameter of 3 to 5 μm and a length of 7 to 10 μm) were found on anodes without electrical stimulation, while none was observed on electrically stimulated anodes. Another marked effect of current stimulation on anodes was that a layer of structure on AC and AN anodes was partially segmented and peeled off from the carbon fibers.

3.3.3 Electrochemical characteristics of MFCs with different treatments

Internal resistance is a rough indicator of the magnitude of electrical energy consumed

by MFC itself, and was linearly fitted from polarization curves (Figure 3-13). In this study, MFC reactors steadily ran for at least 2 months after inoculation before polarization curves were obtained. The current was altered by consecutively decreasing external resistors until the linear relationship between V_{ext} and I no longer held. The range of internal resistances was between 181 and 349 Ω (Table 3-2), and all of these values were markedly lower than the resistances measured immediately after inocula were added: 130 kΩ, 55 kΩ, and 11 kΩ for RS-, AC-, and AN-MFC, respectively. The extrapolated voltage V_b was an estimation of the maximum electron motive force, ranging from 282 to 447 mV. The maximum power output was then calculated from this internal resistance and the maximum voltage output according to the Equation (3-10), which agreed well with the observed data in this study, ranging from 88 to 195 μW (or from 44 to 98 mW m^{-2} when normalized to the anode surface area). These current densities were generally lower than the values reported in other air-cathode studies (e.g., 506 mW m^{-2} [142]).

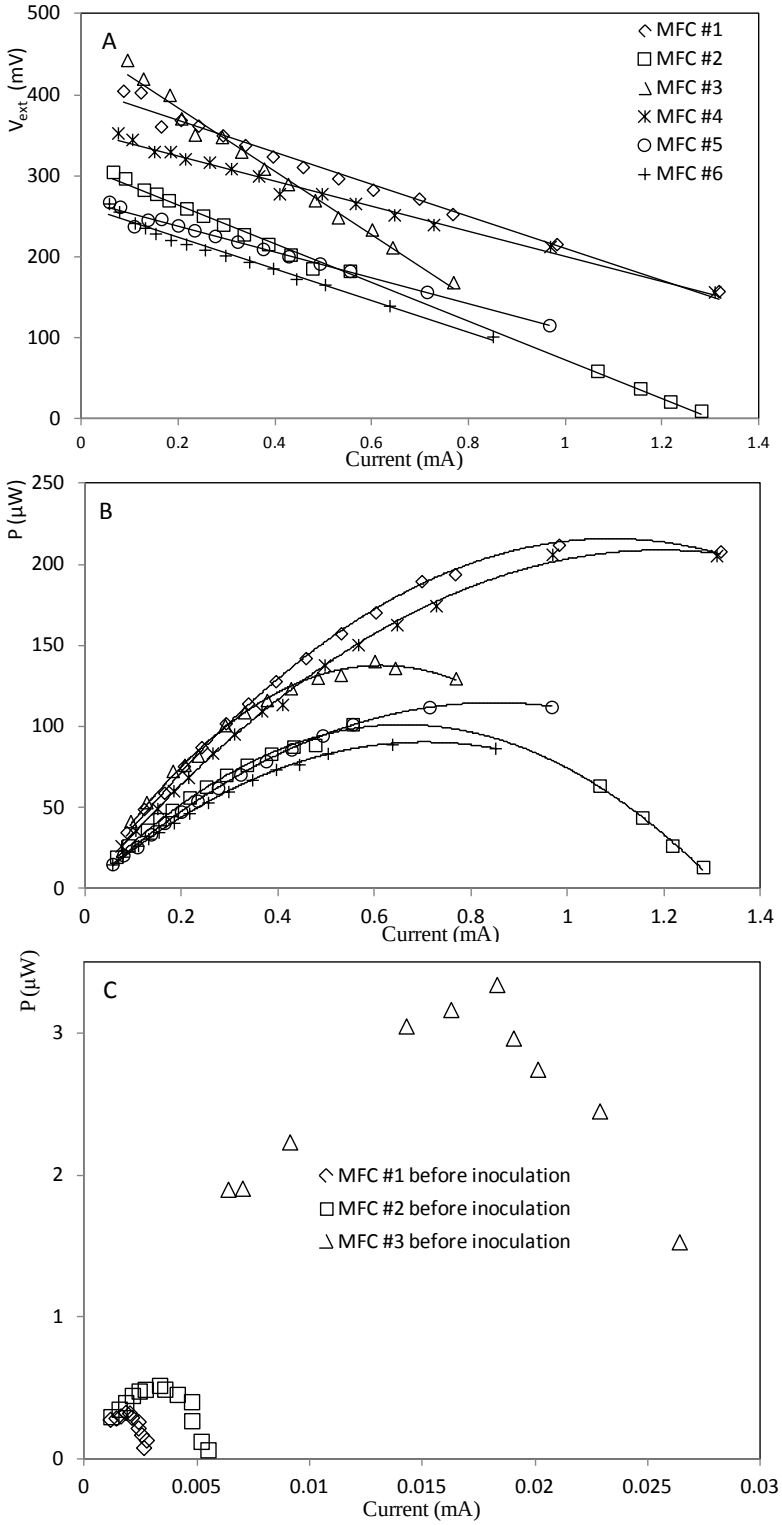

Figure 3-13. Polarization curves of MFC. A, Vext against I; B, P against I; and C, polarization before anodic biofilms were enriched. The reactor numbers indicate different treatment as defined in Table 3-1.

Table 3-2. Electrochemical characteristics (mean ± sd) of MFCs under different treatment during inoculation

Parameters		MFC #1 RS 0	MFC #2 RS +2 V	MFC #3 AC 0	MFC #4 AC +2 V	MFC #5 AN 0	MFC #6 AN +2 V
Internal resistance, R_{int}	Ω	212 ± 20.5	181 ± 36.8	263 ± 33.9	204 ± 62.9	349 ± 62.9	226 ± 42.4
Extrapolated voltage, V_b	mV	405 ± 4.2	366 ± 13.4	339 ± 38.2	309 ± 54.4	447 ± 21.2	282 ± 26.9
Maximum power, P_{max}	μW	195 ± 22.6	187 ± 24.0	110 ± 10.6	118 ± 4.2	145 ± 12.0	88 ± 0.0
Charge transfer resistance, R_{ct}	Ω	754 ± 292	667 ± 220	811 ± 277	1082 ± 812	1235 ± 967	812 ± 322
Capacitance, C	mF	10.2 ± 1.1	57.3 ± 3.9	13.2 ± 11.0	67.9 ± 20.0	9.7 ± 11.7	38.1 ± 22.8

The results of multiple comparisons indicated that RS-MFC had a significantly smaller internal resistance than AN-MFC (196 and 287 Ω, respectively), and that the current stimulation significantly reduced internal resistance ($p < 0.05$; Table 3-3). For example, the internal resistance of AN-MFC was reduced from 349 to 226 Ω after the current stimulation, which was a 35% reduction. These results well agreed with the SEM observation which showed better biofilm coverage on RS anodes and enhanced biofilm coverage on electrical stimulated anodes, as more active bacteria promoted bio-catalytic effect and reduced internal resistance. Therefore, although a DC stimulation may impair MFC inoculation [39], the DC stimulation employed here demonstrated an improvement in MFC electrochemical characteristics. As to the extrapolated voltage V_b, the current stimulation significantly reduced V_b, and the great change happened again on AN-MFC from 447 to 282 mV, which was an 82% reduction. Meanwhile, RS-MFC had a significantly larger V_b than AC-MFC (385 and 324 mV, respectively; $p < 0.05$). As to the power output (P_{max}), RS-MFC significantly ($p < 0.05$) outperformed AC- and AN-MFC by 77 and 75 μW, respectively, denoting that RS-MFC was the best option as a power source. Again, this result was in accordance with the SEM observation of RS anodes. Current stimulation did not change much the power output of RS- and AC-MFC;

however, the power output of AN-MFC reactors was substantially reduced from 145 to 88 μW. And the possible reason was the oxygen gas formed at the anode side as fine gas bubbles were observed during electrical stimulation, which inhibited anaerobic bacterial growth on anode surface and activity.

Table 3-3. ANOVA results (p-values) for MFC electrochemical performance at different treatments

Parameters	***p* values**		
	Inoculum	**Electrical stimulation**	**Interactive term**
Internal resistance, R_{int}	0.080	**0.037**	0.407
Extrapolated voltage, V_b	0.077	**0.005**	**0.039**
Maximum power, P_{max}	**0.001**	0.076	0.052
Charge transfer resistance, R_{ct}	0.728	0.814	0.701
Capacitance, C	0.317	**0.002**	0.449

The charge transfer resistance (R_{ct}) is used to characterize the resistance when the external resistor is large or the current is small, or equivalently, when the activation overpotential is the dominant component of internal resistance [137]. The above-mentioned transient response analysis technique in Section 2.7 provides a way for evaluating both the charge transfer resistance and capacitance (Table 3-3). There was no significant difference found for either inoculum type or current stimulation due to larger standard deviations, but R_{ct} was increased by current stimulation in AC-MFC from 811 to 1082 Ω, and declined for the other two types of inocula. The values of R_{ct} were larger than those of the internal resistances obtained by polarization curves of the corresponding MFC reactors, indicating the domination of activation overpotential in this tested current range.

Capacitance (C) quantifies the capability of MFC to store charges when it is

disconnected from an external load, or when it is between intermittent discharging processes in real applications. MFC capacitance may be derived from the anode, cathode, and biofilm that naturally have double-layers to store charges. It was reported that electrode capacitance was increased by inoculation from 2.2 to 4.2 mF [143], and the capacitance was raised by the abundance of *c*-type cytochromes imbedded in biofilms [144]. ANOVA results suggested that the current stimulation significantly increased MFC capacitance in all three inoculum types, from 11 mF to 54 mF on average. This improvement can be a result of the enhancement of the biofilms under current stimulation as observed by SEM, which consequently improves the double-layer structure of the biofilms but without direct proof observed. A larger biofilm capacitance can be beneficial because it improves simultaneous energy production and storage in MFC [145]. Please note that AC-MFC has obtained the greatest increase in capacitance among the three, which is in accordance with the fact that the maximum power output of AC-MFC was improved by current stimulation. Both phenomena revealed the resilience of the AC biofilm toward the current stimulation.

3.3.4 Effect of electrical stimulation on mature MFCs

When MFCs were operated for 3 months, a series of electrical voltages (±0.5, ±1, ±2, and ±3 V) were applied to an RS-MFC (positive voltages) and AC-MFC (negative voltages) in order to further evaluate responses of MFC biofilms to this type of stimulation. The AN-MFC was not chosen to test because the anaerobic bacteria were found more vulnerable to electrical stimulation (Section 3.3). Table 3-4 records the MFC electrode potentials when the reactors were subject to the DC voltage stimulation. Figure

3-14 shows that the positive voltages severely impaired the maximum power output (by 49% after +3 V stimulation), while the negative voltages substantially improved the power output (by 37% for -3 V stimulation). Within the tested range, the reduction or increase in maximum power output was proportional to the intensity of the stimulation. Both anodic and cathodic potentials of RS-MFC after positive voltage stimulation were reduced: one became less negative positive, and the other less positive, respectively (Figure 3-14C). To the contrary, the negative voltage stimulated AC-MFC had an increasingly negative anodic potential and an increasingly positive cathodic potential (Figure 3-14D). This improvement on power output by negative voltage application was reported for the first time.

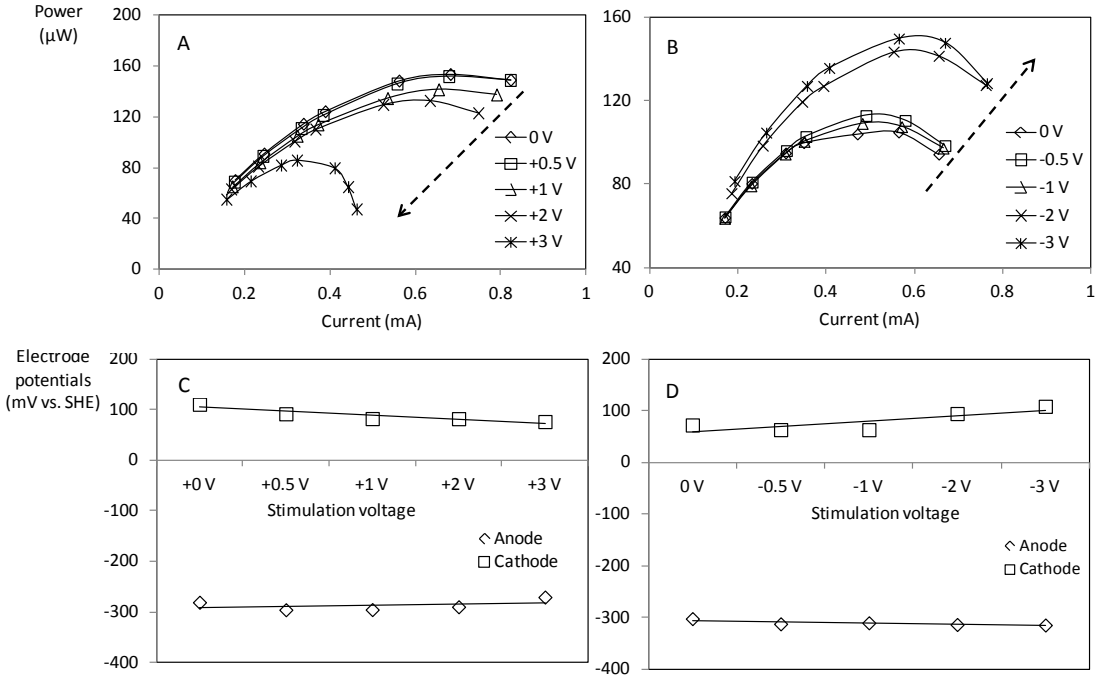

Figure 3-14. Polarization curves (A and B) and electrode potentials (C and D) of two MFCs after electrical stimulation. The dashed arrows indicate the direction of the increasing intensity of the stimulation from 0 to ±3 V. The solid lines in C and D are trend lines for the anodic or cathodic potentials measured at external resistors of 2.2 kΩ.

Table 3-4. Electrode potentials of MFCs under different DC treatments

		Treatment	**0 V**	**+0.5 V**	**+1 V**	**+2 V**	**+3 V**
MFC #1	Anode	V *vs.* SHE	-0.31	+0.19	+0.21	+0.88	+1.60
	Cathode	V *vs.* SHE	+0.08	-0.34	-0.86	-1.11	-1.34
		Treatment	**0 V**	**-0.5 V**	**-1 V**	**-2 V**	**-3 V**
MFC #2	Anode	V *vs.* SHE	-0.29	+0.01	-0.04	-0.41	-1.04
	Cathode	V *vs.* SHE	+0.11	+0.44	+1.03	+1.57	+1.90

The effects continued after the MFC media were replaced (Figure 3-15A and B), which meant that the improvement on power output was a result of the change of electrode surface condition. Cyclic voltammetry was employed to further elucidate the change of the electrochemical activity of MFC cathodes (Figure 3-15C). Voltammograms revealed a substantial difference between cathodes before and after treatment: the higher current response was obtained for the treated cathode than that of the original one (0.018 *vs.* 0.008 A at 1.0 V *vs.* SHE; and -0.009 *vs.* -0.008 A at -0.2 V *vs.* SHE), indicating improved cathode activity [132, 146]. A possible explanation for the improvement is the bactericidal effect which killed bacteria on electrode biofilm, resulting in higher oxygen concentration and better oxygen exposure to Pt particles (catalysts to oxygen reduction) on cathode. A previous study concluded that excessive accumulation of biofilm on cathode reduces the electrochemical activity [132]. In fact, electrodes made from carbon cloth have been found to be effective in drinking water disinfection, and the mechanism was revealed as electrochemical dimerization of intracellular coenzyme A at electrode potentials higher than 0.94 V *vs.* SHE [139]. The potassium permanganate ($KMnO_4$) titration of the effluent immediately after 1 h treatment of the ±3 V DC did not detect H_2O_2 at the detecting limit of 20 mg L^{-1}, suggesting the absence of the bactericidal mechanism by a substantial amount of hydrogen peroxides or free radicals that might form by water electrolysis. A similar electrical treatment has been reported being useful

for fouling reduction in membrane bioreactors, as the DC stimulation enhanced the desorption of EPS and sludge particles from membrane surface [147]. Similarly, the treatment can damage the anodic biofilms as well and it explains the impaired electricity generation. From the polarization curves (Figure 3-14B) it can be known that substantial biofilm impairment happened at the +3, -2, and -3 V stimulations, and these voltages poised the corresponding electrode potentials to be higher than +1.5 V *vs*. SHE (Table 3-4).

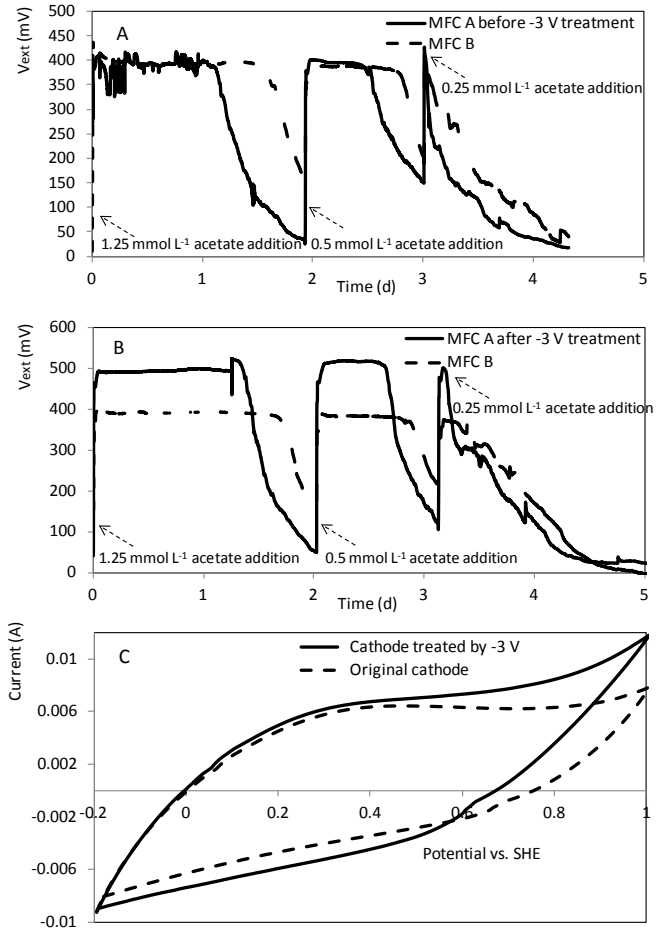

Figure 3-15. Voltage curves (A and B) and cyclic voltammograms (C) of two MFCs. A, voltage curves of MFC A and B before treatment; B, after MFC A treated by -3 V; and C, cyclic voltammograms of cathodes before and after treatment.

3.3.5 Substrate utilization

Acetate and butyrate were originally added to MFCs to provide both carbon sources and reducing power for bacterial growth on anodes. Monitoring the consumption of these two volatile fatty acids as well as total volatile fatty acids (VFA) could also provide data for evaluating MFC's capability for organic contaminants and odor removal from substrate. The VFA concentrations were reduced with time in a sigmoid format for all the MFC reactors shown in Figure 3-16. It can be seen from Figure 3-16A that anaerobic sludge (AN) inoculated MFC utilized VFA most rapidly, while MFC inoculated with river sediment (RS) and activated sludge (AC) removed VFA relatively slowly. A half amount of VFA was decomposed by AN-MFC in 6 d, but 8 to 9 d for MFC inoculated with the other two sources. Over 95% of VFA was removed in 15 d for all 12 MFC reactors. Electric stimulation slightly reduced VFA removal efficiency, as shown in Figure 3-16B, probably due to the bactericidal effect of hydrogen peroxides which might form in the electrolysis of PBS buffered solution.

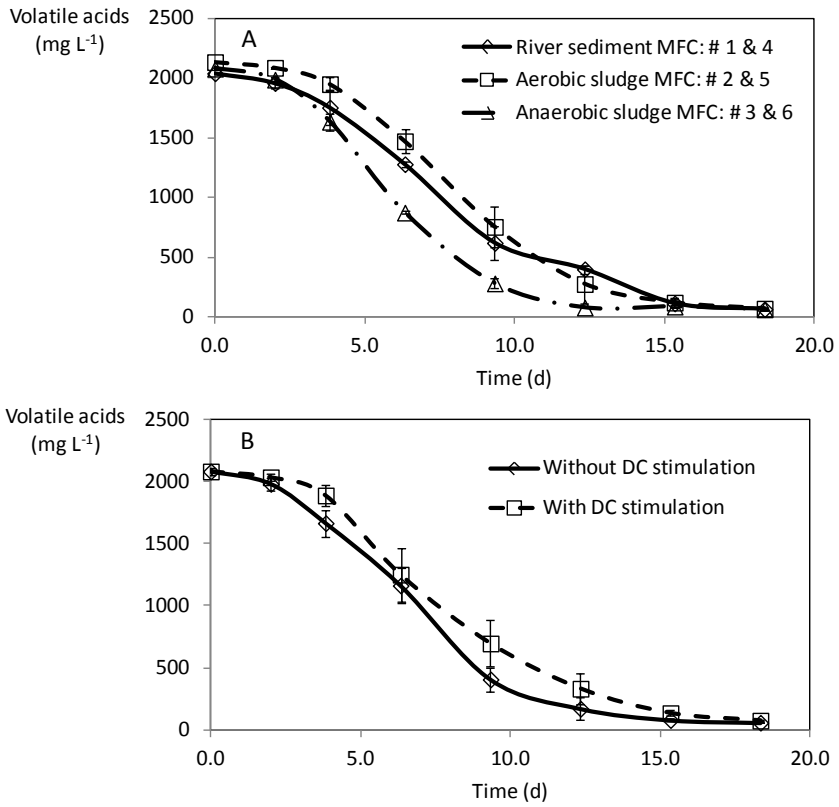

Figure 3-16. Volatile acids utilization in MFC. A, data points were means pooled from the indicated reactors from only the second replicate of the study. B, data points were means pooled from only the second replicate of the study: the open diamonds from reactor #1 to 3 and the open squares from reactor #4 to 6.

The pattern of acetate and butyrate consumption, however, was different from that of VFA. Appearing to be a first order reaction, both acetate and butyrate were degraded at a higher rate when their concentrations were high (Figure 3-17), and at least 90% of these two substrates were degraded in 5 d in all MFC reactors. RS-MFC showed a slightly lower efficiency in degrading acetate and butyrate, which was in accordance with its lower degradation of VFA and a longer lag phase period. In RS- and AC-MFCs, the amount of butyrate surpassed that of acetate after 5 d and its concentration slightly fluctuated, indicating butyrate being a less favorable substrate than acetate for bacteria.

To the contrary, AN-MFC degraded both acids equally (Figure 3-17). The discrepancy between the ways of VFA consumption and two acids reduction might indicate that acetate and butyrate were partially converted by bacteria to other short chain fatty acids and other metabolic products, e.g., propionic and valeric acids, which were detected here by gas chromatography.

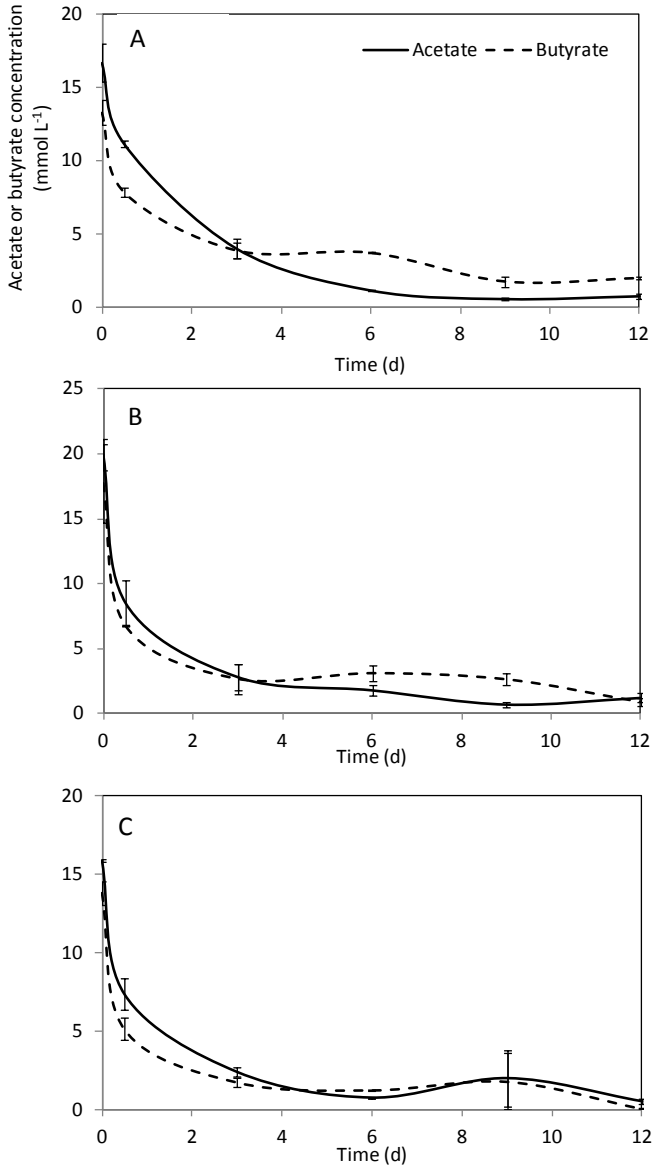

Figure 3-17. Acetate and butyrate evolution in MFC. A, river sediment MFC; B, activated sludge MFC; and C, anaerobic sludge MFC.

3.3.6 Performance under substrate deprivation

It was observed in SEM study that the anodic biofilms mainly consisted of EPS matrices and bacterial cells. During substrate deprivation, EPS may serve as substrate or energy reserves [141]. In this case, different periods of substrate deprivation or starvation were applied to MFCs. It was found that MFCs inoculated under current stimulation demonstrated better and quicker responses when MFCs were subject to this environmental stress of starvation. When the time period of substrate deprivation was 1 d, V_{ext} of all reactors restored to their plateau values within 0.1 d after new substrate was added. When the deprivation time increased to 2 d, V_{ext} of the MFCs treated with current stimulation could still restore within 0.1 d, while the MFC reactors without current stimulation (#1-3) took about 0.1 to 0.2 d to recover (Figure 3-18A). A further increased starvation period of 5 d did not prolong the recovery time for treated MFC #4-6 and MFC #2 (0.1 d), but added 1-2 d for untreated MFC #1 & 3. This longer recovery time suggested that the biofilm of MFCs without current stimulation was partially damaged by the starvation due to bacterial decay or desorption from anodes. In an extreme case, 20 d starvation still did not substantially impair the biofilm of treated MFC #2 and #4-6 (restored in 0.1-0.5 d); however, the biofilm of untreated MFC #1 & 3 seemed to be destroyed, and needed to be inoculated again (Figure 3-18B). In summary, the results demonstrated not only that AC-MFC presented the best biofilm stability among three inoculums types under starvation situation, but also that the biofilm resistance to starvation could be substantially improved by current stimulation, which probably created better bacteria adhesion to the anode surface and enhanced biofilm EPS matrices

[148].

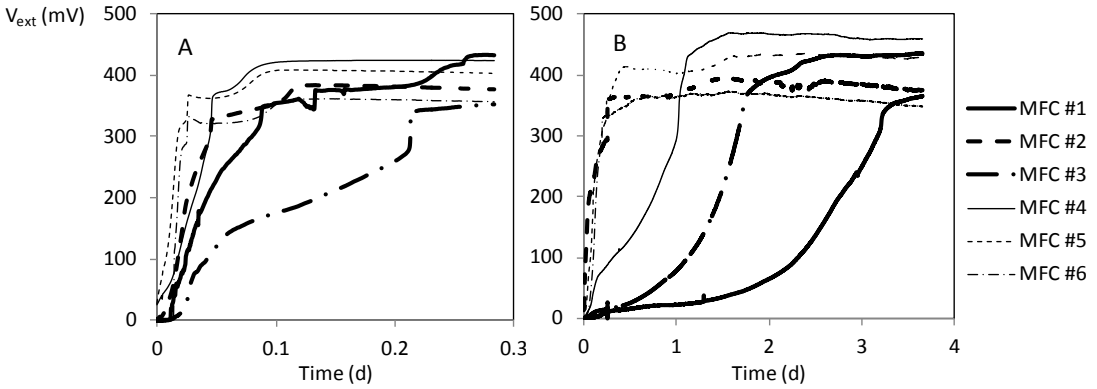

Figure 3-18. Response of MFC after substrate deprivation. A, substrate deprivation for 2 d; B, substrate deprivation for 20 d.

3.4 Conclusions

Among the three types of inoculation sources, activated (AC) and anaerobic (AN) sludge showed faster enrichment of MFC anodic biofilm by 2 to 3 d than river sediment (RS), while AN-MFC presented highest VFA degradation rate, indicating that the bacteria in AN sludge were better adapted to MFC anodes due to the similar anaerobic environment and volatile fatty acid concentrations in a swine manure anaerobic digester. However, RS-MFC anode surface was covered with well-developed layers of biomass (bacterial cells and extracellular polymeric substances) and had a much larger power output (195 μW or 98 mW m^{-2}) than AC- and AN-MFC after one month operation. The electrical current stimulation (+2 V) markedly delayed the MFC startup process for all the inoculum sources, but it efficiently assisted the attachment and homogenous distribution of biomass on anodic carbon fibers, therefore reduced MFC internal resistances by 27%, and improved the resilience of anodic biofilm against long-term substrate deprivation.

For mature MFCs, a transient application of negative voltages (-3 V) improved the cathode activity and maximum power output by 37%. This improvement was due to the bactericidal effect of the electrode potential higher than +1.5 V *vs.* SHE, showing a substantial benefit of treating MFC cathode after long-term operation using suitable electrical current.

Chapter 4. Modeling Single-Chamber Air-Cathode Microbial Fuel Cells Based on Freter Equations

4.1 Introduction

A microbial fuel cell (MFC) is a device oxidizing organic substrates in the liquid environment and releasing electrical energy to external loads. Anode attached biomass works as catalysts for substrate oxidization [24]. The catalytic microorganisms at anodes, mostly enriched from mixed microbial consortia, are capable of handling various organic substrates [121, 122], and can potentially be used in degrading the organic substrates in various types of wastewater.

Due to complicated interactions between various design and operational variables in this hybrid type of reactor, it is not easy to experimentally achieve optimal conditions for power and energy generation and efficient substrate removal. Mathematical models thus provide a simple approach to investigate the effects of different variables and optimize the MFC performances. The electrochemical reactions at anode are emphasized in MFC modeling [116, 149] since the anode reactions are features of MFC and MFC performance can partly be predicted from the growth status of anode attached bacteria [150]. The current MFC anode models are normally based on redox mediators supposed to exist in the medium. Research progress already reveals that outer membrane-bound cytochromes and nanowire of bacteria conduct electricity [24] and so bacteria as a whole, which are directly attached to the anode surface, can be regarded as catalysts. It can thus be assumed that only the directly anode-attached bacteria, or bacteria of a

monolayer [23], contribute to electricity generation. Besides, the suspended bacteria must also be included in the model because the attached and suspended bacterial populations reach a dynamic equilibrium between each other, and because both populations utilize substrate for growth. This inclusion is especially essential when studying substrate utilization between the populations. The Freter model, which originally describes the dynamics of the suspended bacteria and wall-attached bacteria in a bioreactor [151, 152], is herein adopted. The main reason favoring this model is that it emphasizes the formation of a bacterial monolayer on a wall structure which is similar to the process of anode-bacteria attachment. Prior to describing MFC bacterial populations by the Freter model, it is revised to account for the feature of MFC where electricity generation consumes substrate (Figure 4-1).

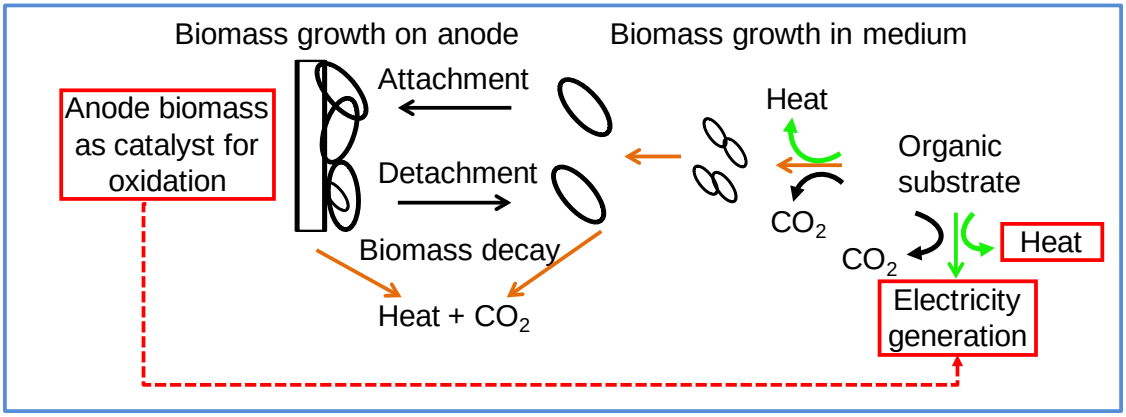

Figure 4-1. A schematic of organic substrate and energy flow in a microbial fuel cell.

In this study, a dynamic model for MFC is developed based on microbial reaction, electrochemical reaction, and mass balances. Numerical simulation of the model is conducted to investigate the effect of varying operational parameters, including initial or influent substrate concentration, dilution rate, and external resistor, on the MFC

microbial populations, substrate removal, power generation, and energy efficiency. Factors influencing the energy efficiency are especially emphasized in numerical simulation for both batch and continuous modes of operation.

4.2 Methods

4.2.1 MFC design and operation

Two identical single-chamber air-cathode MFC reactors, with a total volume of 155 mL, were fabricated from clear/extruded acrylic tubes (5 cm in internal diameter and 7.5 cm in length), covered with 0.25 cm thick plexiglass acrylic endplates at both ends. The anode was made from plain carbon cloth. The air-cathode was made from 0.5 mg cm^{-2} Pt-containing (10% in carbon black) carbon cloth treated with Nafion, and with polytetrafluoroethylene (PTFE) as a gas diffusion backing layer [66]. A 2.2 kΩ resistor was connected in the circuit as an external load.

Anaerobic sludge was obtained for MFC inoculation from a swine manure lagoon at the University of Minnesota Southern Research and Outreach Center in Waseca, MN. The sludge was sieved through a 1 mm mesh to remove sand, gravels, and plant residues prior to use. Sodium acetate was dissolved in 50 mM phosphate buffer solution (pH 7) to prepare a medium with 40 mM acetate. Other nutrients also added to enhance and maintain the development of bacteria included (g L^{-1}): 0.31 NH_4Cl, 0.13 KCl, and mineral and vitamin solutions.

4.2.2 Data acquisition

The voltage (U_{ext}) across an external resistor was measured by voltage probes and recorded by a CR 1000 data logger (Campbell Scientific, Inc., Logan, UT). The anodic and cathodic potentials were monitored against standard Ag/AgCl electrodes (MF-2072, BASi, Inc., West Lafayette, IN). The data logger supporting software, LoggerNet Version 3.4, was used to monitor and collect the voltage data of the MFC reactors.

4.3 Model description

This mathematical model of microbial fuel cells to be developed simulates and predicts the electrochemical performance in batch or continuous mode of operation. A few assumptions are made to simplify the modeling of different MFC reactors. First, the anode-attached microbes are assumed to be the catalyst for the exoelectrogenic process; second, the exchange current density, or the catalytic effect, is proportional to the concentration of the attached biomass; third, the mass transfer of acetate to anode and oxygen gas to cathode, assumed to be fast enough compared to the electrochemical processes, is not a limiting factor and thus is neglected; and fourth, the hydrolytic products of dead cells are assumed not providing carbon source or energy to the suspended or attached bacterial growth.

4.3.1 Electrode potentials

The electrode potential (against the standard hydrogen electrode, SHE or NHE) was dependent on the standard electrode potential and the concentration of active species according to the Nernst equation:

$$E^{o\prime} = E^{0} + \frac{RT}{nF}\sum v_i \ln c_i \quad (4\text{-}1)$$

where $E^{o\prime}$ is the formal potential (pH- and concentration-adjusted reduction potential), E^{o} is the standard electrode potential, v_i is the stoichiometric number for species i (positive for oxidized species, and negative for reduced species), and c_i is the concentration of the species i. In the pH region of this study, the Mineql+ [153] simulation indicated that bicarbonate was the major form in the carbonate equilibrium system. The anodic and cathodic reactions proceeded as follows:

$$2HCO_3^- + 9H^+ + 8e^- \longrightarrow CH_3COO^- + 4H_2O \qquad E^0 = 0.187\ V \quad (4\text{-}2)$$

$$O_2 + 4H^+ + 4e^- \longrightarrow 2H_2O \qquad E^0 = 1.229\ V \quad (4\text{-}3)$$

The anode and cathode electrode potentials ($E_A^{0\prime}$ and $E_C^{0\prime}$, respectively) based on the assumed acetate and bicarbonate concentration can be estimated as follows:

$$E_A^{0\prime} = E_A^0 + \frac{RT}{nF}\sum v_i \ln c_i = -0.335 \qquad [Ac^-]=0.04\ M;\ [HCO_3^-]=10^{-4.5}\ M \quad (4\text{-}4)$$

$$E_C^{0\prime} = E_C^0 + \frac{RT}{nF}\sum v_j \ln c_j = 0.805 \qquad Po_2=0.2 \quad (4\text{-}5)$$

The experimentally measured cathodic potentials usually are much lower than the predicted values [14, 154], partly due to other reactions that might have happened on the cathode surface which results in a mixed cathodic potential of lower values. For

example, hydrogen peroxide production could happen on cathode to deviate the cathode potential to a lower value (e.g., 0.36 V) [14]. In accordance with both the literature information and the cathode potential at open-circuit operation in this study, a cathode potential of 0.51 V (NHE), rather than 0.805 V (NHE), is adopted herein. The electromotive force (E_{emf}) is defined as the difference between the cathode and anode potentials:

$$E_{emf} = E_C^{0'} - E_A^{0'} \tag{4-6}$$

4.3.2 Exchange current and overpotential

Overpotential is defined as the difference of an electrode potential from its formal potential in a fuel cell. The Butler-Volmer equation, neglecting the reverse cathodic reaction [120], is used to express the relationship between the exchange current and anode overpotential:

$$I = j_{oA} A e^{\frac{\alpha_A F \eta_{act,A}}{RT}} \tag{4-7}$$

where I is the electric current, $\mathbf{j_{oA}}$ is the exchange current density of anode, α_A is the transfer coefficient of the anodic reaction, and $\boldsymbol{\eta_{act,A}}$ is the anode overpotential. In a similar way, the cathode overpotential can be formulated with the reverse reaction neglected as follows:

$$I = j_{oC} A e^{\frac{(\alpha_C - 1) F \eta_{act,C}}{RT}} \tag{4-8}$$

where $\mathbf{j_{oC}}$ is the exchange current density of cathode, α_C is the charge transfer coefficient of the cathode reaction, and $\boldsymbol{\eta_{act,C}}$ is the cathode overpotential. The exchange current density of cathode is consistent during the MFC operation due to the unchanging amount of the catalyst (0.5 mg cm^{-2} of Pt), but that of anode is proportional to the increasing catalyst load, which is the attached biomass concentration here [155]:

$$j_{oA} = j_{oAU} w \tag{4-9}$$

where $\mathbf{j_{oAU}}$ is the unit exchange current density of exoelectrogenic biomass, and w is the attached biomass concentration on anode.

4.3.3 Mass balances

A model that was proposed to describe the suspended and attached microbial formation [151, 152] in an aqueous environment is modified and adopted in this study. In this model, bacteria can divide, suspend and decay in the reactor medium, and can also attach to a surface with a dynamic equilibrium between attachment and detachment. Since bacterial growth and electricity generation consume substrate when it is available, the three components of the system, the substrate concentration (S), the suspended biomass concentration (u), and the attached biomass concentration (w), which are dictated by mass balances, are expressed in three ordinary differential equations as follows:

$$\frac{dS}{dt} = D(S_{in} - S) - \gamma^{-1}(u\mu_u + \delta w\mu_w) - r_e \tag{4-10}$$

$$\frac{du}{dt} = u(\mu_u - D - k_u) + \beta\delta w + \delta w\mu_w(1 - G) - \alpha u(1 - W) \quad (4\text{-}11)$$

$$\frac{dw}{dt} = w(\mu_w G - \beta - k_w) + \delta^{-1}\alpha u(1 - W) \quad (4\text{-}12)$$

where D is the dilution rate, S_{in} is the influent substrate concentration, $\boldsymbol{\gamma}$ is the biomass yield of substrate, $\boldsymbol{\mu_u}$ is the suspended bacterial growth rate, $\boldsymbol{\mu_w}$ is the attached bacterial growth rate, $\boldsymbol{\delta}$ is the ratio of projected anode surface area to reactor volume, $\mathbf{r_e}$ is the substrate utilization rate by electricity and heat generation, $\mathbf{k_u}$ is the suspended bacterial death rate, $\mathbf{k_w}$ is the attached bacterial death rate, $\boldsymbol{\beta}$ is the detachment rate of bacteria from wall, $\boldsymbol{\alpha}$ is the attachment rate of bacteria to anode surface, $\mathbf{G}$ is the fraction of daughter cells attached to anode, and $\mathbf{W}$ is the wall occupation fraction. Some of those parameters in the equations can be defined through some more fundamental design and operational parameters:

$$D = Q/V \quad (4\text{-}13)$$

$$\delta = A/V \quad (4\text{-}14)$$

$$\mu_u = \frac{m_u S}{a_u + S} \quad (4\text{-}15)$$

$$\mu_w = \frac{m_w S}{a_w + S} \quad (4\text{-}16)$$

$$G = \frac{(1-W)}{(1.1-W)} \quad (4\text{-}17)$$

where $\mathbf{Q}$ is the dilution rate, $\mathbf{V}$ is the MFC reactor volume, $\mathbf{A}$ is the projected anode surface area, $\mathbf{m_u}$ is the maximum specific growth rate of suspended bacteria, $\mathbf{a_u}$ is the half saturation coefficient of suspended bacteria of the Monod kinetics, $\mathbf{m_w}$ is the maximum specific growth rate of attached bacteria, $\mathbf{a_w}$ is the half saturation coefficient of attached bacteria.

4.3.4 Ohm's law and Kirchhoff's voltage law

By applying Ohm's law, the electrical current of the circuit, the voltage drop (U_m) across the resistance (R_m) of electrolyte solution of MFC medium, and the voltage drop (U_c) across the contact resistance (R_c) of MFC can be obtained:

$$\mathrm{I} = \mathrm{U_{ext}}/\mathrm{R_{ext}} \tag{4-18}$$

$$\mathrm{U_m} = \frac{\mathrm{Id}}{\mathrm{A}\sigma} \tag{4-19}$$

$$\mathrm{U_c} = \mathrm{IR_c} \tag{4-20}$$

where $\mathbf{U_{ext}}$ is the external voltage across the external resistor ($\mathbf{R_{ext}}$), $\mathbf{d}$ is the distance between two electrodes, and $\boldsymbol{\sigma}$ is the conductivity of MFC medium. By combining all the polarization losses along the circuit of MFC, the voltage conservation according to Kirchhoff's voltage law can be denoted as follows:

$$\mathrm{E_{emf}} = \mathrm{E_C^{0'}} - \mathrm{E_A^{0'}} = \mathrm{U_{ext}} + \mathrm{U_c} + \mathrm{U_m} + \eta_{act,A} - \eta_{act,C} \tag{4-21}$$

4.3.5 Power and Energy efficiencies

The power ($\mathbf{P_{ext}}$) extracted by the external load of a resistor is the product of the external voltage and current:

$$P_{ext} = U_{ext}I \tag{4-22}$$

The power extracted by the electrical circuit of MFC ($\mathbf{P_{cell}}$), or termed as an MFC cell, is the product of the electromotive force and current:

$$P_{cell} = E_{emf}I \tag{4-23}$$

The power lost through the polarization of the activation overpotentials of anode and cathode, the contact resistance, and the medium resistance, is the power emitted in a form of heat:

$$P_{heat} = (U_c + U_m + \eta_{act,A} - \eta_{act,C})I \tag{4-24}$$

The rate of the substrate (acetate) loss through MFC cell ($\mathbf{r_e}$) can be calculated as follows:

$$r_e = MP_{cell}/(V\Delta H_c) \tag{4-25}$$

where $\mathbf{\Delta H_c}$ is the heat of combustion of acetic acid, and $\mathbf{M}$ is the relative molecular weight of acetic acid.

Besides the energy loss by heat generation in MFC, the chemical energy of substrate is also lost by providing energy for the growth of the suspended and attached bacteria. The

corresponding powers for the suspended ($\mathbf{P_u}$) and attached ($\mathbf{P_w}$) bacteria can be calculated as follows:

$$P_u = \gamma^{-1}\Delta H_c u \mu_u V/M \tag{4-26}$$

$$P_w = \gamma^{-1}\Delta H_c \delta w \mu_w V/M \tag{4-27}$$

Although some studies [154] suggested that energy efficiency was further reduced by the more positive potential (close to 0 V, NHE) of redox intermediates than that of the substrate, this energy loss was not considered because our experiment achieved anode potentials close to that of the substrate. Therefore, the MFC cell energy efficiency ($\boldsymbol{\eta_{cell}}$) and overall energy efficiency ($\boldsymbol{\eta_{overall}}$) are defined as follows:

$$\eta_{cell} = P_{ext}/P_{cell} \tag{4-28}$$

$$\eta_{overall} = P_{ext}/(P_{cell} + P_u + P_w) \tag{4-29}$$

Please note that at batch mode, the overall energy efficiency is calculated differently:

$$\eta_{overall} = \int_0^t P_{ext} dt\,/(\Delta H_c \Delta SV/M) \tag{4-30}$$

4.3.6 Model parameters

Some constants and parameters involved in microbial fuel cell processes described in Equations (from 3-1 to 3-30) are listed in Table 4-1. During modeling and simulation, units of those parameters and variables are not necessarily SI units, but some are adjusted to the suitable magnitudes. Microbial parameters of acetate utilizers in

anaerobic condition are adopted from literature [156]. Some model parameters associated with electrochemical processes, including charge transfer coefficients (α_A and α_C) and exchange current densities ($\mathbf{j_{oA}}$, $\mathbf{j_{oAU}}$ and $\mathbf{j_{oC}}$) are estimated from the polarization dataset obtained from one of two MFC reactors in this experiment. The quasi-Newton approach is used to minimize the χ^2 test statistic as an error function:

$$\chi^2 = \sum_{i=1}^{n} \frac{(y_i^{cal} - y_i^{exp})^2}{y_i^{exp}} \tag{4-31}$$

where $\mathbf{n}$ is the number of data points, and $\mathbf{y_i^{exp}}$ is the i-th experimental value, and $\mathbf{y_i^{cal}}$ is the i-th calculated value. The polarization curve data of the other reactor is used for validation.

Table 4-1. Constants, and design and operational parameters of a microbial fuel cell system

Parameter symbol	Description	Value	Units
Physical			
F	Faraday's constant	96485	C/mol
R	Ideal gas constant	8.314	J/mol/K
T	Room temperature	298	K
ΔH_c	Heat of combustion of acetic acid	-875000	J/mol
M	Relative molecular weight of acetic acid	60	g/mol
Electrochemical			
$E_A^{0'}$	Formal reduction potential of anode	-0.335	V vs. NHE
$E_C^{0'}$	Formal reduction potential of cathode	0.51	V vs. NHE
Reactor configuration			
A	Projected surface area of electrode	0.002	m^2
d	Distance between anode and cathode	0.075	m
V	Volume of MFC reactor	1.55×10^{-4}	m^3
δ	Ratio of anode surface area to MFC volume	13	m^2/ m^3
R_c	Contact resistance of MFC	20	Ω
Operational			
D	Dilution rate	0-2	d^{-1}
S_{in}	Substrate concentration	10-2400	g/m^3
Q	Flow rate	$0\text{-}7.8\times10^{-5}$	m^3/d
σ	Conductivity of MFC medium	1.1	S/m
R_{ext}	External resistor	2200	Ω
$[HCO_3^-]$	Bicarbonate concentration	$1\times10^{-4.5}$	$kmol/m^3$
P_{O2}	Partial oxygen pressure at cathode	0.2	atm
pH	-log10 of proton concentration	7	Dimensionless
Microbial			
γ	Biomass yield from substrate	0.05	g/g
k_u	Death rate of suspended bacteria	0.02	d^{-1}
k_w	Death rate of attached bacteria	0.02	d^{-1}
α	Bacterial attachment rate	0.05	d^{-1}
β	Bacterial detachment rate	0.05	d^{-1}
m_u	Maximum specific growth rate of suspended bacteria	2.4	d^{-1}
m_u	Maximum specific growth rate of attached bacteria	2.4	d^{-1}
a_u	Half saturation coefficient of suspended bacteria	100	g/m^3
a_w	Half saturation coefficient of attached bacteria	100	g/m^3
w_{max}	Maximum bacterial attachment	0.33[a]	g/m^2

[a] The maximum amount of bacteria attached on electrode is calculated from the bacteria dimensions observed in SEM images, and this value is close to the literature values of 0.47 to 0.52 g/m^2 [23].

4.4 Results and discussion

4.4.1 Parameter estimation

Two identically-made MFC reactors with respect to reactor configuration and electrode materials were inoculated with the same anaerobic sludge and operated in parallel. After MFC were fully inoculated and operated for 30 d, polarization curves of MFC was obtained by varying the external resistor from 2200 Ω to 220 Ω, with the electrode potentials recorded (Figure 4-2A). The resultant electrochemical parameters estimated by fitting polarization curves of electrodes are listed in Table 4-2. The simulation results based on the estimated parameters are in good agreement with the experimental data of both reactors, as shown in Figure 4-2B and C. The anodic exchange current density of 62.5 mA m^{-2} is in the same order of a literature value of 29 mA m^{-2} [157]. The cathodic exchange current density (0.975 mA m^{-2}) observed in this study is higher than that of non-catalyzed and bio-catalyzed cathodes [158, 159] but lower than another Pt-based cathode [160]. To further validate the model, the external voltage (U_{ext}) during inoculation stage is simulated based on the listed parameters except the unit exchange current, which is fitted from the experimental data of the inoculation stage to be 0.129 mA mg^{-2} biomass and has a difference of 32% from 0.189 mA mg^{-1} which is fitted from polarization curves. This difference can be a result of the change of the activity or catalytic effect of the attached biomass during the inoculation and 30 d operation. The simulated data and the experimental data of the inoculation stage generally show good agreement to each other (Figure 4-2D).

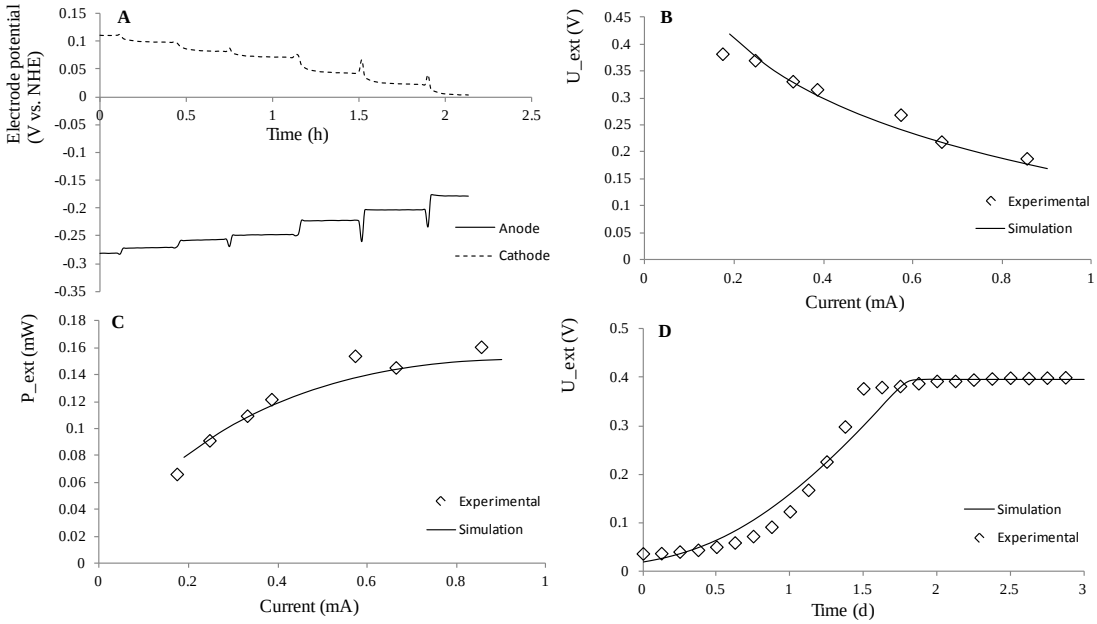

Figure 4-2. Electrochemical parameters estimation and validation. These figures plot the electrode potential during polarization experiment (A), model validation for experimental data from another identical MFC reactor (B for *Uext*, and C for *Pext*), and comparison of the simulated and experimental *Uext* during inoculation stage.

Table 4-2. Estimated electrochemical parameters for MFC in this study

Estimated parameters	Description	Value	Units
α_A	Charge transfer coefficient, anode	0.318	Dimensionless
α_C	Charge transfer coefficient, cathode	0.694	Dimensionless
j_{oA}	Exchange current density, anode	62.5	mA/m^2
j_{oAU}	Unit exchange current, anode	0.189	mA /mg
j_{oC}	Exchange current density, cathode	0.975	mA/m^2

4.4.2 Simulation of batch mode MFC

Effect of initial substrate concentration

Simulation of the proposed model is performed through Matlab on a personal computer to illustrate the processes of substrate utilization, biomass concentration evolution, and voltage generation across an external resistor. Since most MFC studies in literature are

carried out in batch mode, this simulation assumes the medium dilution rate D=0 with initial substrate (HAc) concentrations of 10, 100, 1000, and 2400 mg L^{-1}, consecutively.

The simulation results are shown in Figure 4-3. Initial substrate concentrations of 1000 and 2400 mg L^{-1} do not show obvious decrease in the first 4 d (Figure 4-3A), but substrate is consumed dramatically after this period. MFCs started with the other lower substrate concentrations behaved differently from the higher strength cases, as a continuous and gradual decrease is observed. The substrate in the case of 1000 mg L^{-1} lasts the longest, i.e., 9 d, which almost doubles that of the higher strength cases. These results indicate that it is not always the case that more concentrated substrate sustains the longest period, and a moderate substrate concentration should be chosen for keeping MFC from starvation. Trends of substrate utilization are generally the work of suspended bacteria, which can accumulate to a high level and subsequently consume substrate at a high rate that rapidly reduces substrate concentration (Figure 4-3B). For example, in the cases of 100 and 2400 mg L^{-1} initial substrate concentrations, the peak suspended biomass concentrations are 2.5 and 117 mg L^{-1}, respectively. The latter is 47 times higher than the former, which consumes substrate in a higher rate due to two reasons: the higher level of biomass concentration and the enhanced specific substrate utilization rate which is indicated by the Monod equation (Equations 3-15 & 3-16).

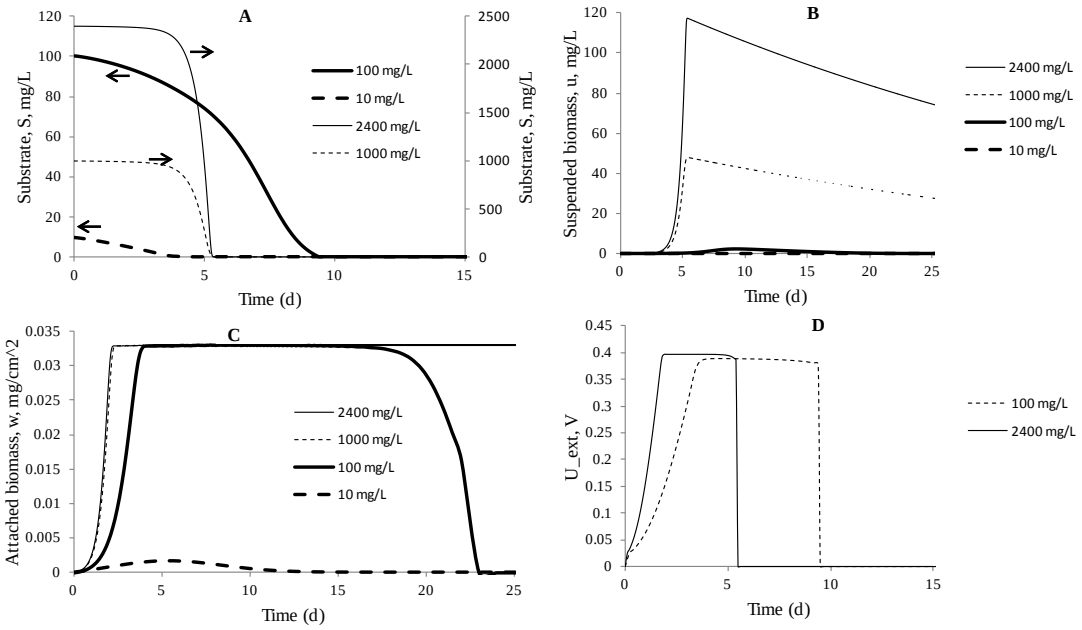

Figure 4-3. Simulated time-course profiles of process variables at different initial substrate concentration. The simulated variables are the substrate concentration (A), suspended (B) and attached (C) biomass concentration, and the external voltage *Uext* (D).

The attached biomass concentrations (Figure 4-3C) accumulate to their plateau values (0.033 mg cm^{-2}) for all of those initial substrate concentrations (in 2 d for 1000 and 2400 mg L^{-1}, and in 4 d for 100 mg L^{-1}), except for the one with 10 mg L^{-1} substrate, indicating that there may exist a lower limit for substrate concentration and thus substrate concentration lower than 10 mg L^{-1} should be avoided during inoculation stage. The more the initial substrate concentration is, the longer the attached biomass sustains: both last more than 25 d for 1000 and 2400 mg L^{-1}, but only 23 d for 100 mg L^{-1} before the biomass disappears. The electricity generation (Figure 4-3D) is simulated in a form of external voltage (U_{ext}) for the initial substrate concentrations of 100 and 2400 mg L^{-1}, because both of them fully develop the attached biomass, and are also typical levels for the low and high substrate concentrations, respectively. During the first few days of

anode inoculation, the growing voltage is caused by the growing attached biomass and eventually reaches a plateau value of about 0.39 V. Since the substrate lasts a longer period in the 100 mg L^{-1} MFC than in the 2400 mg L^{-1} MFC, the electricity generation also lasts longer by 4 more days. Energy generated is 25.1 and 40 J for 2400 mg L^{-1} MFC and for 100 mg L^{-1} MFC, with overall energy efficiencies extracted from acetate ($\eta_{overall}$) of 0.46% and 17.7%, respectively. Therefore, based on electricity energy generation and overall energy efficiency, the MFC with 100 mg L^{-1} of substrate substantially outperforms the one with 2400 mg L^{-1}. Controlling the initial substrate concentration is demonstrated as a way for regulating the suspended biomass concentration, and is helpful to harvest more energy out of the substrate for electricity.

The growing amount of the attached biomass not only enlarges the external voltage (U_{ext}), but also improves the external power, evidenced by the gradual expansion of the polarization curves by the time in Figure 4-4. These simulations are based on the high initial substrate concentration of 2400 mg L^{-1} in order to avoid a noticeable substrate decrease in 2 d. The pattern of the curve expansion is similar to what was observed in literature [116, 150], illustrating the importance of the attached biomass on power generation.

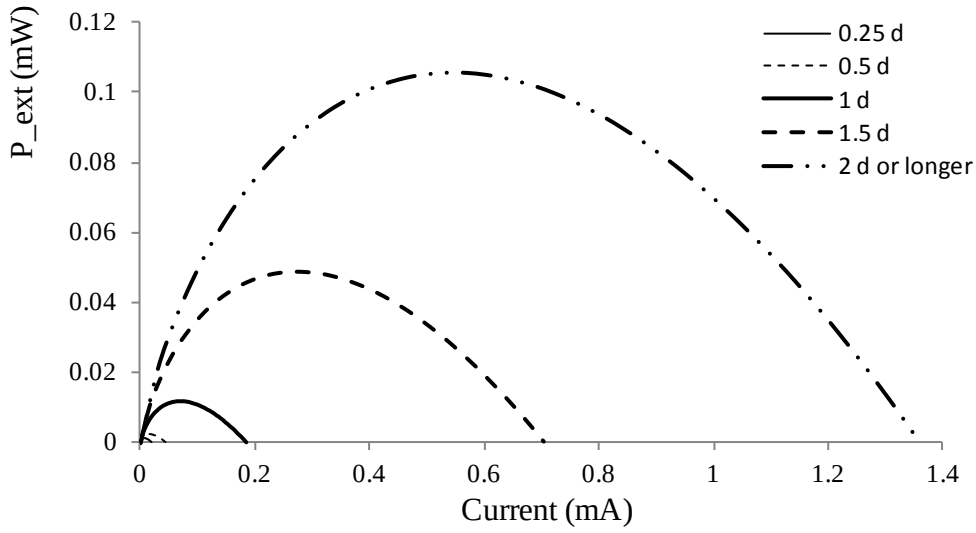

Figure 4-4. Simulated polarization curves at different moments of inoculation. Attached bacteria concentration reach a plateau value after about 2 d, and the polarization curves do not change much anymore.

Effect of external resistor

From the comparisons of external voltage and overall energy efficiency, it can be seen that under this experimental condition, a 100 mg L^{-1} of initial substrate works best among the four tested substrate concentrations. The next step of this study simulates the impact of the external resistor on the batch mode MFC voltage and power generation as well as overall energy efficiency. In MFC study, the internal resistance (R_{in}) is used for indicating the overall resistance of a reactor, which is a useful index because varying an external resistor to the value of internal resistance generates the maximum external power density [35]. Depending on the reactor design and operation, the values of R_{in} may differ but usually is within a range of several hundreds of Ohms, which is also in accordance with the observations (332 Ω in experimental study; and 471 Ω in simulation study) in MFC reactors in this study. In order to see the effect of external resistors on

MFC energy and power generation, a range of resistor covering the values of internal resistance is chosen for simulation: 10, 300, 1000, and 2200 Ω.

The simulation results are presented in Figure 4-5. The smaller value the external resistor is, the more rapid the substrate is consumed (Figure 4-5A), which was also observed in two-chamber MFC reactors for organic matter removal [111, 161]. The main reason is that the heat generation, which depicts the part of energy loss through overpotentials (Equation 3-24), is substantially increased with the smaller external resistor which corresponds to a greater electrical current [162]. When the resistor reduces to 10 Ω, a major part of substrate is lost via heat so that there is not enough substrate to support suspended (Figure 4-5B) and attached microbial growth. On the other hand, the small resistor is beneficial to organic substrate removal because of its substrate utilization rate, and this value would be appropriate for treating high strength wastewater such as swine wastewater [163]. A greater external resistor harvests a higher external voltage (Figure 4-5C), and takes a longer reaction period. The 10-Ω resistor causes an apparently impaired performance due to the failure of the microbial growth. Simulation of external power generation (Figure 4-5D) confirms that 300 Ω, which is the closest among the three to the internal resistance observed in this study, generates the largest power. A similar trend is also observed in a previous experimental study [161]. However, this value of resistor sustains a shorter reaction time by 2 to 3 d compared to that of 1000 and 2200 Ω. In overall, the 1000 Ω resistor harvests the most energy from substrate, achieving overall energy efficiency of 20.7% (Table 4-3). Energy efficiency

between 15% and 20% is achieved in experimental studies as best cases [164, 165], while a value of around 5% is more frequently observed for general cases [165, 166].

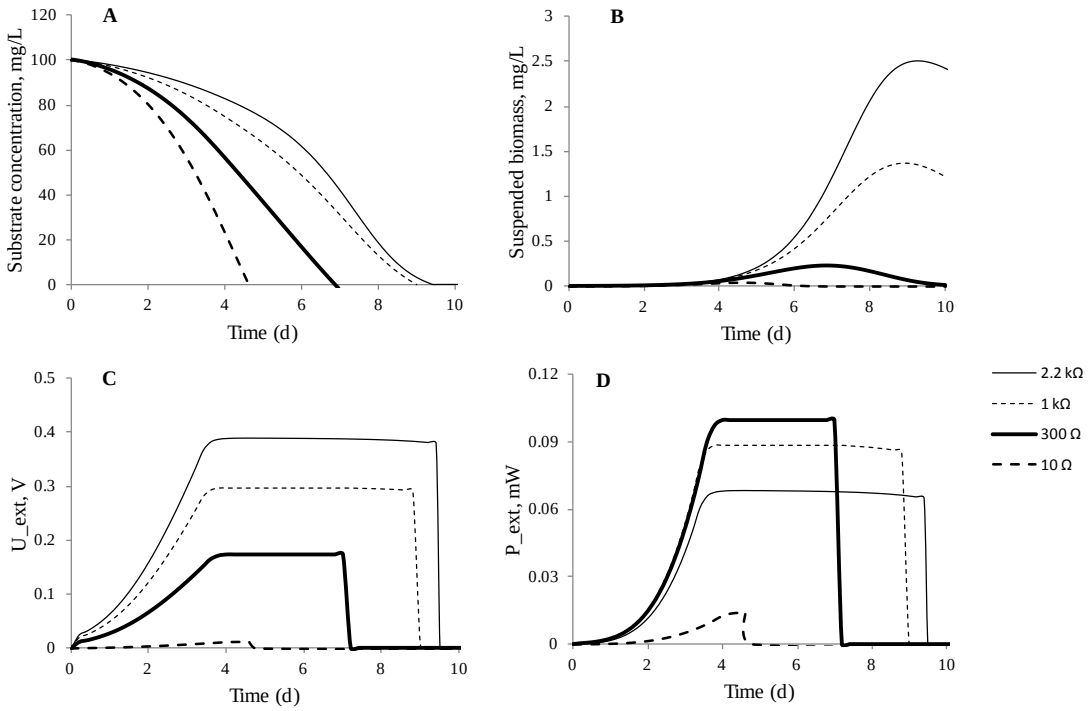

Figure 4-5. Simulated batch performance of MFC with 100 mg L^{-1} initial substrate at different external resistors. The plots include the following variables: A, substrate concentration; B, suspended biomass concentration; C, external voltage; and D, power generation.

Table 4-3. Simulated peak power and energy recovery from external resistor, and overall energy efficiency ($\eta_{overall}$) at different external resistors

External resistor	**Peak power**	**Energy recovered**	$\eta_{overall}$
10 Ω	0.0142	1.96 J	0.87%
300 Ω	0.0998 mW	37.1 J	16.4%
1000 Ω	0.0882 mW	47.3 J	20.7%
2200 Ω	0.0685 mW	40.0 J	17.7%

4.4.3 Simulation of continuous mode MFC

Effect of influent substrate concentration and dilution rate

When MFC reactors are operated in continuous mode, the operational variables that may have pronounced effects are dilution rate (D) and influent substrate concentration (S_{in}). These two variables control the substrate inflow rate and biomass washout rate, and therefore will eventually impact MFC power generation and energy efficiency at steady state. So in the simulation the dilution rate is varied between 0.1 to 2 d^{-1}. The upper limit is chosen to be less than the maximum microbial specific growth rate (2.4 d^{-1}) to prevent biomass washout. The influent substrate (HAc) concentration is between 10 to 2400 mg L^{-1}. The results, including the substrate concentration, suspended biomass concentration, attached biomass concentration and overall energy efficiency, are plotted in Figure 4-6. Please note that the external power (P_{ext}) is not considered in the simulation of varying S_0 and D, because it is found that when assuming the attached biomass is fully grown at steady state, the external power is rather a function of the external resistor than a function of these two operational variables. It should be noted that little MFC studies of varying these operational parameters are implemented in continuous mode, so literature data for comparison are inaccessible.

At a given level of the influent substrate concentration, the steady state substrate concentration goes up with the increasing dilution rate, basically due to the increased substrate inflow to the reactor (Figure 4-6A). When the influent substrate concentration is higher than 500 mg L^{-1}, the concentration does not have much impact on the steady

state substrate concentration at a given dilution rate. But when the influent concentration is lower than 500 mg L^{-1} and the dilution rate is greater than 1.5 d^{-1}, the steady state concentration increases along with the influent concentration. The suspended biomass concentration is obviously increases with the influent substrate concentration in a linear way at any dilution rate (Figure 4-6B). The dilution rate between 0.5 and 1 d^{-1} results in a maximum suspended biomass at a given influent substrate concentration, because a lower rate causes substrate limitation and a higher rate partially washes suspended biomass. The attached biomass is more stable and can generally achieve its maximum in most cases (Figure 4-6C), except for the cases of S_{in} which are much less than 100 mg L^{-1} and are too low to provide enough carbon sources for supporting the bacterial growth and attachment. As to the overall energy efficiency, it can be concluded that a higher influent substrate concentration reduces the efficiency (Figure 4-6D). The only exception is the case with about 10 mg L^{-1} of influent substrate and 0.1 d^{-1} of dilution rate, under which condition the attached biofilm is not fully mature due to substrate deficiency so that MFC does not generate electricity. Considering the tradeoff between higher electrical power generation (reflected by the attached biomass concentration, which is the catalyst) and acceptable overall energy efficiency, it is recommended to operate MFC with about 100 mg L^{-1} of influent substrate concentration. Meanwhile, at this substrate concentration, the choice of a lower dilution rate, e.g., 0.1 d^{-1}, will help achieve lower effluent substrate and better removal efficiency, and the choice of a larger dilution rate, e.g., 2 d^{-1}, may help generate more electricity energy.

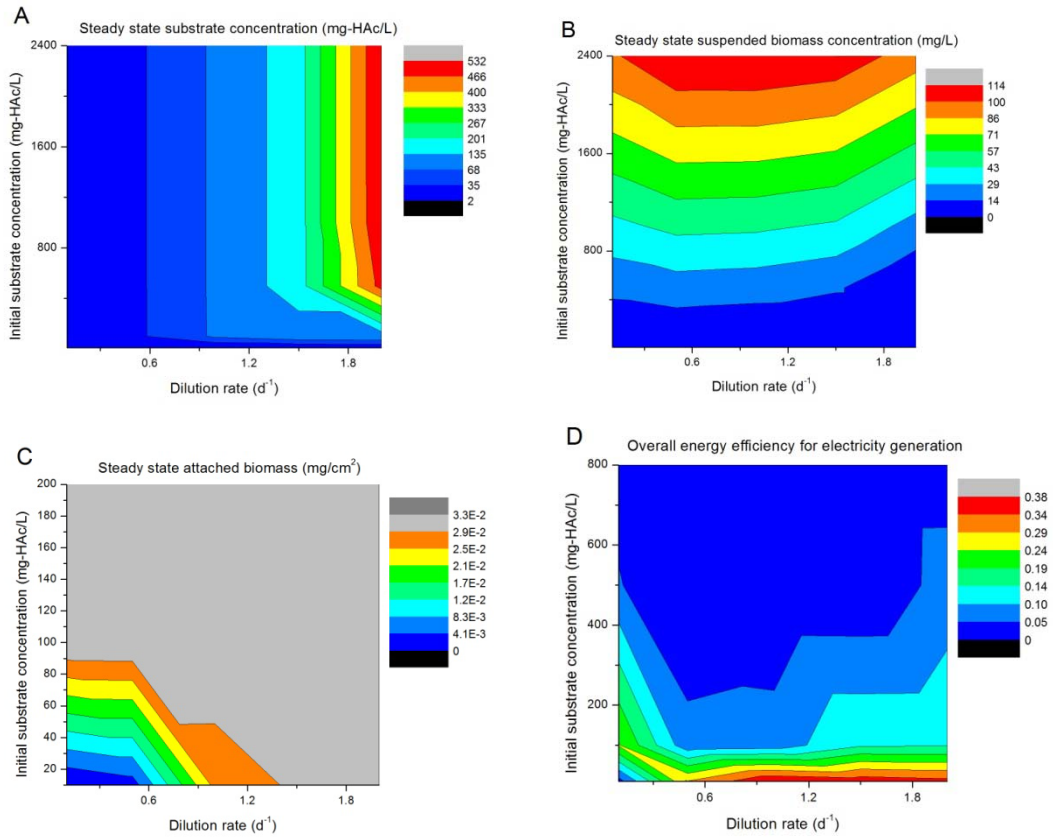

Figure 4-6. Process variables and MFC performance predicted at steady state under different dilution rates and influent substrate concentrations. The simulated variables are the steady state substrate concentration (A), suspended (B) and attached (C) biomass concentration, and the overall energy efficiency η_{ext} (D).

Effect of external resistor

The next simulation is implemented for changing electrical currents by varying R_{ext} at the operational conditions of S_{in} and D listed in Table 4-4. The relationship between R_{ext} and current I is depicted in the inset of Figure 4-7A. These results are useful for determining a suitable range of the external resistor for better substrate removal, power generation or overall energy recovery. As shown in Figure 4-7A and Table 4-4, all cases result in a maximum power generation ($P_{ext,\,max}$) of 0.106 mW at R_{ext} of 352 Ω, except for the case of the lowest substrate loading (S_{in} = 100 mg L^{-1} and D = 0.1) which has a

highest power of 0.091 mW at R_{ext} of 1007 Ω. For the lowest substrate loading case, a further decrease of R_{ext} distributes more organic substrate utilization for heat generation, and would finally lead to a system failure without electrical generation due to substrate limitation for biomass growth. To the contrary, all the MFCs with enough substrate generate the same external powers at given R_{ext}. Figure 4-7B plots the results of MFC cell efficiency (η_{cell}, defined in Equation 3-28) which shows that MFC cell efficiency decreases with the increasing circuit current (or the decreasing external resistor) because of the increased heat loss through the cell (Equation 3-24). Again, the curve of the lowest substrate loading differs from the others and is interrupted at R_{ext} less than 928 Ω due to insufficient substrate available for biomass growth.

Table 4-4. Simulated MFC performance: substrate removal, power generation and overall energy efficiency

S_{in} mg/L	D d^{-1}	Steady state S mg/L	S removal %	$P_{ext,\,max}$ mW	$\eta_{overall,\,max}$	R_{in} [a] Ω	$R_{ext,\,P}$ [b] Ω	$R_{ext,\,\eta}$ [c] Ω
100	0.1	0 - 5.26	> 94.7	0.091	0.322	471	1007	928
	1	57.6 - 73.5	26.5 - 42.4	0.106	0.105		352	405
	2	79 - 100	< 21.0	0.106	0.156		352	1017
2400	0.1	5.17 - 5.26	100	0.106	0.0167		352	352
	1	73.9	96.9	0.106	0.0017		352	352
	2	531	77.9	0.106	0.0011		352	352

[a] The internal resistance is estimated from the transiently simulated polarization curves in the electrical current range between 0.18mA to 0.82 mA.
[b] This is the value of the external resistor where the $P_{ext,\,max}$ is achieved.
[c] This is the value of the external resistor where the $\eta_{overall,\,max}$ is achieved.

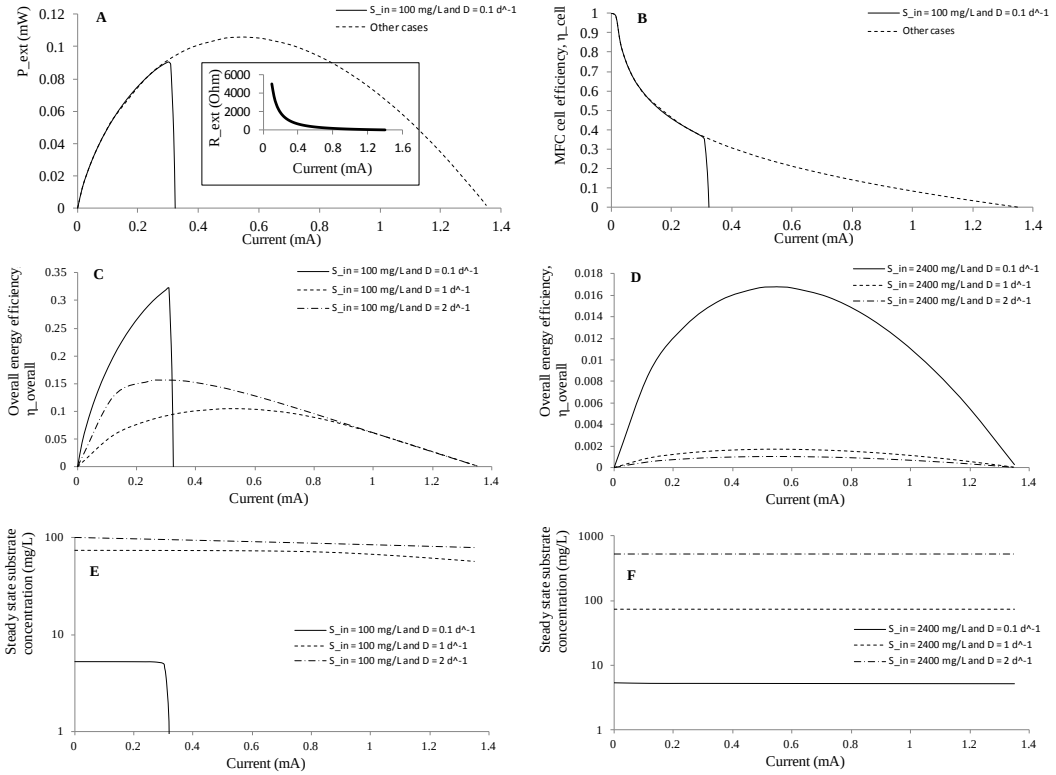

Figure 4-7. Simulated MFC performance at steady state under different electrical currents (or external resistors), dilution rates and influent substrate concentrations. The simulated variables are the steady state power density (A), MFC cell energy efficiency (B), overall energy efficiency at *Sin*=100 mg L^{-1} (C) and *Sin*=2400 mg L^{-1} (D), and effluent substrate concentration at *Sin*=100 mg L^{-1} (E) and *Sin*=2400 mg L^{-1} (F).

Figure 4-7C and D show the overall energy efficiencies for the influent substrate concentrations of 100 and 2400 mg L^{-1}, respectively. For the lower substrate cases, the maximum overall energy efficiencies ($\eta_{overall,\,max}$) are between 0.105 and 0.322, and achieved at external resistors depending on dilution rates (928 Ω at D= 0.1 d^{-1}; 405 Ω at D=1 d^{-1}; and 1017 Ω at D= 2 d^{-1}). For the higher substrate cases, the maximum overall energy efficiencies are between 0.0011 and 0.0167, and are achieved at R_{ext} = 352 Ω at which the $P_{ext,\,max}$ values are concurrently obtained. So the lower substrate concentration reactor has one or two orders of magnitude of higher overall efficiency than that of the

higher substrate concentration. This substantial difference is a result of more proliferated biomass growth at higher substrate concentration, and the biomass in turn consumes more substrate. Please also note that the internal resistance R_{in} estimated by polarization curves is 471 Ω, and is independent of these operational parameters. The steady state substrate concentration (S) and substrate removal almost keep unchanging at different electrical current (Figure 4-7E and F), but depend on the influent substrate concentration and dilution rate as discussed earlier. Removal efficiencies greater than 94.7% or about 100% are achieved at S_{in} = 100 mg L^{-1} and D = 0.1 d^{-1}, and S_{in} = 2400 mg L^{-1} and D = 0.1 d^{-1}, respectively.

4.5 Conclusions

The model proposed in this study is based on the assumption that the anode attached bacterial monolayer serves as biocatalysts for MFC exoelectrogenesis. By modifying the Freter model and combining it with Butler-Volmer equation, this model adequately describes the processes of electricity generation, substrate utilization, and suspended and attached biomass growth, in both batch and continuous operational mode. MFC performances are impacted by various operational variables such as initial substrate concentration, external resistor, influent substrate concentration, and dilution rate, and their interactions, which are revealed by data simulation to be complicated. The simulation results explain that in batch mode, an intermediate initial substrate concentration (S_0 about 100 mg L^{-1} at this reactor configuration) is appropriate to achieve maximum overall energy efficiency. With the S_0 of 100 mg L^{-1}, an external resistor (about 300 Ω) with the value around the internal resistance (R_{in} of about 471 Ω)

boosts the power generation, and a resistor of about two times (about 1000 Ω) of that value achieves better overall energy efficiency. However, a small external resistor should be adopted for MFC reactors aiming to rapidly remove organic substrates. In continuous mode and at R_{ext}= 2200 Ω, the anode-attached biomass can fully grow when the influent substrate concentration is equal to or higher than 100 mg L^{-1} at any dilution rates within the tested range. The maximum external power of 0.106 mW can be achieved at R_{ext}= 352 Ω when there is enough substrate to sustain the power generation. An influent substrate concentration of 100 mg L^{-1} achieves the overall energy efficiency greater than 10%. The high substrate concentration, e.g., 2400 mg L^{-1}, encourages substantial biomass growth and thus reduces the overall energy efficiency to less than 2%. For the low influent substrate concentration (100 mg L^{-1}), the maximum power generation and overall energy efficiency cannot be concurrently achieved, and to operate MFC at an external resistor R_{ext} close to the internal resistance (R_{in}) or two times of R_{in} is recommended to obtain optimal values for both indices. Overall, this relative simple model provides a convenient way for evaluating and optimizing performance of MFC reactors by regulating operational parameters.

Chapter 5. Electricity Generation, and Organic Matters and Nutrients Removal for Swine Wastewater Using Microbial Fuel Cells

5.1 Introduction

The larger and intensified swine production in recent years generates an increasing amount of high-strength wastewater that needs to be treated before disposal. The liquid waste from swine industry is mainly in the form of pig wastewater or slurry, a mixture of feces, urine, and washing water. The wastewater has a varying amount of chemical oxygen demand (COD, roughly between10000 and 50000 mg/L), total N (3000 to 5200 mg-N/L), NH_4-N (1820-3330 mg-N/L) and phosphorus (660-920 mg/L) [10]. The production facility, manure storage, and even the manure treatment unit [7] may release air pollutants such as volatile fatty acids and ammonia. A poor management and treatment of the waste would lead to severe environmental issues to soil, water, and air [6]. Therefore, developing better management and treatment technologies of the swine waste to reduce those pollutants becomes urgent and crucial to sustain the industry.

Microbial fuel cells (MFCs) are known as a type of bioelectrochemical reactors that may find potential uses in energy extraction from and treatment of swine wastewater due to the rich amount of degradable volatile fatty acids and high energy density available in this type of wastewater [69]. Basically, the MFCs carry out biological oxidation at anode for organic carbon, and electrochemical or biological reduction at cathode [14]. Despite a large amount of studies related to using synthetic wastewater of acetate and butyrate solution, this technology has also been tested to treat wastewater. It has been shown that

wastewater can be used as substrate for electricity generation with simultaneous reduction of COD and nitrogen concentrations [74, 75]. Among the removed organic matters, volatile fatty acids, an indicator of odorous chemicals, can be completely degraded (>99%) in MFCs at the end of a batch (260 h). The ammoniacal nitrogen removal by MFCs is another advantage among its applications in treating animal wastewater [100]. One study compared an air-cathode MFC and a two-chamber MFC for their ammonium removal performance and mechanism [100] and found that the former removed 60% ammonium in 5 d at an initial concentration of 188 mg NH_4-N/L with little accumulation of nitrite and nitrate (<1.5 mg/L). In the latter, ammonium was removed mainly by a physical way of air sparging. A lack of direct ammonium oxidation on anode was confirmed by the cyclic voltammetry test in another study, where a direct oxidation would only happen after a long period of acclimation in solution containing high ammonium concentration [56]. High strength of ammonium, e.g., a concentration of higher than 500 mg-NH_4-N/L, was found severely inhibitory to electricity generation and substrate removal in MFCs based on studies using synthetic wastewater [15]. This inhibition indicates that a careful control over ammoniacal nitrogen level is important for MFCs. Since zeolite is a natural alumino-silicate mineral, and an effective and selective sorbent for ammonium adsorption in wastewater [93, 95], its adsorption capability could be beneficial for controlling ammonium concentration, thus reducing the inhibitory effect of ammonium in MFCs.

In this study, experiments were conducted to evaluate the electricity generation and treatment performance for swine wastewater using air-cathode microbial fuel cells. For

electrochemical performance, the voltage and power output, and energy and Coulombic efficiencies were calculated. The kinetics (zero-, first- or second-order degradation) of organic matter and major nutrients changes in the MFC medium, such as COD, total ammoniacal nitrogen, nitrite, nitrate, and phosphate, were evaluated. In order to optimize the MFC performance, pretreatment methods including wastewater dilution and adsorption, and different external resistors were evaluated to determine if power output, energy and Coulombic efficiencies were improved by eliminating chemical inhibitions and by reducing external resistors.

5.2 Materials and methods

5.2.1 MFC design

Single-chamber air-cathode MFC reactors, with a total volume of 150 mL, were fabricated from clear/extruded acrylic tubes (5 cm in internal diameter and 7.5 cm in length), covered with 0.25 cm thick plexiglass acrylic endplates at both ends. The anode was made from plain carbon cloth. The air-cathode was made from 0.5 mg/cm^2 Pt-containing (10% in carbon black) carbon cloth treated with Nafion, and with polytetrafluoroethylene (PTFE) as a gas-diffusion backing layer [66]. The projected surface area of both anode and cathode was 20 cm^2. The inoculum source for MFC reactors was the anaerobic sludge obtained from a covered lagoon in Southern Research and Outreach Center (SROC) of University of Minnesota, Waseca, MN. During MFC operation, about 2 mL of distilled water was daily added to reactor to maintain liquid volume as it was lost through volatilization through cathode. A 2200 Ω resistor was

connected in the circuit as an external load. The voltage (V_{ext}) evolution across resistors was measured by voltage probes and recorded by a CR 1000 data logger (Campbell Scientific, Inc., Logan, UT). For some experiments, the anodic and cathodic potentials were monitored using standard Ag/AgCl electrodes (MF-2072, BASi, Inc., West Lafayette, IN).

In order to determine the ammonia volatilization through cathode, one of the swine wastewater-fed MFCs was slightly modified so that the air facing the outside of cathode was trapped and slowly conducted via a peristaltic pump to an Erlenmeyer flask containing 100 mL of 1 mol/L sulfuric acid solution. The final solution was analyzed for concentrations of ammonium-N (NH_4^+-N), nitrate-N (NO_3^--N), nitrite-N (NO_2^--N). A small amount of solid was observed to precipitate at the cathode side, and so it was dissolved in 100 mL of distilled water for determination of the amounts of the soluble phosphate and the inorganic nitrogen compounds.

5.2.2 MFC operation

The swine wastewater collected from a swine farm in SROC was sieved through a 1-mm mesh to remove sand, gravels, and plant residues, and stored at 4°C in a refrigerator prior to use. The prepared wastewater was then fed to MFCs as full-strength substrate, or after diluted in distilled water in order to investigate the effect of the strength of swine wastewater on MFC power generation. Dilution was made at different levels (defined as the ratio of the final volume after dilution to the initial volume) of 10, 5, 3, 2 and 1, and the diluted wastewater were fed to an MFC sequentially. Another MFC was fed with

non-diluted and two-fold diluted wastewater. When the voltage readings were stabilized after two days since the medium replacements, the corresponding polarization curves were obtained by varying external resistors on the circuits.

Another pretreatment method was adsorption of potentially inhibitory components in swine wastewater, e.g., the high strength of organic matters indicated by COD or VFA, and ammonium using natural zeolite (St. Cloud Mining Company, Tucson, AZ) or granular activated carbon (GAC; Sigma-Aldrich, St. Louis, MO). The wastewater samples were shaken for 24 h in flasks filled with a zeolite dose of 75 g/L-wastewater, or with a GAC dose of 150 g/L, or a combination of both the zeolite and GAC. The pretreated wastewater samples were then filtered through 1-mm mesh to remove the adsorbents, and the filtrates were used as substrates in different MFCs, which were operated until the generated voltages sharply declined.

In order to evaluate the effect of external resistors on MFC performance such as wastewater treatment efficiency and power generation, the MFC was fed with 8-fold diluted swine wastewater but connected to different external resistors of 2200, 330, and 33 Ω in each batch. Each experiment was repeated once.

5.2.3 Characterization of swine wastewater

Swine wastewater and MFC medium were collected and filtered through 0.25 μm syringe filters for characterization. The soluble chemical oxygen demand (COD), volatile fatty acids (VFA), ammonium-N (NH_4^+-N), nitrate-N (NO_3^--N), nitrite-N (NO_2^--N), and phosphate-P (PO_4^{3-}-P) were analyzed using a spectrophotometer (Hach DR

2800, Hach Company, Loveland, CO), pH a pHTestr10 pH meter (Oakton Instruments, Vernon Hills, IL), and conductivity an HI 8700 conductivity meter (Hannah Instruments, Woonsocket, RI).

The acetate and butyrate concentrations were quantified using a gas chromatograph (GC; CP-3800, Varian Inc., Palo Alto, CA) equipped with a flame ionization detector. A fused-silica capillary column (HP-FFAP, 30 m×0.25 mm×0.25 μm) was used. The injector and detector temperatures were set at 220°C and 250°C, respectively. The temperature in the oven was kept at 60°C for 2 min, ascended to 140°C at 8°C min^{-1}, and then kept constant at 140°C for another 6 min. Helium with a flow rate of 25 mL min^{-1} was used as the carrier gas.

5.2.4 Calculation

Electrochemical performance

The current (I) and power (P) outputs of MFC were calculated as follows:

$$I = \frac{V_{ext}}{R_{ext}} \quad (5\text{-}1)$$

$$P = \frac{V_{ext}^2}{R_{ext}} \quad (5\text{-}2)$$

The maximum power output can be calculated as follows:

$$P_{max} = {V_b}^2/(4\,R_{int}) \quad (5\text{-}3)$$

where V_b was the maximum voltage output, and R_{int} was the internal resistance, both of which were estimated from polarization curves of $V_{ext} = V_b - IR_{int}$ [88].

The total power (P_{cell}) extracted by the electrical circuit of MFC, including both the power for the electrical energy and heat, was the product of the electromotive force (E_{emf}, assumed to be 0.8 V) and the measured current:

$$P_{cell} = E_{emf} I \tag{5-4}$$

The total chemical energy [165] released from swine wastewater was estimated from the change of its COD concentration (ΔCOD) and its higher heating value (ΔH_c, -460 kJ/mol) [167]:

$$U = \Delta H_c \Delta CODV/M \tag{5-5}$$

where V was the liquid volume of an MFC reactor, and M was the COD value (g-COD/mol) of the organic matter which was expressed in the chemical formula of $CH_{1.69}N_{0.06}O_{0.51}$ with the carbon normalized to be 1 [167]. Therefore, the MFC energy efficiency ($\boldsymbol{\eta_e}$) based on the generated electrical energy, and the total energy efficiency ($\boldsymbol{\eta_t}$) based on both electrical energy and heat, were defined as follows:

$$\eta_e = \int_0^t \frac{P}{U} dt \tag{5-6}$$

$$\eta_t = \int_0^t \frac{E_{emf} I}{U} dt \tag{5-7}$$

The Coulombic efficiency, defined as the ratio of the recovered charge to the total available charge in organic matter, was calculated as follows [14]:

$$C_e = \int_0^t \frac{I}{F\Delta CODV/8} dt \tag{5-8}$$

where F was the Faradic constant (96,485 C/mol), and the number 8 denoted that 8 grams of COD could donate 1 mol of electrons.

Decay kinetics

The experimental data of COD, VFA, nitrite, nitrate, and total ammoniacal nitrogen (TAN) concentrations were fitted to the most suitable one of the following kinetic models, the pseudo zero-, first-, or second-order equations:

$$C = C_0 - kt \quad (5\text{-}9)$$

$$C = C_0 e^{-kt} \quad (5\text{-}10)$$

$$C = \frac{C_0}{1+ktC_0} \quad (5\text{-}11)$$

where C_0 was the initial concentration of a wastewater characteristic (mg/L), k was the rate constant different in each equation, and t was the reaction time (d).

5.3 Results and discussion

5.3.1 Organic matter and nutrients removal

Electricity generation, and COD and VFA degradation kinetics

An external voltage of 249 mV on average (Figure 5-1A) was generated over the 40 d period when the pre-inoculated MFCs were fed with the un-pretreated, un-diluted swine wastewater. This wastewater was initially of high strength as indicated by its high soluble COD of 12700-14300 mg/L and total ammoniacal nitrogen (TAN) of 1370-1800 mg/L. As the average voltage for the 40 mM acetate solution-fed MFC was 383 mV, there was a voltage reduction of 134 mV after the swine wastewater was induced as the MFC medium. The corresponding decrease of power output was more substantial, from 66.7 to 28.2 μW by 58%. The trend of the monitored anode and cathode potentials

(Figure 5-1B) during the first 15 d suggested that when the swine wastewater replaced the acetate solution, both anodic and cathodic overpotentials increased, by about 30 mV and 90 mV on day 15, respectively. As such, this high strength wastewater probably impacted more on activity of the cathodic catalyst of Pt/C than on that of the anodic biofilm, which was quite a surprising result because a previous study revealed a more substantial impact on anode than on cathode, as suggested by delayed acetate consumption at higher ammonium concentrations [15]. Free ammonia was found toxic to Pt catalyst in some chemical reactions, e.g., combustion [168] or low temperature oxidation of methanol [169] due to the site competition between ammonia and methanol molecules on catalyst . More seriously, oxygen reduction reaction catalyzed by Pt was reported to be inhibited by the presence of ammonia/ammonium [170], while the mechanism was not clear. Nevertheless, the removal of ammoniacal nitrogen from swine wastewater can be beneficial to MFC power generation as a result of the reduction of inhibition effect either on anode biofilm or cathode catalyst Pt. The high concentration of VFA may also impose inhibitory effect to electricity generation due to reduced microbial activity, but the effect had not been directly tested yet in MFCs. Throughout the batch operation of 40 d, the average energy and Coulombic efficiencies were 0.37% and 1.50% (Table 5-1), respectively. These values, which were not optimized in this experiment, were lower than literature values for MFCs fed with pure organic substrates, e.g., energy efficiency about 5% and Coulombic efficiency >10% [165, 166].

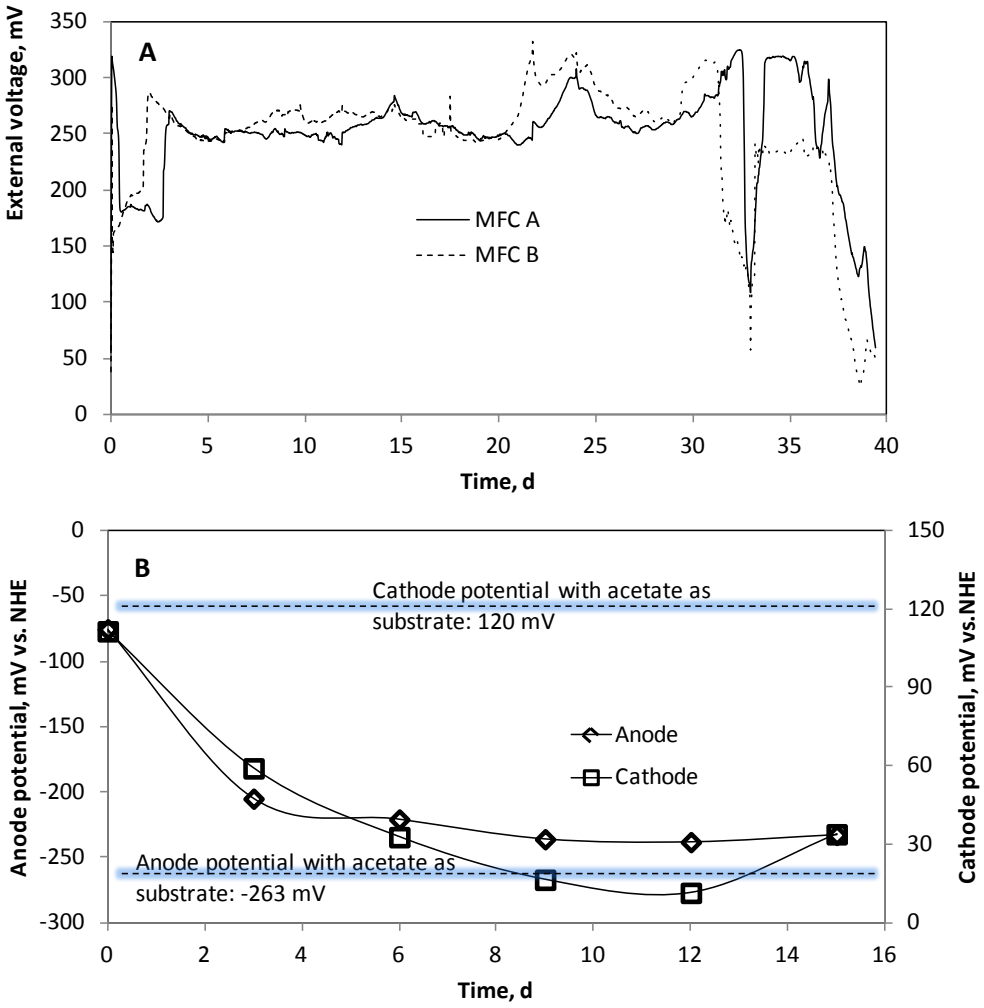

Figure 5-1. Electricity generation from swine wastewater in two identical microbial fuel cells (A) and the electrode potentials of one reactor (B).

Table 5-1. Energy and Coulombic efficiencies of two MFCs fed with swine wastewater

Parameters	MFC A	MFC B	Unit
Recovered electrical energy	101	99.0	J
Recovered charge	389	381	C
COD removal	2.15	2.10	g
Energy efficiency	0.37	0.37	%
Coulombic efficiency	1.50	1.50	%

The degradation of the soluble COD and VFA followed pseudo first-order kinetics (Figure 5-2). The time course of degradation can be categorized into two stages according to the scatterplots: during the first stage (before 30 d), the fitted curve showed a larger slope than that of the second stage (between 33 d and 48 d), illustrating that the organic matters were decomposed more quickly in the first stage. The resulting kinetic parameters were listed in Table 5-2. The half-life for COD and VFA degradation was 7.36 and 4.99 d^{-1}, respectively. After 24 d of operation, 91% of initial soluble COD was removed from the wastewater, while 92% of VFA removal was achieved in 18 d. Interestingly, the suspended biomass concentration (represented by volatile suspended solids, VSS; results not shown) of the wastewater did not increase when COD and VFA were decomposed, suggesting that the suspended sludge production in MFCs was negligible during organic matter degradation and that a substantial part of organic carbon was oxidized to carbon dioxide rather than converted to suspended biomass. It should also be noted that the prolific growth of biomass on cathode surface may take up some organic matter and nutrients, although it was not quantified in this study. The more rapid removal of VFA indicated by the shorter half-life time, especially the acetate removal evidenced in Figure 5-3, was consistent with previous studies that VFA was

less recalcitrant than other organic matter in swine wastewater [75] and that VFA was suitable substrate for microbial consortia in MFCs. Given the availability of high concentration of VFA, swine wastewater has a promising potential to provide substrate for MFC electricity generation compared to other wastewater sources [171, 172].

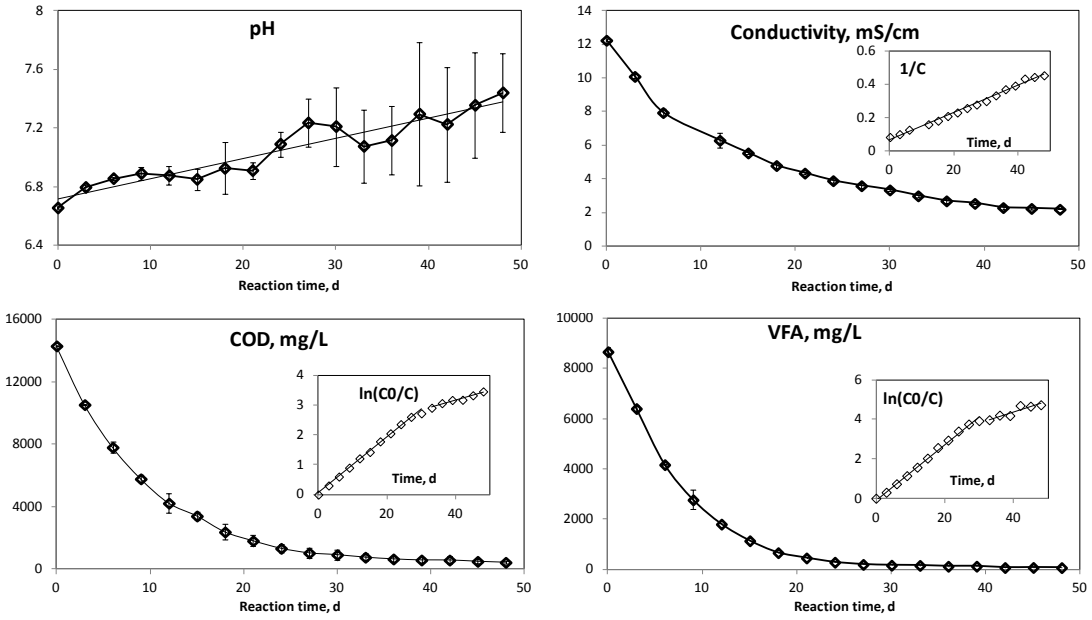

Figure 5-2. Evolution of pH, conductivity, COD, and VFA concentrations in microbial fuel cells.

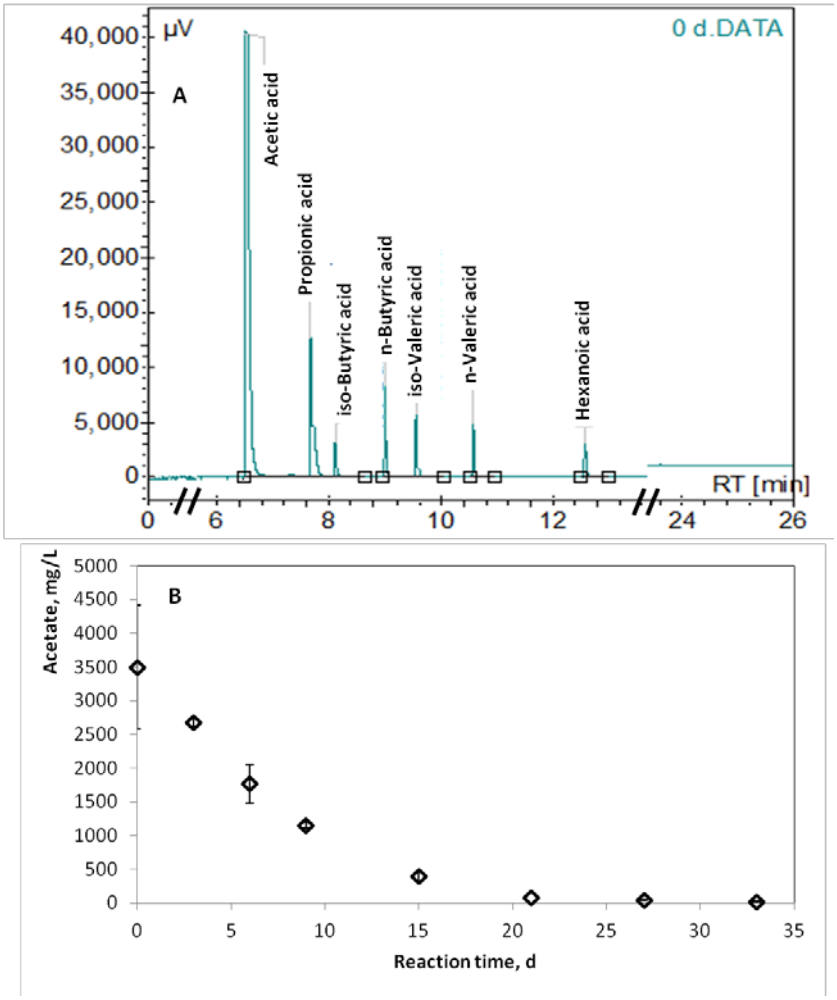

Figure 5-3. Volatile fatty acids in swine manure, and acetate degradation in microbial fuel cells.

Table 5-2. Kinetic models and parameters for organic matters and nutrients decay of wastewater in microbial fuel cells

Characteristics	**Suitable models**	**Initial value**		***k***		***$t_{1/2}$* (d) ***
pH	Linear	6.7	-	-	-	-
Conductivity	Pseudo-2nd order	12.3	mS cm^{-1}	0.0082	L mg^{-1} d^{-1}	9.96
COD	Pseudo-1st order	14300	mg L^{-1}	0.0942	d^{-1}	7.36
VFA	Pseudo-1st order	8680	mg L^{-1}	0.139	d^{-1}	4.99
NH_4^+-N	Pseudo-1st order	1370	mg L^{-1}	0.0884	d^{-1}	7.84
NO_2^--N	Pseudo-0th order	0.9	mg L^{-1}	0.0173	mg L^{-1} d^{-1}	26.0
NO_3^--N	Pseudo-1st order	2.2	mg L^{-1}	0.0301	d^{-1}	23.0
PO_4^{3-}-P	-	155	mg L^{-1}	-	-	-

*The half-time $t_{1/2}$ is a term only suitable for use in pseudo first-order kinetics, but for other kinetic equations here it means the time required for the reduction of the first half amount of an initial concentration or a characteristic.

During the operation, the pH value gradually increased in a linear manner from 6.7 to 7.4, while the conductivity of the wastewater decreased from 12.3 to 2.2 mS/cm following the pseudo second-order kinetics. This reduction in conductivity led to an increase of the Ohmic resistance of the liquid medium from about 30 to 170 Ω, which had little impact on the external voltage as it was still small compared with the 2200 Ω external resistor. But for MFCs connected to small external resistors, this decrease of the conductivity may theoretically have noticeable impact on external voltage output.

Nutrients removal and kinetics

Swine wastewater is characteristic of high concentrations of various nutrients, making its treatment more challenging. Ammonium was the major component of inorganic nitrogen compounds in swine wastewater, while the concentrations of nitrite and nitrate were otherwise as low as 1 mg/L and 7 mg/L, respectively (Figure 5-4). The TAN removal followed the pseudo first-order kinetics (Table 5-2) with 90% of the initial TAN (1370 mg-TAN/L) removed from the wastewater on day 27. The nitrite and nitrate concentrations, despite low, increased abruptly after the swine wastewater was fed to MFCs, and the decays of these compounds were slow and followed the pseudo zero- and first-order kinetics, respectively. So the oxidation of ammonium to nitrite/nitrate in swine wastewater in MFC was negligible throughout the experiment. This result was quite different from an earlier study using synthetic wastewater where nitrite accumulated to be high after acetate depletion [15], but consistent with another study using diluted swine wastewater that reported only a little amount of nitrite/nitrate accumulation, i.e., up to 11.3 mg-N/L in total [74].

The rapid ammonium removal in MFCs was impressive, and its mechanisms were diverse. As the assimilation of suspended biomass in MFCs was low, the conversion of ammonium as nitrogen source to organic nitrogen was deemed negligible. The conversion of the ammonium to nitrite or nitrate, either by biological or chemical pathways, was also unnoticeable because these concentrations were low and continuously declining after the first few days. Some abiotic processes may facilitate the ammonium removal as a result of spatial heterogeneity of the liquid body in MFCs, e.g., by ammonia volatilization on cathode proposed in a previous study [100] and by struvite formation [63]. Driven by an elevated local pH value near cathode [173] because of oxygen reduction reaction, the partial pressure of gas phase ammonia ($NH_{3\ (g)}$) increased and was finally volatized through the gas-diffusion layer of the cathode, with the equations shown as follows:

$$NH_4^+ <--> NH_{3\ (l)} + H^+ \quad (5\text{-}12)$$

$$NH_{3\ (l)} <--> NH_{3\ (g)} \quad (5\text{-}13)$$

So after 42 d operation, the analysis of the air captured from the outside of the MFC cathode in sulfuric acid solution detected an amount of 13.6% of the initial TAN in swine wastewater. The balance of the TAN loss may be a result of assimilation, and N_2 formation due to nitrification-denitrification process which was not quantified in this study. For comparison, anaerobic digestion of swine wastewater without MFC process had a stable TAN concentration but a little reduction due to biogas volatilization. Anaerobic digestion of synthetic wastewater (10 mM of sodium acetate and 10 mM of sodium chloride) resulted in a TAN concentration reduction in the two days and

approximately recovered to the initial level in the next three days, as a result of sequential assimilative and dissimilative metabolism of microorganisms. The idea of collecting ammonia through gas-diffusion or gas-permeable membrane, mostly PTFE materials, was tested in air cleaning [174] and livestock wastewater [175]. Compared to the direct use of the membrane, an obvious advantage of using MFC is the local pH elevation in vicinity of cathode, which accelerated ammonia volatilization. So MFC technology demonstrated its promising use in complete extraction of ammonia from wastewater. The released ammonia then can be captured by sulfuric acid to generate ammonium sulfate [$(NH_4)_2SO_4$] solution that can be used as a fertilizer provided suitable concentrations. However, since the recovered ammonia only accounted for 13.6% of the TAN loss, some modifications are needed to polish this process. For example, decreasing the thickness of the cathodic biofilm, which imposes resistance to ammonium transfer to cathode surface, may increase the ammonia flux through the diffusion layer. Alternatively, increasing the ratio of the surface area of the cathode to liquid volume will theoretically increase the flow of ammonia through the diffusion layer.

Phosphate was gradually removed in the first 10 d operation, and its concentration thereafter remained quite stable, but the removal was far from completion even after 42 d operation, resulting in PO_4^{3-}-P concentration of 94 mg/L or a 39% reduction of the initial concentration of 155 mg/L. The removal was realized by phosphate salt precipitation and struvite formation on cathode [64]. The solid collected on the air-facing side of the cathode was dissolved in water for analysis, and it collected 95.5% of the removed phosphate, and also 1.4% of the removed inorganic nitrogen compounds.

Even though MFC can play an effective role in TAN removal for swine wastewater, it is not very efficient in phosphate removal. If the solid precipitation or struvite formation on cathode can be accelerated and improved by optimizing reaction conditions, the phosphate removal may be improved as well. The precipitate needs further analysis by X-ray diffraction (XRD), which will qualitatively determine the type of the crystalline after comparing to synthesized struvite and other salt samples [176].

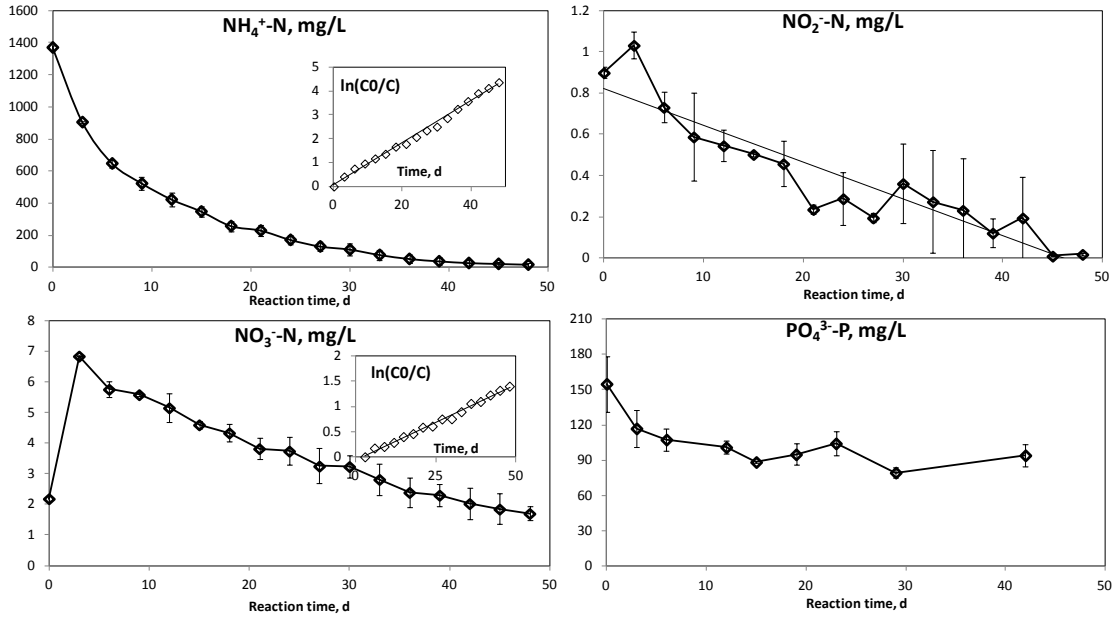

Figure 5-4. Nutrients (ammonium, nitrite, nitrate, and phosphate) removal in microbial fuel cells.

5.3.2 Effects of dilution

It was mentioned above that the MFC fed with swine wastewater generated less external voltage than that fed with acetate solution, due to the increased electrode overpotentials as a result of certain types of inhibition induced by swine wastewater (Figure 5-1). To clarify this, swine wastewater diluted at different ratios (dilution factors between 2 and

10) was used as MFC substrate to see if the power output could be increased. The soluble COD, VFA, conductivity (as low as 1.8 mS/cm) and nutrients concentrations were proportionally decreased when the wastewater was diluted, and the resulting pH values were between 6.5 and 6.8.

Figure 5-5A showed the polarization curves of an MFC fed with wastewater of different dilution factors in a descending order. The diluted swine wastewater, from 10 to 2 folds, generated comparable power output at 2.2 kΩ, with a decrease of power from 50 to 40 μW when less diluted; however, when the undiluted wastewater was used as the substrate, the power output was abruptly reduced to only 11 μW, which was only about 20% of the power generated in the 10-fold diluted wastewater and clearly demonstrated an inhibitory effect on power generation by the high strength swine wastewater. The similar effect happened to the maximum power output, which was determined at an optimized external resistor according to polarization curves. Again, as free ammonia was found toxic to anodic bacteria [15] and also possibly to Pt-catalyst on cathode, the high TAN (1370 mg/L) in swine wastewater can be attributed to the occurrence of inhibition to electricity generation. High concentration of VFA, especially the propionate, an anion of three-carbon volatile fatty acid, showed inhibition to methanogens as a result of end-products inhibition [177]; however, it was not clear if the VFA displayed any toxicity to MFCs here. Dilution of the wastewater reduced the inhibition to electricity generation, but also increased the amount of the waste stream and, consequently, the burden of treatment.

This finding that a lower substrate concentration stimulated power generation was inconsistent with previous results based on acetate or swine wastewater [74, 165]. Assuming there are three factors playing roles in the power output, i.e., TAN inhibition, Ohmic resistance of the solution, and the external resistors, these contradictory results can be explained by the overall effects of the varying levels of these three influential factors. Simply put, when the value of the external resistor was comparable to or less than the Ohmic resistance of the solution (depending on the solution conductivity or dilution factors), the more diluted medium generated less external voltage and power as more voltage was distributed to the Ohmic resistance; however, when the external resistor was much higher than the Ohmic resistance, most of the voltage was distributed to the external resistor, so the inhibition of ammonia on the overall voltage was reflected on the reduced external voltage and power.

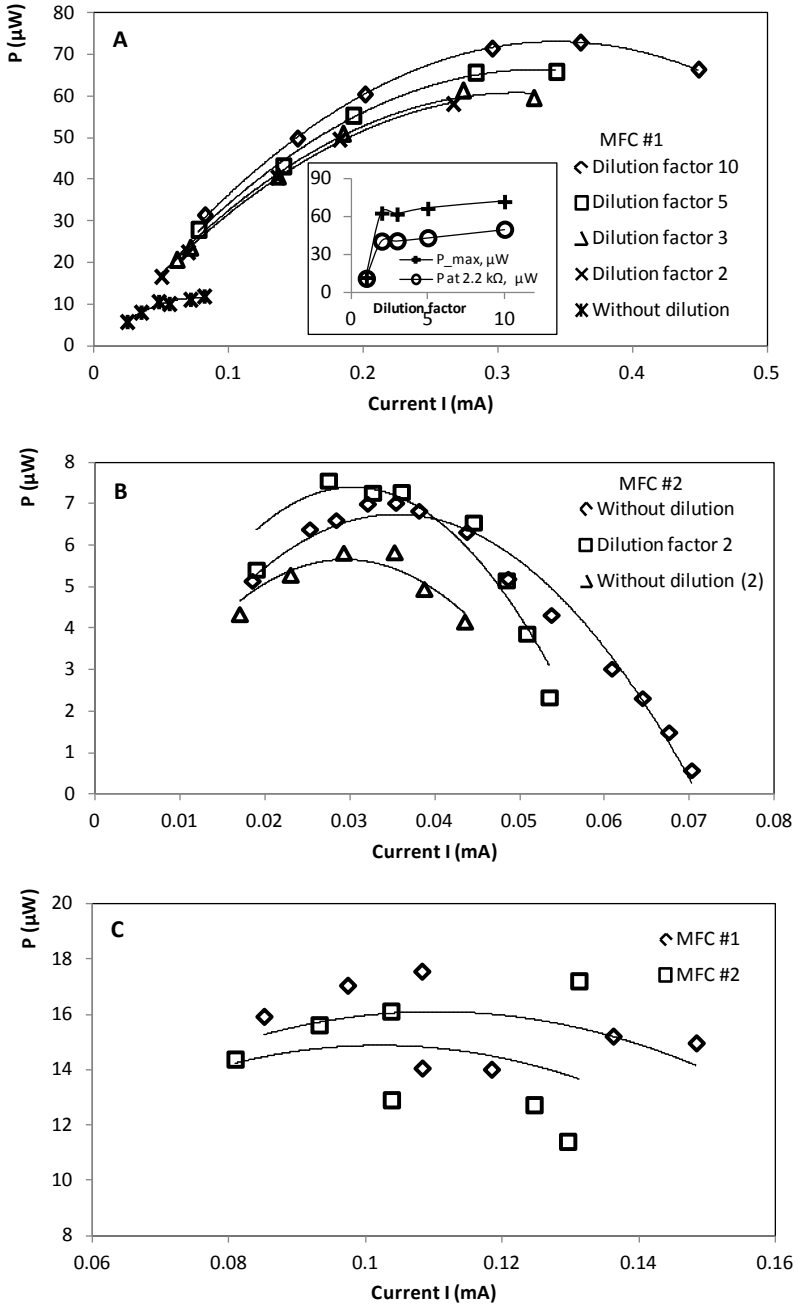

Figure 5-5. Polarization curves of microbial fuel cells fed with swine wastewater of different dilution factors.

5.3.3 Effects of external resistors

The external resistor was another factor that might impact the MFC performance, so this study evaluated MFCs which were fed with the same diluted swine wastewater (a dilution factor of 8) but sequentially operated at external resistors of 2200, 330, and 33 Ω (Figure 5-6). The average internal resistance of these two reactors, regardless of the external resistors, was 547 Ω. As expected, the lowest external resistor (33 Ω) generated the largest electrical current, and the external resistor (330 Ω) closest to the internal resistance produced the largest power (Table 5-3). The energy efficiency of the MFC connected to 330 Ω was 1.10%, the highest among the three. However, the total energy efficiency achieved was highest (7%) with the lowest external resistor of 33 Ω. Similarly, the highest Coulombic efficiency was achieved (8.96%) also with the lowest resistor. As more chemical energy was converted to electricity and heat for lower resistors, the substrate was consumed at higher rates. As a result, the required operation time of MFCs was shortened by 5.3% from 4.33 to 4.10 d when the 2200 Ω external resistor was changed to 33 Ω, demonstrating a little higher rate of organic matter removal. The further reduction of the external resistor, e.g., to 0 Ω as in a short circuit, would not substantially reduce the operation time because the internal resistance would override the external resistor. Smaller external resistors of MFCs were previously observed being able to expedite the glucose degradation [161]. The effect of reducing external load was also found useful in electron donor removal. When nitrate was used as the electron donor, the lower external resistor of 10 Ω removed all nitrate in 25 h while the higher external resistor of 1000 Ω removed only 38% [111]. It can be concluded

from those results that although the power and energy efficiency decrease with a lower external resistor, the wastewater treatment performance is expedited. Even though it was not experimentally demonstrated, a reduction in internal resistance should also improve MFC performance in both energy efficiency and wastewater treatment.

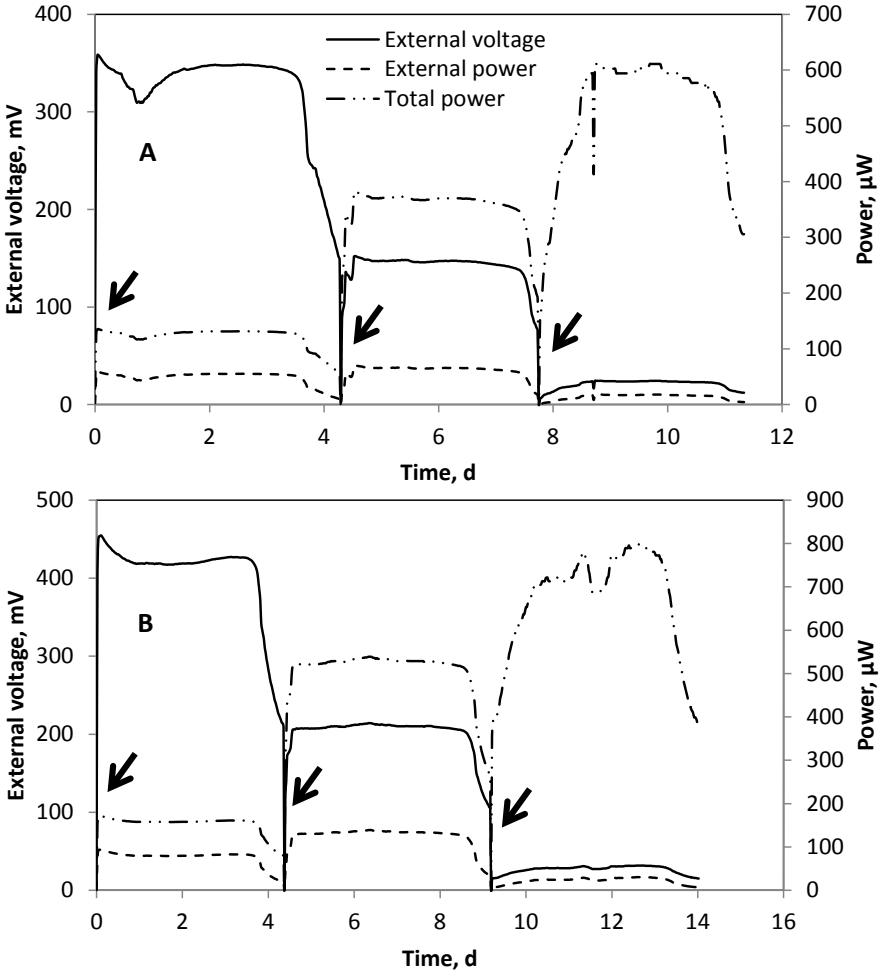

Figure 5-6. External voltage and power of microbial fuel cells fed with swine wastewater at different external resistors.

Table 5-3. Effects of external resistors on MFCs performance

External resistor	Voltage	Power	Reaction time	Efficiencies*, %		
Ω	mV	μW	d	Energy	Cell energy	Coulombic
2200	384	67	4.33	0.73	1.62	2.07
330	179	100	4.14	1.10	5.00	6.40
33	28	28	4.10	0.21	7.00	8.96

*The efficiencies were calculated based on the COD concentration of the diluted swine wastewater.

5.4 Conclusions

This study modeled the kinetic data of swine wastewater characteristics in MFCs, including conductivity, COD, VFA, total ammoniacal nitrogen (TAN), nitrite, nitrate, and phosphate concentrations. The removals of VFA and TAN had the half-life times of 4.99 and 7.84 d, respectively. Among the removed TAN, 13.6% was recovered from the evaporated air outside of MFC cathode, indicating its potential use for ammonium recovery from animal wastewater. The mechanism for phosphate removal was principally the salt precipitation from cathode, and needed improvement as the removal was far from completion. MFC with an external resistor of 2.2 kΩ and fed with raw swine wastewater generated relatively small power (28.2 μW), energy efficiency (0.37%) and Coulombic efficiency (0.15%). The main reason for the impaired performance was the inhibitory effects associated with TAN on Pt activity and VFA on anodic biofilm activity. Diluted swine wastewater, with a dilution factor of 2 or higher, dramatically improved the power generation as the inhibitory effect was reduced. Smaller external resistor in the circuit promoted the organic matter degradation and shortened the required reaction time in the batch mode.

Chapter 6. Selective Sorption of Ammonium and Volatile Fatty Acids from Swine Wastewater: Kinetics, Equilibrium, and Improvement in Electricity Generation

6.1 Introduction

Swine wastewater (SW) is a relatively concentrated wastewater source in both chemical oxygen demands (COD) and total ammoniacal nitrogen (TAN) compared to most other wastewater sources such as domestic wastewater, landfill leachate and grey water. When biological treatment processes are adopted for SW treatment, the high-strength level of contaminants can inhibit microbial activities and result in an impaired performance. For example, ammonia inhibition can happen to anaerobic digestion. A 50% reduction of methane generation may occur due to the TAN concentration exceeding 1700 mg/L [178]. Excessive ammonia (TAN higher than 5000 mg/L) was also reported to delay biohydrogen production in dark fermentation [179]. For microbial fuel cells, the inhibition to the power density was observed for TAN levels of 1000 mg/L [15] and 3500 mg/L [180]. Despite not being completely removed in pretreatment, partial reduction of TAN to 1000 mg/L, regardless of the mitigation methods used, is beneficial to the subsequent biological processes.

There are several options for ammonium removal from swine wastewater, such as air stripping, nitrification-denitrification, anammox, and sorption [95]. Among these methods, ammonium sorption can be a superior way because an excessive loading of TAN will not damage reactor systems, and it is a rapid and reversible process: the

ammonium absorbed can be released [93] to the aqueous phase again when its counterpart in water is consumed. Another advantage of sorption is that this process can be easily incorporated into other biological processes through packed-bed columns or teabags [96, 181].

Zeolite is a natural alumino-silicate mineral, found to be an effective and selective sorbent for ammonium in wastewater [93-95]. The sorption is a result of its building block, a tetrahedron structure, where a silicon or aluminum atom is located at the center and four atoms of oxygen outside. The substitution of Si^{4+} by Al^{3+} leaves the structure a negative charge, and thus allows cation exchange and sorption with the external environment. The ammonium sorption performance depends on factors such as chemical components of zeolite, modification methods used, initial ammonium concentrations, presence of other competing cations, the amount of zeolite added, reactor types, pH, temperature, and reaction time. In a sorption study based on batch operation of stirred shakers, 4.5 mg/g of sorption capacity was achieved in 24 h reaction for synthetic wastewater containing 500 mg/L initial TAN [96]. The Langmuir model fitting showed a maximum sorption capacity up to 10.84 mg/g. Another study using high TAN (4500 mg/L) swine wastewater also revealed a 46% ammonium removal within 24 h with a zeolite loading of 5 g/25 mL [98]. All these results show a possibility of using zeolite as sorbents to reduce ammonium nitrogen for swine manure.

Literature survey shows that studies on zeolite for ammonium sorption in swine wastewater are relatively rare [98, 181], let alone studies on isotherm, kinetics, and thermodynamics regarding this high-strength wastewater source. The objectives of this

study were to evaluate the performance of zeolite for ammonium removal in high-strength swine wastewater at various experimental conditions, e.g., at different dosages, TAN concentrations, pH, and temperatures, and with the addition of granular activated carbon (GAC). Sorption isotherm, kinetics, and thermodynamics were investigated for the first time in literature to fully understand ammonium sorption for swine wastewater treatment. Finally, the selectively treated swine wastewater by zeolite and GAC were fed into MFC to see its improvement on electricity generation

6.2 Materials and methods

6.2.1 Natural zeolite and GAC

Natural zeolite used in this study was bought from St. Cloud Mining Company, Tucson, AZ. It was a granular product prepared from natural minerals, with 8-14 mesh, which corresponded to 1.40-2.38 mm of sieve size. The major oxides components were SiO_2 (70%) and Al_2O_3 (12%). Granular activated carbon (GAC), with 8-20 mesh, was procured from Sigma-Aldrich (Sigma-Aldrich, St. Louis, MO).

6.2.2 Swine wastewater

The swine wastewater (SW) was collected from a temporary container in a swine barn located in Waseca, MN, which was then screened through 1-mm sieve and kept in a refrigerator at 4 ^{o}C before use. The initial TAN concentrations of the swine wastewater were between 1310 and 2080 mg/L.

6.2.3 Experimental design for batch studies

Different doses of zeolite were added into 40 mL of SW in 125-mL flasks, from 1 g to 6 g with 1 g increment. The flasks were then shaken on a continuously stirred mechanical shaker for 12 h at room temperature, followed by 36 h settling. The initial and final COD and ammonium nitrogen concentrations were evaluated using a spectrophotometer (Hach DR 2800, Hach Company, Loveland, CO).

For adsorption kinetics studies, 3 g zeolite in 40 mL SW was added to a flask with 250 mL SW. The flask was then subject to shaking in a mechanical shaker reactor, and the supernatant was sampled for analysis at 5, 10, 20, 30, 45, 60, 90, 120, 180, 240, and 300 min.

In order to investigate the effects of initial ammonia concentration, pH, and temperature on ammonia removal, sorption experiments were conducted at different dilution factors (1, 2, 4, 8, and 16), initial pH values (5, 6, 7, 8, and 9), temperatures (25 °C, 35 °C, 45 °C, and 55 °C), and filtration pretreatment (filtered through sieves of 1, 0.25, 0.15, and 0.075 mm).

6.2.4 Analysis for sorption kinetics

Multiple steps or mechanisms occur in sorption processes, so it is necessary to evaluate and choose suitable kinetic models. Four kinetic models, including pseudo first-order, pseudo second-order, intra-particle diffusion, and Elovich equations, were chosen to describe the sorption processes of ammonium onto zeolite. The experimental data were

fitted to these models for kinetic parameter estimation. The pseudo first-order model [182] is widely used for adsorption kinetics, and its equation is given as follows:

$$\frac{\mathrm{dq_t}}{\mathrm{dt}} = k_f(q_e - q_t) \tag{6-1}$$

After integrating the above equation by applying boundary condition (q_t= 0 at t = 0), it can be arranged and linearized as:

$$\ln(q_e - q_t) = \ln q_e - k_f \mathrm{t} \tag{6-2}$$

where q_t (mg/g) is the adsorbed amount of adsorbate at time t, q_e is the equilibrium adsorption capacity (mg/g), and k_f is the rate constant (h^{-1}) of the pseudo first-order kinetic model.

The pseudo second-order model [183] assumes that adsorption follows a second-order reaction:

$$\frac{\mathrm{dq_t}}{\mathrm{dt}} = k_s(q_e - q_t)^2 \tag{6-3}$$

After integrating the above equation and applying boundary condition, it can be arranged in a linear form:

$$\frac{t}{q_t} = \frac{1}{k_s q_e^2} + \frac{t}{q_e} \tag{6-4}$$

where k_s is the rate constant (g mg^{-1} h^{-1}) of the pseudo second-order kinetic model. Please note that both q_e values of the first- and second-order models were chosen to be the sorption capacities of the very last samples during kinetic experiments.

The experimental data were also fitted to intra-particle diffusion model [95], which is expressed as follows:

$$q_t = k_d t^{1/2} + C \quad (6\text{-}5)$$

where k_d is the rate constant (mg g^{-1} $h^{-1/2}$) of intra-particle diffusion, and C is the intercept.

The Elovich equation [95] was expressed as follows:

$$\frac{dq_t}{dt} = \alpha e^{-\beta q_t} \quad (6\text{-}6)$$

The linear form of the Elovich model is as follows:

$$q_t = (1/\beta)\ln(\alpha\beta) + (1/\beta)\ln t \quad (6\text{-}7)$$

where α is the initial adsorption rate (mg g^{-1} h) and β is a parameter (g mg^{-1}) considered to be related to desorption constant [184].

6.2.5 Analysis for adsorption isotherms

Parameters, such as the maximum adsorption capacity and energy constant, are also important to understand sorption process and essential for designing sorption-based reactors. These parameters can be determined in sorption isotherms studies which model the amount of absorbed sorbate in sorbents and sorbate concentrations in solution at equilibrium. Various empirical or theoretical models were considered in this study for their adequacies for modeling ammonium sorption. The Freundlich model is one of the most widely used empirical models for sorption, expressed as follows:

$$q_e = K_F C_e^{1/n} \quad (6\text{-}8)$$

The linearization of the Freundlich [185] model is as follows:

$$\ln q_e = \ln K_F + \frac{1}{n} \ln C_e \quad (6\text{-}9)$$

where q_e is the amount of substrate sorbed (mg/g), K_F is the Freundlich absorption constant (L/mg) related to bonding energy, C_e is the equilibrium sorbate concentration in solution (mg/L), and $\frac{1}{n}$ is the heterogeneity factor.

The Langmuir model [186] is represented as follows:

$$q_e = \frac{q_m K_L C_e}{1 + K_L C_e} \quad (6\text{-}10)$$

The linearization of the Langmuir model is as follows:

$$\frac{1}{q_e} = \frac{1}{q_m} + \frac{1}{q_m K_L C_e} \quad (6\text{-}11)$$

where q_m is the maximum adsorption capacity (mg/g), and K_L is the Langmuir constant relating to binding energy (L/mg).

The Temkin model is given as follows:

$$q_e = \frac{RT}{b} \ln (K_T C_e) \quad (6\text{-}12)$$

The linear form of the Temkin equation is as follows:

$$q_e = \frac{RT}{b} \ln K_T + \frac{RT}{b} \ln C_e \quad (6\text{-}13)$$

where $\frac{RT}{b}$ is a term relating to the heat of sorption, R is the ideal gas constant (8.314 J mol^{-1} K^{-1}), T is the absolute temperature (K), and K_T is the binding constant (L/mg) relating to binding energy.

In order to calculate mean sorption energy, the Dubinin-Radushkevish (D-R) model [187] was used for some sets of isotherm data:

$$q_e = q_m e^{-\beta' \varepsilon^2} \quad (6\text{-}14)$$

where q_m is the maximum adsorption capacity (mg/g), β' is a constant related to sorption energy (mg^2 J^{-2}), and ε is the Polanyi potential (defined as $\varepsilon = RTln(1 + \frac{1}{C_e})$). Note that sorbate concentration needs converted to mol unit for this model. Through this model the mean sorption energy (E) of unit amount of sorbate separation from solution to solid can be calculated as follows:

$$E = \frac{1}{\sqrt{2\beta'}} \quad (6\text{-}15)$$

6.2.6 Analysis of adsorption thermodynamics

Thermodynamic parameters, including the change of the Gibbs free energy of adsorption (ΔG^o, in kJ/mol), enthalpy (ΔH^o, in kJ/mol), and entropy (ΔS^o, in kJ/mol/K), can be obtained by sorption constants calculated from Langmuir or Temkin isotherm models [95]:

$$\Delta G^o = -RTlnK \quad (6\text{-}16)$$

$$\Delta G^o = \Delta H^o - T\Delta S^o \quad (6\text{-}17)$$

where K (L/mol) is the sorption constants.

6.2.7 Statistic analysis

When experimental data were transformed and fitted to linearized models, the lease square method was used to determine a best fit. This method minimizes the objective function of the residual sum of squares (RSS; or sum of squared errors, abbreviated as SSE or ERRSQ):

$$\mathrm{RSS} = \sum_{i=1}^{n}(y_{cal,i} - y_{exp,i})^2 \quad (6\text{-}18)$$

where $y_{cal,i}$ is the i-th estimated value and $y_{exp,i}$ is the i-th experimental value. The coefficients of determination (r^2) were calculated as follows:

$$r^2 = \frac{\sum_{i=1}^{n}(y_{cal,i}-\bar{y})^2}{\sum_{i=1}^{n}(y_{cal,i}-\bar{y})^2+\sum_{i=1}^{n}(y_{exp,i}-\bar{y})^2} \quad (6\text{-}19)$$

where $\bar{y}$ is the average value of the experimental variable. Non-linear regression was also performed in order to avoid the distortion of error functions during the data transformation in linearized models, and here χ^2 test was adopted as an error function for non-linear regression:

$$\chi^2 = \sum_{i=1}^{n}\frac{(y_{cal,i}-y_{exp,i})^2}{y_{exp,i}} \quad (6\text{-}20)$$

Another error function, the hybrid fractional error function (HYBRID), was used to compare different regression models. The advantages of this error function are that it improves the fit of RSS at low values of dependent variable values, and that it accounts for the degrees of freedom in its definition [188]:

$$\text{HYBRID} = \frac{100}{n-p}\sum_{i=1}^{n}\frac{(y_{cal,i}-y_{exp,i})^2}{y_{exp,i}} \quad (6\text{-}21)$$

where p is the number of parameters in a model. For the same set of data, HYBRID and χ^2 test of non-linear regression would yield the same result about the order of the model preference, because the degrees of freedom (n - p) of the three regression models were identical.

6.3 Results and discussion

6.3.1 Sorption kinetics of TAN on zeolite

The porous morphology of natural zeolite was revealed by scanning electron microscopy (Figure 6-1A), and this structure was considered facilitating the sorption process. The sorption of TAN in SW on zeolite continued for about 5 h until it was complete (Figure 6-2). This result showed a longer sorption time of ammonium than literature values, e.g., 1.3 h [93] and 2 h [95], which were based on either synthetic wastewater or wastewater with substantially lower ammonium concentrations. When the ammonium concentration increased in real wastewater in which other contaminants were also in presence, the time to reach equilibrium was elongated.

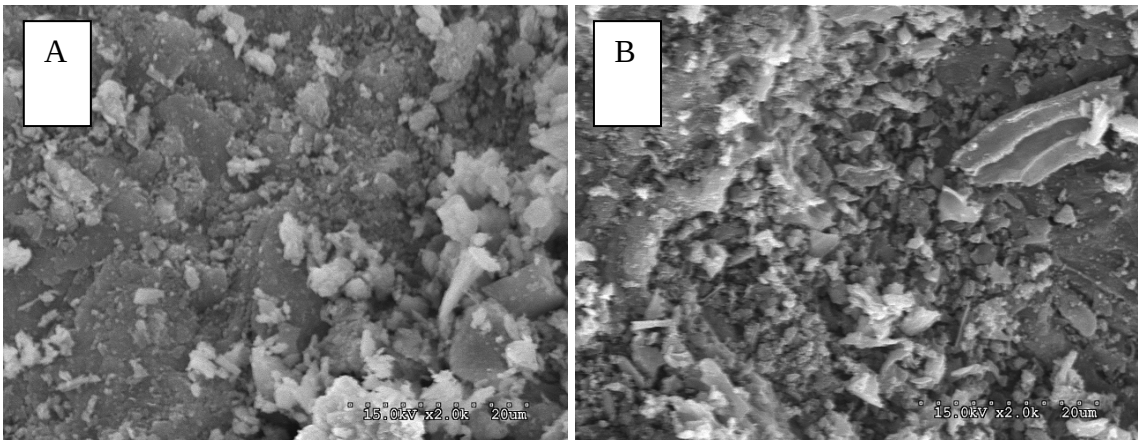

Figure 6-1. Scanning electron microscopy (SEM) of natural zeolite (A) and activated carbon (B).

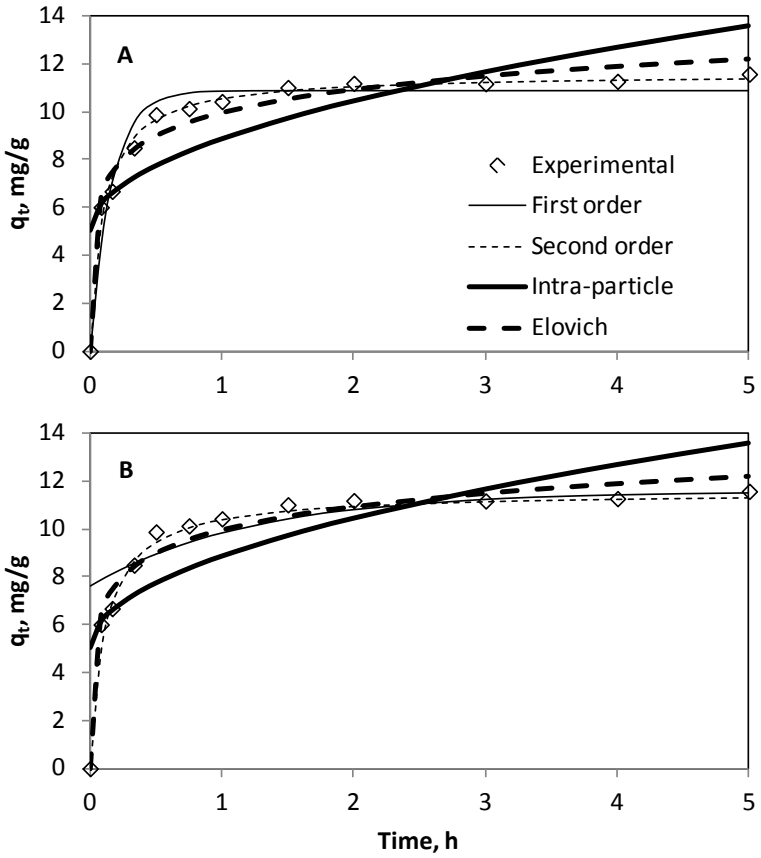

Figure 6-2. Regression analysis of ammoniacal sorption on zeolite. A, results of non-linear regression; B, results of linear regression.

The four chosen kinetic models, including the pseudo-first-order, pseudo-second order, intra-particle diffusion, and Evolich, fitted experimental data with varying accuracies, shown in Figure 6-2 and Figure 6-3. For each model, both linear and non-linear regression methods were examined to fit experimental data with better estimated parameters. The rate constants, equilibrium sorption capacities, and other estimated parameters were listed in Table 6-1. The χ^2 values of the non-linear regressions indicate that the pseudo-second-order model best described the sorption process among the four models (χ^2=0.0899), followed in a descending order by Elovich, pseudo-first-order, and intra-particle diffusion models, which agreed well with the results of the linear regression. The non-linearly estimated equilibrium sorption capacity, q_e, was 10.85 mg g^{-1} by the pseudo-first-order and 11.60 mg g^{-1} by the pseudo-second-order model. The latter was more close to the experimental value of 11.58 mg g^{-1}. Under these sorption capacities and the zeolite dose (75 g L^{-1} wastewater), about 800 mg L^{-1} ammonium nitrogen can be removed from the initial wastewater.

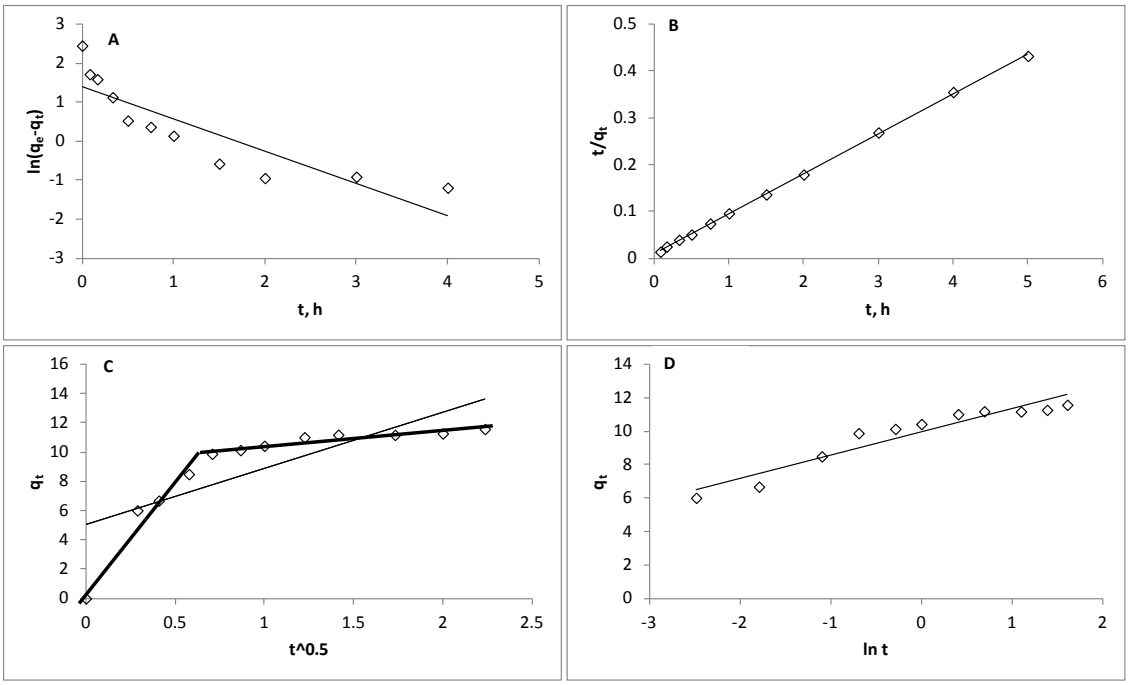

Figure 6-3. Linear regression of ammoniacal nitrogen sorption. A, pseudo-first-order kinetic model; B, pseudo-second-order kinetic model; C, intra-particle diffusion model; and Elovich model.

Table 6-1. Results of regression analysis using various kinetic models for ammonium sorption on zeolite

		Pseudo-1st order		**Pseudo-2nd order**		**Intra-particle**		**Elovich**	
Non-linear	Parameters	k_f, h^{-1}	6.28	k_s, g mg^{-1} h^{-1}	0.861	k_d, g mg^{-1} h^{-1}	3.83	α, mg g^{-1} h	1800
		q_e, mg^{-1} g	10.85	q_e, mg^{-1} g	11.60	C, mg g^{-1}	5.01	β, g mg^{-1}	0.72
	χ^2	0.391		**0.0899**		6.05		0.184	
	HYBRID	8.06		**1.96**		21.9		4.11	
Linear	Parameters	k_f, h^{-1}	0.8209	k_s, g mg^{-1} h^{-1}	0.768	k_d, g mg^{-1} h^{-1}	3.83	α, mg g^{-1} h	1800
				q_e, mg^{-1} g	11.71	C, mg g^{-1}	5.01	β, g mg^{-1}	0.72
	r^2	0.767		**0.999**		0.635		0.909	
	HYBRID	12.1		**2.70**		21.9		4.11	

The suitability of the pseudo-second-order model for ammonium sorption was previously reported elsewhere [183, 189], which indicated that the sorption overall followed a second-order reaction. However, it cannot be concluded that there is no diffusion-controlled step in sorption. The agreement between experimental data and the

model can be a mathematical coincidence [93] due to the severe simplicity of the model, and more importantly, this model does not elucidate the mechanisms of SW ammonium sorption on zeolite. As the intra-particle diffusion model poorly fitted to experimental data, the assumption of this model may not really hold in ammonium sorption, so the intra-particle diffusion may not be the sole rate-controlling step. In fact, when the linear regression curves were examined (Figure 6-3C), it can be found through the intra-particle diffusion model that there were two separate stages happening: the fitting curve for the data before 0.5 h passed the origin, indicating that the intra-particle diffusion dictated the sorption; afterwards, the curve was still straight but the intercept C increased, indicating that the surface diffusion is the rate limiting step. Similar results were observed for other sorbents and sorbates in liquid/solid sorption studies [95, 190].

The different regression models and methods yielded substantially different HYBRID values. The smaller HYBRID values corresponded to smaller χ^2 values in non-linear regression and larger r^2 values in linear regression. For both the pseudo-first- and second-order models, the non-linear regression resulted in lower HYBRID values than linear regression. For the intra-particle diffusion and Evolich models, linear and non-linear regressions generated the same HYBRID. So when HYBRID was used as a criterion for choosing better model parameters, non-linear regression performed better than linear regression. This finding is in accordance with literature reports in which non-linear regression was recommended to achieve better fitting [191], as the data transformation for the linear regression usually implicitly distorted error functions.

Besides ammonium ion removal, phosphate-P in swine wastewater was substantially absorbed by zeolite (Figure 6-4). After 5 h reaction, 46% of initial phosphate-P was removed, reduced from 342 to 186 mg/L with an equilibrium adsorption capacity of 2.08 mg/g. Volatile fatty acids and COD were also slightly reduced by a percentage of 6% and 5%, respectively. As a result of ion removal, conductivity of the wastewater was decreased from 12.7 to 10.8 mS/cm; pH value was meanwhile increased from 6.79 to 7.37, while it was still under the tendency of a slight increase.

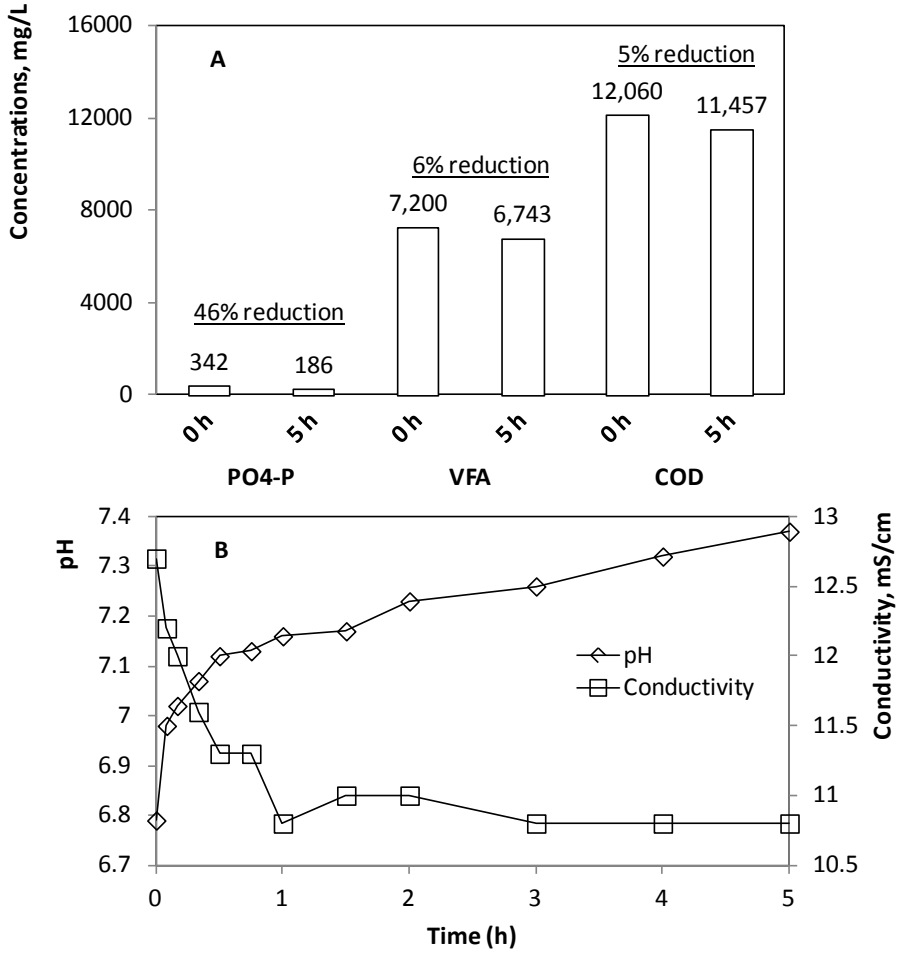

Figure 6-4. Removals of other components (A: phosphate-P, volatile fatty acids, and COD) of swine wastewater by zeolite addition and the changes of pH and conductivity (B).

6.3.2 Sorption equilibrium of ammonium sorption on zeolite

The results of linear and non-linear regressions for ammonium sorption on zeolite at 298 K (25 °C), mainly in terms of sorption constants and adsorption capacities, were tabulated in Table 6-2. All the three isotherm models well fitted experimental data regardless of the regression analysis methods used. The Langmuir model was suggested to be the most suitable one as indicated by its smallest χ^2 value (0.0188) and greatest r^2 (0.995) value, followed in a descending order by Temkin and Freundlich models. However, when the results of linear regression were examined by HYBRID, the Temkin model achieved the best fit (0.962) among the three models. Similar to the kinetics studies, non-linear regression produced HYBRID values smaller than those generated by linear regression, indicating non-linear regression can be a more accurate fitting method [192].

Table 6-2. Results of regression analysis using various isotherm models for ammoniacal nitrogen sorption on zeolite at 298 K

		Freundlich		**Langmuir**		**Temkin**	
Non-linear	Parameters	K_F *	1.63	K_L, L mg^{-1}	0.00104	K_T, L mg^{-1}	0.00805
		n	1.94	q_m, mg g^{-1}	34.2	b_1, mg mol g^{-1} J^{-}	296
	χ^2	0.058		**0.0188**		0.0193	
	HYBRID	2.89		**0.935**		0.962	
Linear	Parameters	K_F	0.405	K_L, L mg^{-1}	0.00098	K_T, L mg^{-1}	0.00806
		n	1.84	q_m, mg g^{-1}	35.3	b_1, mg mol g^{-1} J^{-}	296
	r^2	0.980		**0.995**		0.991	
	HYBRID	2.90		0.968		**0.962**	

Isotherm models elucidate the sorbate distribution between liquid and solid phases at equilibrium, and the model parameters can provide information about binding energy

and binding capacity. The non-linear regression result of Freundlich parameter K_F (mg g^{-1} (L mg^{-1})$^{1/n}$) indicated that 1.63 mg TAN could be absorbed by every gram of zeolite for a unit increase in equilibrium concentration. The n value (1.94) greater than 1 indicated a normal Langmuir isotherm [193]. The Langmuir sorption constant K_L (0.00104 L mg^{-1}) indicated the affinity of the ammonium sorption on zeolite, and the maximum sorption capacity q_m (34.2 mg g^{-1}) represented the amount of the saturated monolayer ammonium on unit weight of zeolite at equilibrium. The parameters of Temkin models were also listed in Table 6-2. Similar to the sorption constant in the Langmuir model, the Temkin sorption constant K_T (0.00805 L mg^{-1}) indicated the affinity of the ammonium sorption to zeolite, and can be used to calculate the change of Gibbs free energy.

The non-linear regressions of the three models were further examined for the sorption isotherm data at higher temperatures, i.e., 308, 318, and 328 K, with the model parameters listed in Table 6-3. At these higher temperatures, all these models fitted well to the experimental data (Figure 6-5), while the Freundlich model slightly outperformed the other two. The higher the temperature, the smaller the adsorption constants are (K_F, from 1.63 to 1.16 mg g^{-1} (L mg^{-1})$^{1/n}$; K_L, from 0.00104 to 0.000471 L mg^{-1}; and K_T, from 0.00805 to 0.00517 L mg^{-1}), and the larger the maximum sorption capacity (q_m, from 34.2 to 52.0 mg g^{-1}). These trends of the change of adsorption constants and maximum sorption capacities were not in agreement with the results from a previous study of ammonium sorption in grey water using natural zeolite [95], and this discrepancy will be further discussed in the next section. The trend of the change of the maximum sorption

capacity was similar to that of the methylene blue adsorption onto zeolite [189]and the trend of the change of the sorption constant was similar to the result of the dye sorption onto cashew nut shell [190].

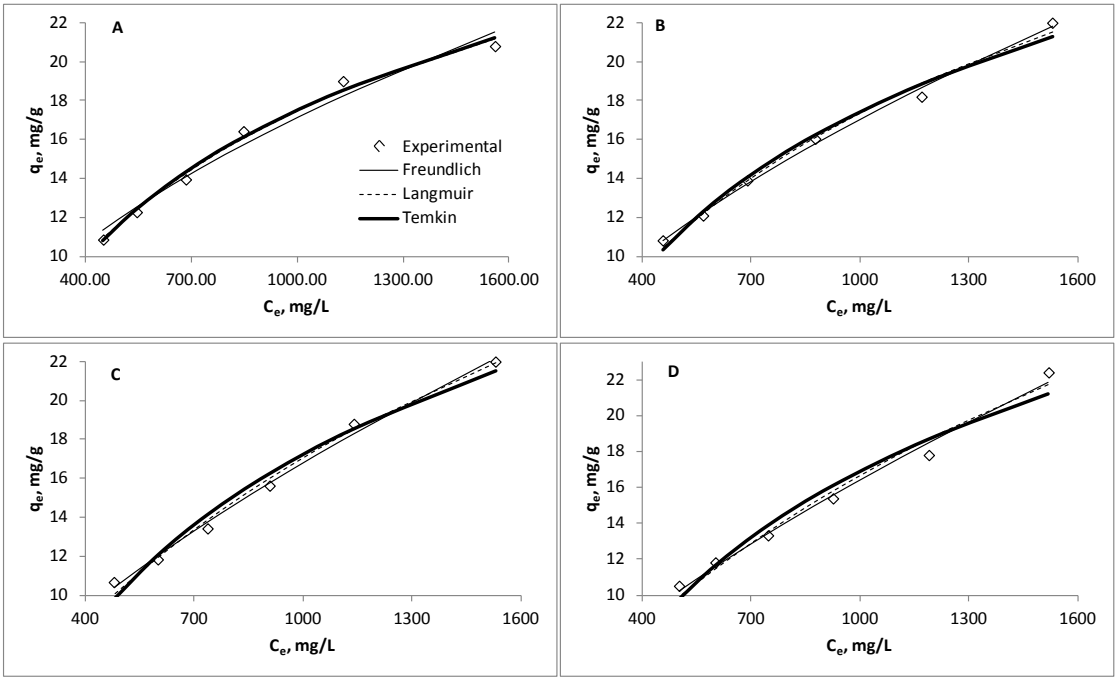

Figure 6-5. Non-linear regression of ammoniacal nitrogen sorption at different temperatures. A, 298 K; B, 308 K; C, 318 K; and D 328 K.

Table 6-3. Results of non-linear regression analysis using various isotherm models for ammoniacal nitrogen sorption on zeolite at different temperatures (308, 318, and 328 K)

		Freundlich		**Langmuir**		**Temkin**	
308 K	Parameters	K_F	1.36	K_L, L mg^{-1}	0.00079	K_T, L mg^{-1}	0.00681
		n	1.72	q_m, mg g^{-1}	39.3	b_1, mg mol g^{-1} J^{-}	273
	χ^2	**0.0109**		0.0256		0.0388	
318 K	Parameters	K_F	1.20	K_L, L mg^{-1}	0.000554	K_T, L mg^{-1}	0.00552
		n	1.53	q_m, mg g^{-1}	47.8	b_1, mg mol g^{-1} J^{-}	246
	χ^2	**0.0177**		0.0342		0.0774	
328 K	Parameters	K_F	1.16	K_L, L mg^{-1}	0.000471	K_T, L mg^{-1}	0.00517
		n	1.46	q_m, mg g^{-1}	52.0	b_1, mg mol g^{-1} J^{-}	241
	χ^2	**0.0272**		0.0603		0.108	

6.3.3 Thermodynamic parameters of ammonium sorption

The Gibbs free energy change (ΔG°) of ammonium sorption onto zeolite was calculated from the sorption constants obtained in both Langmuir and Temkim models (Figure 6-6 and Table 6-4). All the ΔG° values were negative (between -5.14 and -11.7 kJ/mol), which indicated that the ammonium sorption was a spontaneous process and naturally feasible at the tested temperature range. When plotting ΔG° against temperature, it was found that the intercept (the enthalpy change ΔH°) was -22.3 kJ/mol for the Langmuir model and -14.9 kJ/mol for the Temkin model. These negative values indicated that the sorption was exothermic in nature [194, 195]. But this result was opposite to some other studies [95, 196], indicating the complexity of ammonium sorption process by zeolite. The entropy change (ΔS°) associated with ammonium sorption was -0.0525 or -0.0107 kJ/K mol depending on the selected model, comparable but less than a literature value of -0.0729 kJ/K mol [195]. This negative value indicated that even though the randomness of the whole system always tended to increase, the randomness of the subsystem concerning ammonium sorption decreased, which was a result of the sorption of ammonium ions into the tetrahedral crystal structure of zeolite. The mean sorption energy calculated from the Dubinin-Radushkevish (D-R) model was between 5.29 and 5.59 kJ/mol. The literature reported that an E value between 1.0 to 8.0 kJ/mol was typical for physisorption, and a value between 9.0 to 16.0 kJ/mol was typical for chemical ion-exchange adsorption [197]. So this relatively low sorption energy, as well as ΔG° the absolute values of which were less than 20 kJ/mol, categorized the SW

ammonium sorption on zeolite mainly as a physisorption process which was in accordance with sorption studies based on synthetic wastewater streams [194, 195, 198].

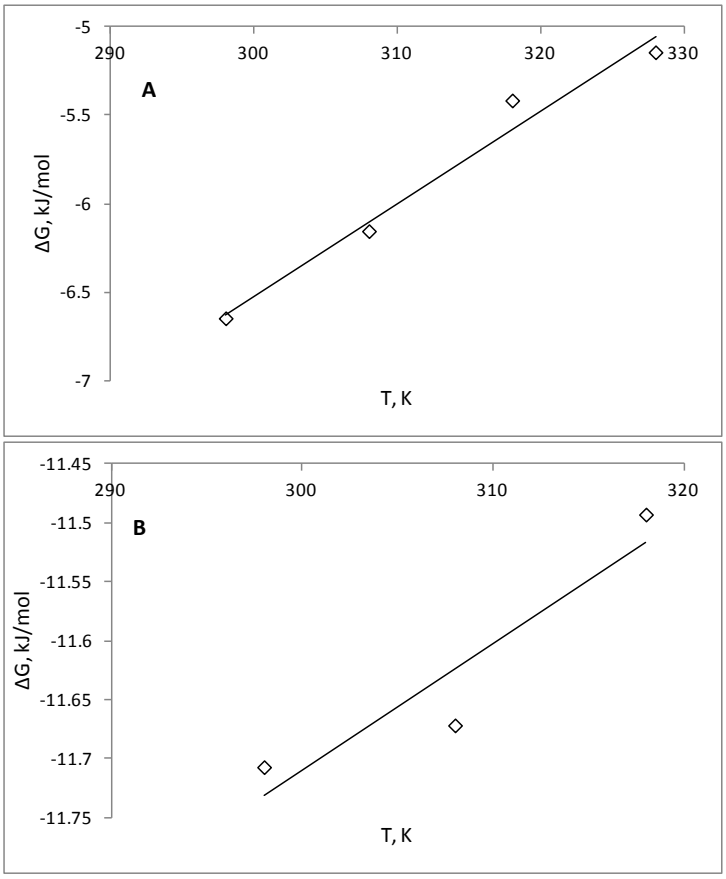

Figure 6-6. Gibbs free energy change of sorption at different temperatures. A, ΔG° estimated using Langmuir model; and B, ΔG° estimated using Temkin model.

Table 6-4. Thermodynamic parameters of ammoniacal nitrogen sorption on zeolite

Temperature	**Langmuir model**		**Temkin model**		**D-R model**
	K_L	**ΔG°**	**K_T**	**ΔG**	**E**
K	L/mol	kJ/mol	L/mol	kJ/mol	kJ/mol
298	14.6	-6.65	113	-11.7	5.59
308	11.1	-6.15	95.4	-11.7	5.47
318	7.76	-5.42	77.3	-11.5	5.29
328	6.59	-5.14	72.4	-11.7*	5.33
ΔH° (kJ/mol)	-22.3		-14.9		na
ΔS° (kJ/mol)	-0.0525		-0.0107		na

* This data point was not included for estimation of ΔH° and ΔS°.

6.3.4 Effects of operational parameters on ammonium sorption on zeolite

When zeolite is used to mitigate ammonium nitrogen in swine wastewater, the performance of sorption either in batch mode or continuous mode may be dependent on several operation parameters. As the kinetic of ammonium sorption was rapid and usually not the rate limiting step in a reactor, the performance of zeolite was mainly compared based on the final ammonium concentration and removal efficiency.

Effect of ammonium concentrations and sorbent doses

The swine wastewater was diluted into distilled water at different dilution rates, resulting in a series of concentrations: 130, 260, 520, 1040, and 2080 mg-TAN/L. The ammonium removal efficiencies were recorded to be higher than 90% when the initial concentration was lower than 520 mg/L (Figure 6-7). The corresponding final concentrations were lower than 48 mg/L after 24 h or 46 mg/L after 48 h. Even for the non-diluted SW, the final TAN concentration at 48 h can reach 780 mg/L, which value did not cause ammonia inhibition for most bioreactors.

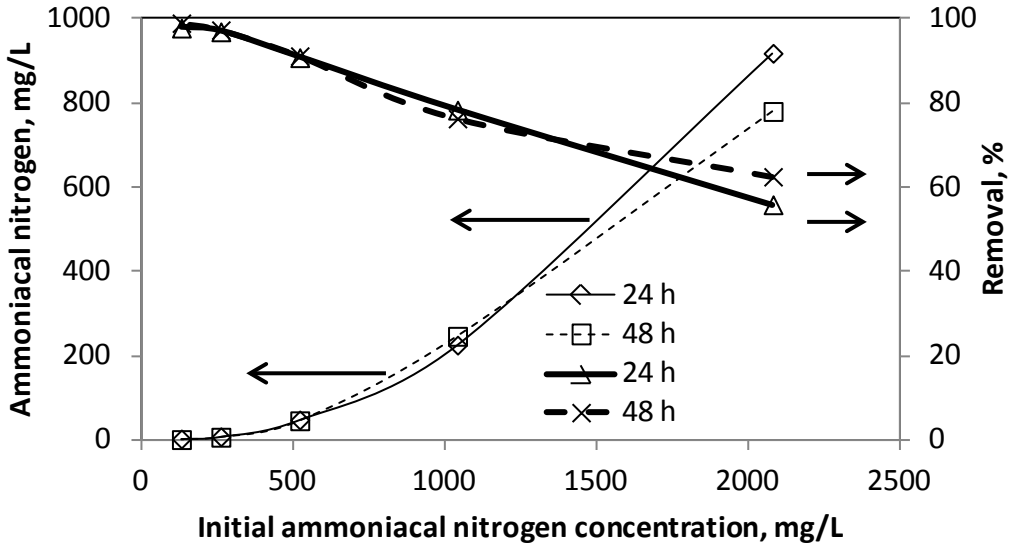

Figure 6-7. Ammoniacal nitrogen removals at different initial TAN concentrations between 130 and 2080 mg/L.

The amount of TAN that can be absorbed from the wastewater increased with increasing the zeolite doses (Figure 6-8). For doses greater than 3 g-zeolite/40 mL-wastewater (or 75 g/L), the final TAN concentrations reached values lower than 848 mg/L after 24 h. Again, although this performance was acceptable for avoiding ammonia inhibition in bioreactors, it was insufficient for ammonium removal.

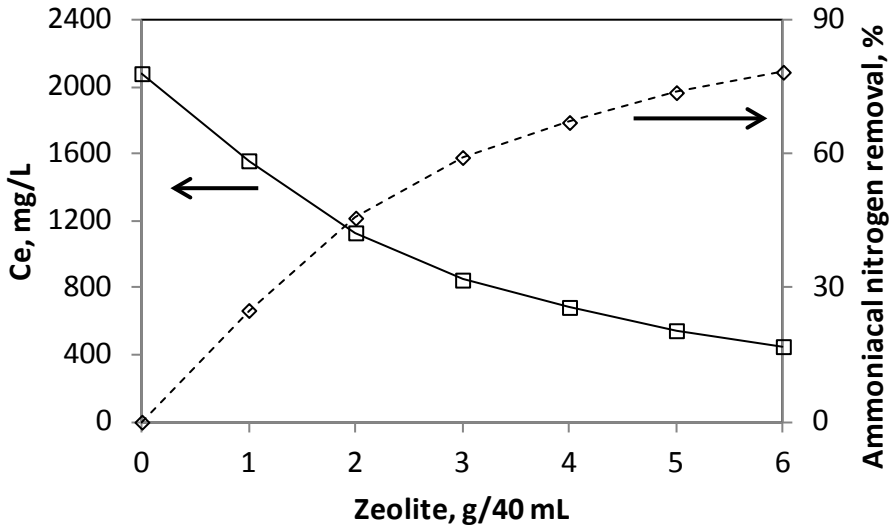

Figure 6-8. Ammoniacal nitrogen removals at different zeolite doses between 0 and 6 g/40 mL (or 0 to 150 g-zeolite/L).

Effects of pH, filtration treatment, and temperatures

Figure 6-9 showed that the initial pH value had a slight impact on ammonium removal. When the pH varied from 5 to 9, the removal efficiencies were between 53% and 61% and peaked at pH 7 to 8, which was the pH range of the unadjusted wastewater samples. These effects were also reported by other studies using zeolite as sorbents [95]. This slight change in removal efficiency could be attributed to the fact that zeolite helped maintain neutral pH in the liquid: the final pH all recovered to between 6.9 and 7.6 except for the case with the initial pH of 5 (Figure 6-9). It was not recommended to adjust pH beyond the range tested in this study basically because extreme pH values would be detrimental to the sorption process: zeolite may be partially dissolved at lower

pH, while at higher pH the ammonium/ammonia dissociation equilibrium would be shifted towards the direction favoring ammonia formation.

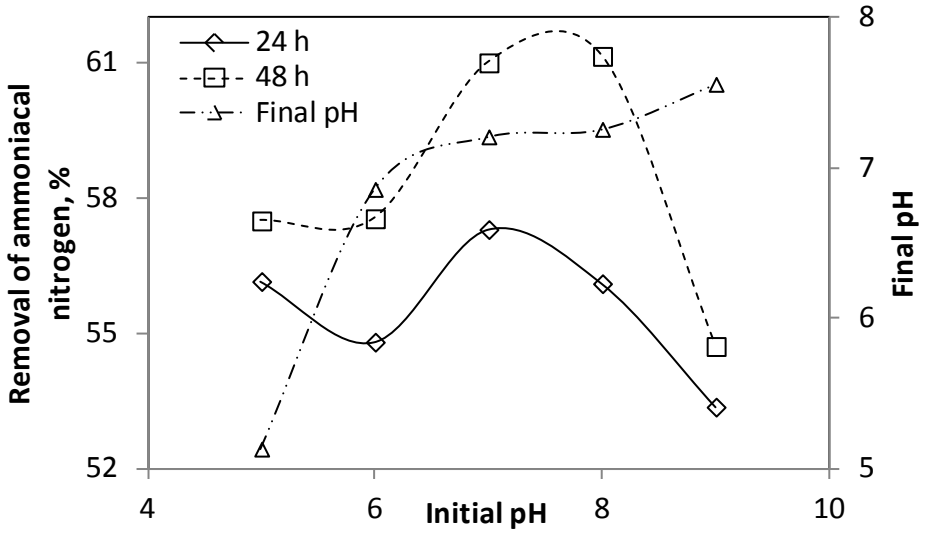

Figure 6-9. Ammoniacal nitrogen removals at different initial pH.

As suspended solids of various sizes could be present in swine wastewater, the wastewater samples were filtered though sieves from 0.075 mm to 1 mm of pore sizes. The filtration of suspended solids displayed complex effects on ammonium sorption (Figure 6-10). Generally speaking, filtrated wastewater speeded up the rate of ammonium sorption on zeolite: suspended solids of larger sizes may attach to zeolite particles and block ammonium ions to diffuse further inside. So the existence of suspended solids may explain the longer time needed to reach equilibrium in this study than those of other studies using synthetic wastewater that were actually water solution [93].

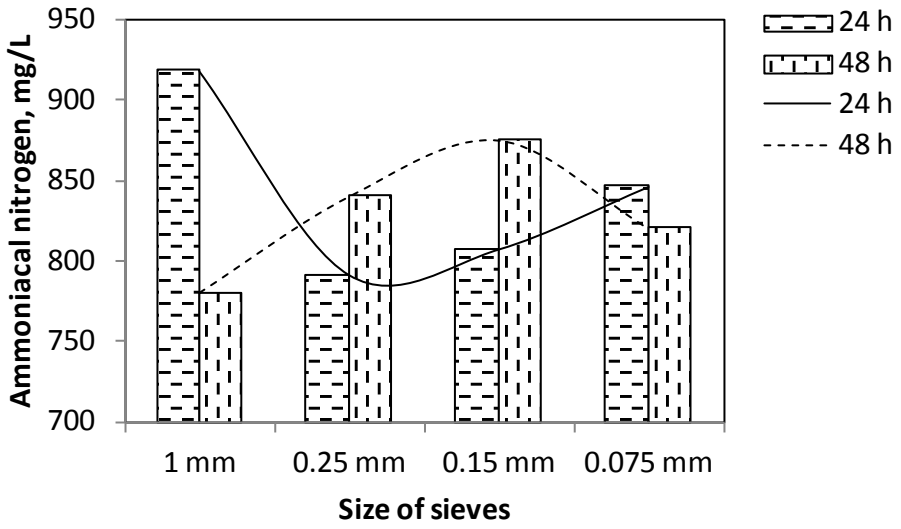

Figure 6-10. Ammoniacal nitrogen removals after filtration treatment using sieves of different sizes.

Ammonium removals were investigated with respect to the effect of temperatures (Fig. A5). For most zeolite doses, ammonium removals decreased when the temperature increased, except for the data set of 1 g/40 mL wastewater; however, the effect was small in that the greatest decrease was only 3.8%, which occurred for the data set of 3 g/40 mL. So when designing and operating ammonium sorption reactors using zeolite, the effect of temperature can be practically neglected.

6.3.5 Effect of adding GAC on ammonium sorption

The experimental data and fitted kinetic models of COD sorption on GAC were presented in Figure 6-11A and Table 6-5. Different from zeolite sorption, the pseudo-first-order kinetic model achieved the smallest χ^2 value (1.91), followed in an ascending order by pseudo-second-order, Elovich, and intra-particle diffusion models. The

equilibrium COD sorption capacity q_e was experimentally measured to be 62.7 mg/g, which was close to the estimation (59.5 mg/g) by the pseudo-second-order model.

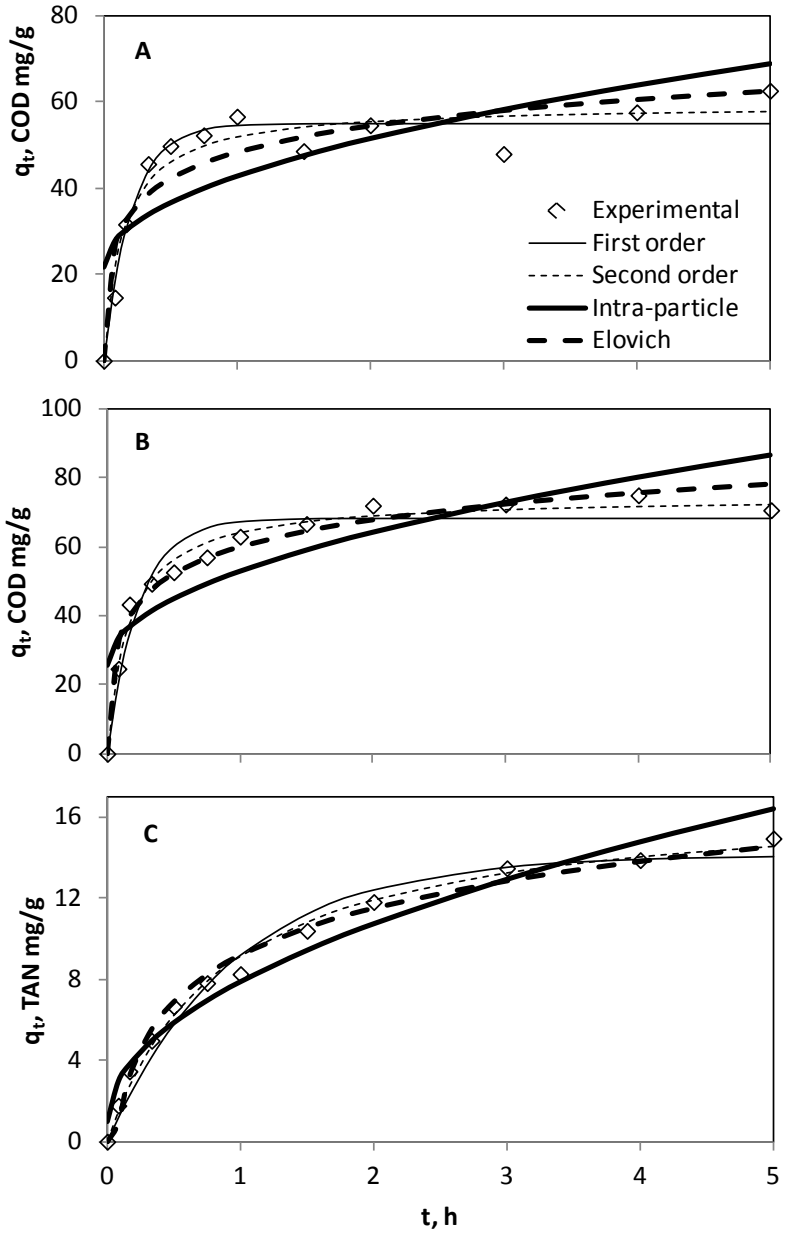

Figure 6-11. COD and ammoniacal nitrogen removal using GAC and zeolite, and mixture of GAC and zeolite. A, COD sorption on GAC alone; B, COD sorption on GAC and zeolite mixture; and C, TAN sorption on GAC and zeolite mixture.

Table 6-5. Results of non-linear regression analysis using various kinetic models for COD and ammoniacal nitrogen sorption

		Pseudo-1st order		Pseudo-2nd order		Intra-particle		Elovich	
GAC for COD removal		k_f, h^{-1}	4.86	k_s, g mg^{-1} h^{-1}	0.115	k_d, g mg^{-1} h^{-1}	21.1	α, mg g^{-1} h	2140
		q_e, mg g^{-1}	54.8	q_e, mg g^{-1}	59.5	C, mg g^{-1}	21.7	β, g mg^{-1}	0.113
	χ^2	**1.91**		3.20		34.8		6.82	
GAC + Zeolite for COD removal		k_f, h^{-1}	4.34	k_s, g mg^{-1} h^{-1}	0.0815	k_d, g mg^{-1} h^{-1}	27.5	α, mg g^{-1} h	2290
		q_e, mg g^{-1}	68.3	q_e, mg g^{-1}	74.7	C, mg g^{-1}	25.4	β, g mg^{-1}	0.0886
	χ^2	3.25		**0.867**		32.8		1.73	
GAC + Zeolite for TAN removal		k_f, h^{-1}	1.05	k_s, g mg^{-1} h^{-1}	0.0675	k_d, g mg^{-1} h^{-1}	6.91	α, mg g^{-1} h	53.1
		q_e, mg g^{-1}	14.1	q_e, mg g^{-1}	17.1	C, mg g^{-1}	0.955	β, g mg^{-1}	0.300
	χ^2	0.621		**0.189**		1.58		0.384	

Zeolite and GAC, mixed in quantities of 3 g-zeolite and 6 g-GAC in 40 mL wastewater, were used as sorbents for both ammonium and COD sorption. The fitted models were shown in Figure 6-11C for COD and 10D for TAN, and parameters were summarized in Table 6-5. The pseudo-second-order was the best fitted model, with χ^2 values of 0.867 and 0.189 for COD and TAN, respectively. The equilibrium sorption capacities (q_e) for both COD and TAN were increased in the mixed sorbents, based on the pseudo-second-order model, from 59.5 to 74.7 mg/g for COD and from 11.6 to 17.1 mg/g for TAN. This could resulted from the facts that GAC alone showed a capability of ammonium sorption for swine wastewater (15% reduction in 24 h), and zeolite alone also showed slight COD removal, as confirmed in this study. However, the rate constants (k_s) of both COD and TAN decreased after sorbents were mixed, based on the pseudo-second-order model, from 0.115 to 0.0815 g mg^{-1} h^{-1} for COD and from 0.861 to 0.0675 g mg^{-1} h^{-1} for TAN. The reduction on the TAN sorption rate was substantial, which obviously was reflected in the shape of the experimental data shown in Figure 6-2A and Figure 6-11C. The possible reason can be the exchange of liquid between the bulk liquid phase and the highly porous GAC particles (shown in Figure 6-1B), and this process could delay the

TAN sorption between liquid phase and zeolite. This change was also accompanied by the improved fit of intra-particle diffusion model for the mixed sorbents, indicated by the substantial change of χ^2 value from 6.05 to 1.58. It can thus be concluded that the mixed sorbents disturbed the sorbate diffusion process, especially the ammonium diffusion to zeolite.

6.3.6 Effects of pretreatment by selective adsorption

The swine wastewater was treated prior to being fed in MFCs, by selective removal of potentially inhibitory components from it, i.e., TAN removal by zeolite and VFA removal by granular active carbon (GAC). Four MFC reactors performed almost identically when fed with 40 mM acetate at the beginning, and then was fed with different swine wastewater (untreated, zeolite treated, GAC treated, and both zeolite and GAC treated) and examined with respect to power output, energy efficiency, and Coulombic efficiency. The wastewater characteristics were listed in Table 6-6. The soluble COD was substantially absorbed by GAC, and lowered by 40% from 12700 to 7610 mg/L. Zeolite neither absorbed COD from the wastewater, nor prevented COD adsorption by GAC when it was added to GAC. The adsorption of VFA followed the same trend as that of COD although the adsorption capacity was smaller, and VFA was reduced by 16% from 7050 to 5900 mg/L. The TAN was reduced by 52% by zeolite alone from 1800 to 865 mg/L, and by 17% to 1490 mg/L by GAC if used. Phosphate, with an initial concentration of 401 mg-PO_4^{3-}/L (or 131 mg-P/L), was reduced by zeolite or GAC by 65% or 57%, respectively. The removal of these ions yielded reduced

solution conductivity, but the resulting increase of Ohmic resistance was insignificant compared to the external resistor of 2.2 kΩ. The pH value was between 7.5 and 7.7.

For the untreated swine wastewater, the inhibitory effect was obvious and the generated voltage and power were substantially smaller than those of the reactors fed with the pretreated wastewater (Figure 6-12 and Table 6-6).

Table 6-6. Effects of swine wastewater pretreatment on characteristics and MFCs performance after zeolite or GAC adsorption

Pretreatment	**COD**	**VFA**	**TAN**	**PO_4^{3-}-P**	**Cond.**	**Power**	**Efficiencies*, %**	
	mg L^{-1}	mg L^{-1}	mg L^{-1}	mg L^{-1}	mS cm^{-1}	μW	**Energy**	**Coulombic**
Zeolite & GAC	7620	5880	760	49.9	12.8	51.2	0.59	1.98
Zeolite	13500	7120	865	45.7	14.2	51.1	0.51	1.75
GAC	7610	5900	1490	58.1	12.8	49.7	0.71	2.30
Untreated	12700	7050	1800	131	16.2	27.3	0.40	1.68

*All of the efficiencies were calculated based on the COD concentration of the untreated swine wastewater.

For the average power, the untreated wastewater generated a value of 27.3 μW, while the others generated 51.2, 51.1, and 49.7 μW after the treatments by adsorption of zeolite and GAC, zeolite alone, and GAC alone, respectively. The improvements on power generation were 88%, 87%, and 82% by the selective adsorption processes, respectively. Given the data in Table 6-6, the improvements of energy efficiency and Coulombic efficiency were also remarkable, each by 48%, 28% and 78%, and 18%, 4.2% and 37%, respectively. Therefore, the selective removal of the overloaded components in swine wastewater, either TAN or COD, was very effective in reducing their inhibitory effects, and consequently beneficial to improving MFC performance with respect to voltage, power, energy and Coulombic efficiencies. Similarly,

advantages of zeolite addition were observed in methane production in various types of anaerobic digestion, most possibly as a result of the adsorption of overloaded ammonium in swine wastewater [199-201].

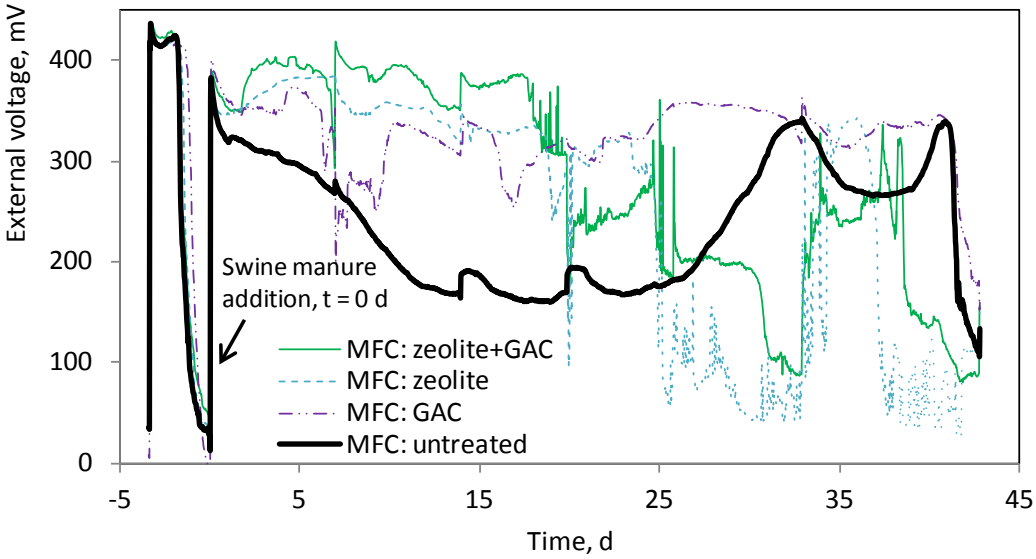

Figure 6-12. External voltage evolutions in microbial fuel cells fed with swine wastewater after different pretreatment.

6.4 Conclusions

This study showed that sorption using natural zeolite was an effective way for ammonium mitigation in swine wastewater. The kinetic process of the ammonium sorption on zeolite was best described by the pseudo-second-order model, and the resulting TAN sorption capacity at equilibrium was 11.6 mg/g. The isotherm data were best fitted by the Langmuir model, and the maximum TAN sorption capacity was 34.2 mg/g. For both kinetic and equilibrium studies, the non-linear regression yielded better model parameters than the regression after linear transformation, with respect to the

HYBRID values. The thermodynamic parameters indicated the spontaneity (ΔG° = -6.65 kJ/mol by the Langmuir model) and exothermic nature (ΔH° = -22.3 kJ/mol) of ammonium sorption on zeolite. The small values of the ΔG° and the mean sorption energy (E, obtained using the D-R model) indicated that the swine wastewater ammonium sorption on zeolite tended to be more of a physisorption process. Addition of GAC in zeolite decreased ammonium diffusion to zeolite particles, but it enhanced the maximum zeolite sorption capacity and COD removal.

For the practical use of zeolite for swine wastewater ammonium sorption at an initial TAN concentration of 2080 mg/L and zeolite dose of 75 g/L-wastewater in a batch-shaken reactor, a reaction time of 1 h was enough to achieve an ammonium concentration below the level causing ammonia inhibition, or less than 1000 mg/L. Operational parameters such as pH and temperature did not have a substantial effect, while the removal of suspended solids through filtration reduced the time for reaching equilibrium. Zeolite and granular activated carbon were effective in the selective adsorption of ammonia and organic matter in swine wastewater, and consequently improved the power generation, energy efficiency, and Coulombic efficiency in microbial fuel cells substantially.

Chapter 7. Improved ammonia removal from wastewater in microbial fuel cell-based membrane contactors

7.1 Introduction

Animal industry is thought to contribute over 50% of annual anthropogenic ammonia emission globally and in the US [202]. In concentrated animal feeding operations, ammonia originates from the input step of nitrogen uptake and the output step of manure excretion, and is later emitted from animal housing, manure storage and treatment facilities, and manure land application [203]. The nitrogen in fresh swine manure mainly exists in the forms of urea and uric acid, and these components go through hydrolysis via the enzyme urease to be converted to ammonium [203]. The direct discharge of swine wastewater to water bodies or land releases the most part of ammonium in manure to the environment. When swine slurry is subjected to storage or anaerobic digestion, the produced biogas also contains gaseous ammonia with typical concentrations of 10-100 ppm (volume-based). Ammonia emissions from animal housing and manure storage/treatment are comparable, for example, 3.7 kg-NH_3/year-finisher pig for swine housing and 2.4 kg-NH_3/year-pig from lagoon [204].

Ammonia is a chemical agent that can cause adverse environmental impacts through deposition of acidifying species and aerosol formation [205] and through indirect N_2O emission which is a greenhouse gas [206]. According to results of life cycle assessment for swine slurry from finishing pig farms, the release of ammonia is the dominant contributor both to eutrophication and acidification, equivalent to 498 g-PO_4/m^3-slurry

and 2276 g-SO_2/m^3-slurry, respectively [207]. Effective ammonia emission control technologies are further needed due to two supplemental air quality laws, CERCLA and EPCRA, that require any stationary major source to report NH_3 emissions exceeding 45.4 kg in any 24 h period [208].

The corresponding ammonia mitigation strategies can be incorporated in these emission stages, and manure and wastewater management and mitigation is a critical step in controlling the emission from swine farms. Microbial fuel cells may offer a potential application in ammonium removal from swine wastewater according to the Literature Review section, as the air cathode provides a microenvironment that favors the ammonia volatilization. The mechanism for ammonia removal through MFC cathode resembles a membrane contactor, which offers a large and stable interfacial area of hydrophobic membrane for ammonia volatilization.

So this study tried to modify the regularly used air-cathode and MFC configuration (i.e., membrane contactor mode) for improving ammonium removal. A suitable level of hydrophobic treatment on cathode should allow the best ammonia volatilization. Increasing the cathode surface area may also improve the ammonium removal efficiency. At last, the volatilized ammonia from cathode may be captured by sulfuric acid solution after channeling the striping air to it.

7.2 Materials and methods

7.2.1 MFCs and cathode treatment

The configuration of MFCs A, B, and C were the same as previously reported [209]. The reactors were inoculated with anaerobic sludge obtained from a swine manure lagoon at the University of Minnesota Southern Research and Outreach Center in Waseca, MN. The sludge was sieved through a 1 mm mesh to remove sand, gravels, and plant residues prior to use.

The anode material of the three MFCs was plain carbon cloth, and the cathodes had the same Pt/black carbon catalyst layer with 0.5 mg-Pt/cm^2. The cathode carbon cloth for MFC A and C was with 20% PTFE treatment (Figure 7-1), while the cathode carbon cloth for MFC B was with 5% PTFE treatment. To prevent potential water leak, the cathode carbon cloth of the MFC A and B was applied with three layers of PTFE.

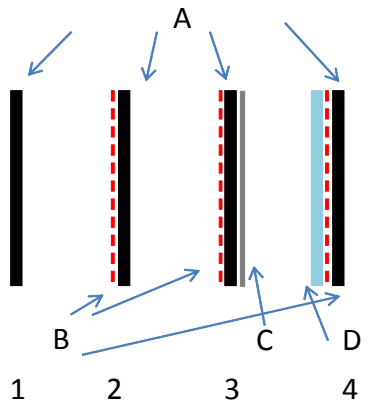

Figure 7-1. Different cathode structures and different layers. A: wet-proofed carbon cloth; B: Pt/black carbon catalyst; C: diffusion (hydrophobic) layer; D: ion exchange membrane. Schematics of commonly used carbon-cloth cathodes: 1, wet-proofed carbon cloth; 2, Pt-containing wet-proofed carbon cloth; 3, carbon cloth with a hydrophobic diffusion layer; 4, membrane electrode assembly.

7.2.2 Design of MFC-membrane contactor

The electrode materials in MFC-membrane contactor were the same as in the MFC C, with plain carbon cloth as anode (20 cm^2) and 20% PTFE treated carbon cloth (45 cm^2) as the cathode. The total liquid volume of this MFC was 50 mL. The cathode formed the tubular surface of the MFC column supported by plastic tubes at both ends (Figure 7-2). The MFC column was encompassed by a plastic bottle which had inlet and outlet ports for stripping gas which was pumped by a peristaltic pump. The stripping gas was induced to 1 M sulfuric acid solution to recover ammonia. The reactor was inoculated as previous described for other MFCs.

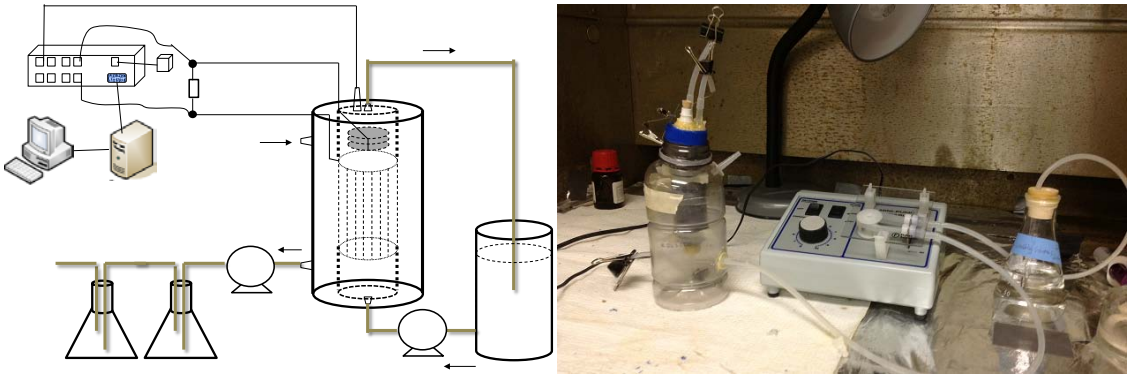

Figure 7-2. Diagram and photo of MFC-membrane contactor used in this study.

7.2.3 Description of ammonia volatilization

According to Fick's law of diffusion, the mass balance of ammoniacal nitrogen in the lumen [210] is expressed as follows:

$$\frac{\partial C_{ta}}{\partial t} + \vec{U}\nabla C_{ta} = D_{ta}\nabla^2 C_{ta} + R_{ta} \quad (7\text{-}1)$$

where C_{ta}denotes the local nitrogen concentration of ammoniacal species, $\vec{U}$ is the velocity vector, $D_{ta}$is the diffusivity of ammoniacal component in water, and R_{ta} is the rate of ammoniacal species generation due to chemical or physical reactions. When the reactor is operated in a batch mode without mixing, the Equation (7-1) can be simplified to Fick's second law of diffusion:

$$\frac{\partial C_{ta}}{\partial t} = D_{ta}\nabla^2 C_{ta} \quad (7\text{-}2)$$

Ammonium ion is a weak acid and ammonia is a gas dissolvable in water, so the equilibrium of ammonia concentration is dictated by the ammonium dissociation constant ($K_d = \frac{C_{NH3} * 10^{(-pH)}}{C_{NH4+}}$) and the Henry's law constant ($K_h = \frac{P_{NH3\,(g)}}{C_{NH3\,(l)}}$, in atm·(mg/L)$^{-1}$, where $P_{NH3\,(g)}$=RT$C_{NH3\,(g)}$) through ammonium-ammonia dissociation equilibrium (Equation 4) and gas-liquid equilibrium (Equation 5):

$$NH_4^+ <--> NH_{3\,(l)} + H^+ \quad (7\text{-}3)$$
$$NH_{3\,(l)} <--> NH_{3\,(g)} \quad (7\text{-}4)$$

Both of these two constants are temperature-dependent [211]:

$$K_d = 10^{-(0.09018+\frac{2729.92}{T})} \quad (7\text{-}5)$$
$$K_h = 1.1561 \times e^{-\frac{4151}{T}} \quad (7\text{-}6)$$

As a result, the total concentration is the sum of the concentrations of the protonated form, ammonium, and the unprotonated form, ammonia:

$$C_{ta} = C_{NH3} + C_{NH4+} \quad (7\text{-}7)$$

The total unprotonated ammonia includes the dissolved gaseous ammonia and dissolved liquid ammonia:

$$C_{NH3} = C_{NH3(l)} + C_{NH3(g)} \quad (7\text{-}8)$$

The flux of total ammoniacal nitrogen to the inner side of cathode is equal to the gaseous ammonia diffused outside the cathode, so the mass balance across the cathode can be expressed as follows:

$$-D_{ta} \frac{\partial C_{ta}}{\partial x}\Big|_{x=0} = k_g \frac{\mathrm{P_{NH3(g),int}}}{\mathrm{RT}} \quad (7\text{-}9)$$

where $k_g$denotes the overall mass transfer coefficient of gaseous ammonia in carbon cloth and gas diffusion layer, and $\mathrm{P_{NH3(g),int}}$ is the partial pressure of gaseous ammonia at the interface of the liquid and cathode.

7.3 Results and discussion

7.3.1 Power generation

The MFC using 5% PTFE-treated carbon cloth as cathode material did not well function due to heavy liquid leak. To prevent liquid leak, diffusion layers are necessary to apply to the air-facing side of the cathode. The other four MFCs did not have the leak problem, and the results of the overall electrochemical performance were summarized in Figure 7-3 and Table 7-1. When fed with the same feed, the MFCs had very different electrochemical performance with regard to maximum power, maximum current, internal resistance and open circuit voltage (OCV). Among the four MFCs, the MFC A with 20% PTFE and GDLs had the largest internal resistance of 469 Ω, and the smallest

maximum power of 106 μW, maximum current of 0.95 mA, and OCV of 472 mV. When using 5% PTFE and GDLs in MFC B, the electrochemical performance was substantially improved, so it can be concluded that too much hydrophobic treatment on carbon cloth intervened oxygen gas diffusion to the catalyst side which impaired the electrochemical performance of the MFC. The MFC C did not have additional GDLs except the 20% PTFE treatment, and it achieved better performance than MFC B. So the cathode used in the MFC-membrane reactor adopted the same structure as in MFC C. The MFC-membrane contactor achieved the best performance among the four reactors: the internal resistance of 189 Ω, the smallest maximum power of 815 μW, maximum current of 415 mA, and OCV of 825 mV. This improvement was mainly a result of the increased cathode surface area from 20 cm^2 to 45 cm^2, which reduced the activation overpotential of cathode [212], and a result of the reduced electrode spacing, which reduced Ohmic resistance of the medium [165].

Table 7-1. Power generation of microbial fuel cells with different cathode materials or configurations

Configuration	**Cathode**	**Calc. max. P** μW	**Calc. max. I** mA	**Int. resistance** Ω	**OCV** mV
Regular, MFC A	20% PTFE+GDLs	106	0.95	469	472
Regular, MFC B	5% PTFE+GDLs	197	1.57	319	541
Regular, MFC C	20% PTFE	368	2.29	280	753
Membrane contactor	20% PTFE	815	4.15	189	825

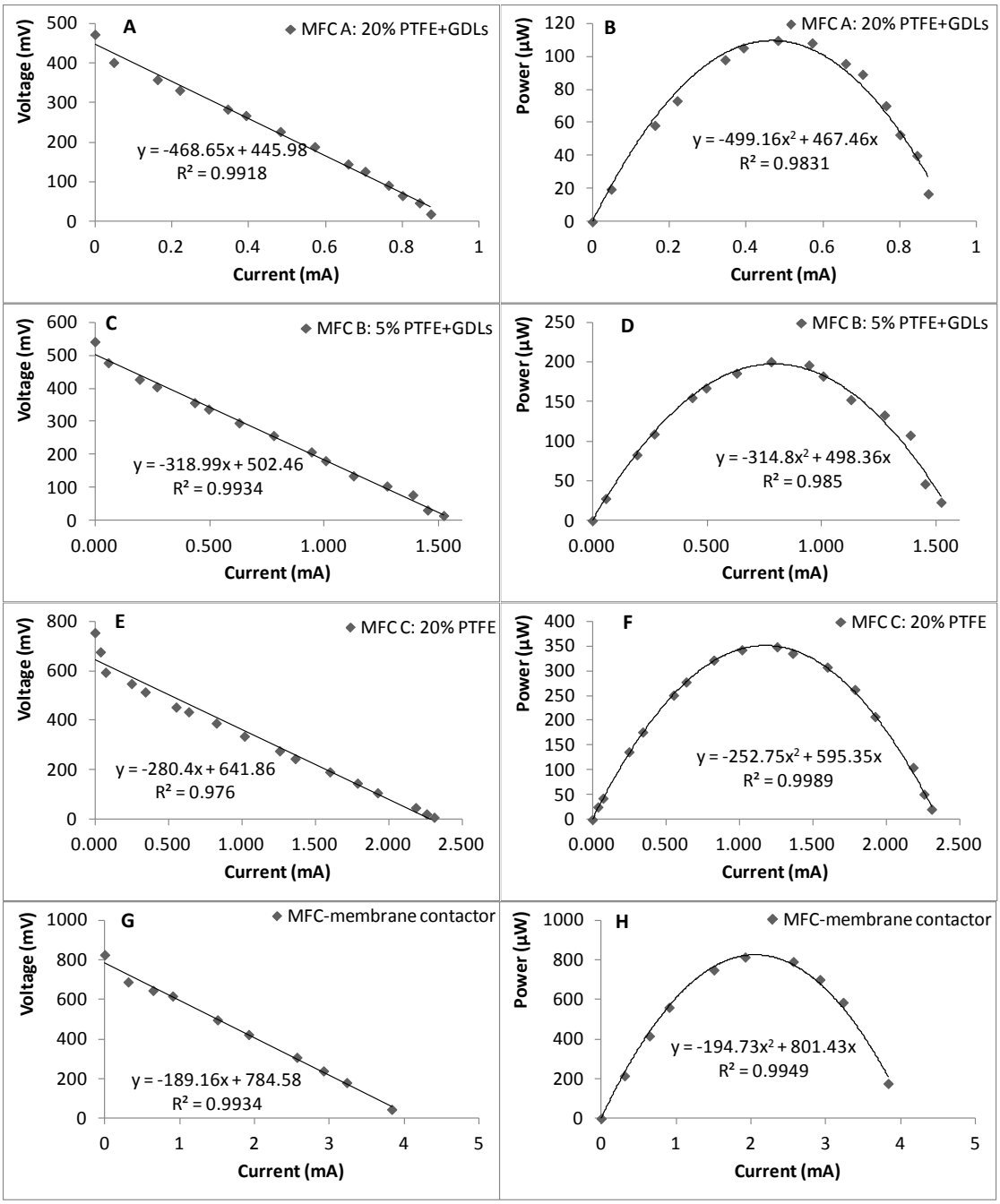

Figure 7-3. Polarization curves of different microbial fuel cells.

7.3.2 Effect of current on ammonium removal

Two parallel experiments were conducted with the regular reactors MFC A and MFC C, the former achieving the lowest electrochemical performance and the latter achieving the best. Three levels of electrical current were chosen: the first level was with a small current (< 0.1 mA), the second level was with a current where maximum power density was obtained, and the third one was the one close to the maximum current. Each of these current was controlled by choosing a suitable external resistor (Table 7-2). The profile of the total ammoniacal nitrogen concentrations in MFCs media were reported in Figure 7-4. In both reactors, the TAN removal can achieved more than 0.6 (or 60%) when MFCs finished electricity generation, and denitrification was found not obvious (both NO_2^--N and NO_3^--N less than 1.0 mg/L). In the control group, the highest TAN removal of 31% was achieved on day 3, and the TAN concentration started to recover when bacteria decayed and hydrolyzed to release ammonium from the nitrogen of organic form such as proteins. So the TAN removal was most possibly by cathode volatilization [100], and the TAN removal was the most rapid when the largest electrical current was employed in both MFC reactors, indicating the current generation improved ammonia removal.

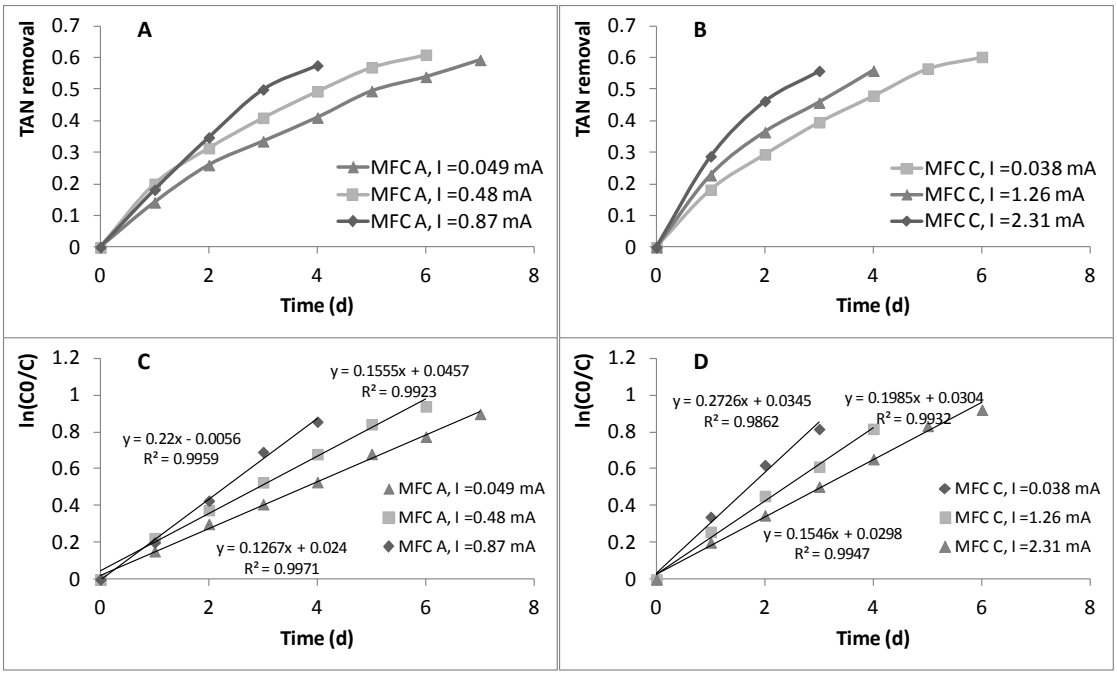

Figure 7-4. Total ammoniacal nitrogen removal in MFCs and the kinetic estimations.

Table 7-2. Ammonium removal in MFCs

MFCs	**External R** Ω	**Current** mA	**TAN half-life** d
MFC A	8200	0.049	5.46
MFC A	470	0.48	4.44
MFC A	22	0.87	3.15
MFC B	10	1.52	3.01
MFC C	18000	0.038	4.47
MFC C	220	1.26	3.48
MFC C	3.9	2.31	2.54
Membrane contactor	12	3.83	**0.67**

The explanation for the improved TAN removal was the local pH increase on cathode [100]. As oxygen reduction reaction at the vicinity of catalyst layer of the cathode generates hydroxide, the pH around cathode increased when the ORR reacted more rapidly. Meanwhile, oxygen gas served as electron donor, so an increased electrical

current indicated a more rapid ORR. The equilibrium of ammonium/ammonia would then shift to the direction favoring the formation of ammonia as a result of increased pH, which then improved ammonia volatilization through cathode (Figure 7-5). A useful index for ammonia removal was the half-life time based on pseudo-first order reaction, which indicates the time needed to remove half an amount of initial TAN from the medium. So the relationship between these two variables was further confirmed by plotting the half-life time of TAN against electrical current, which showed a strong correlation between them (R^2 = 0.9908 for MFC A and R^2 = 0.9992 for MFC C, Figure 7-6). An increase of 1 mA in current reduces half-life time by 2.8 and 0.85 d on average, for MFC A and MFC C, respectively. Therefore, when using air-cathode MFCs for TAN removal, the current density should be set large or external resistors set smaller to accelerate the ORR at cathode.

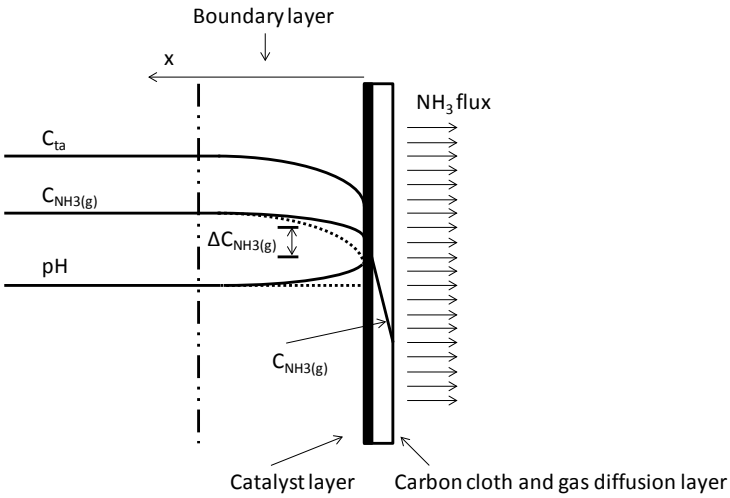

Figure 7-5. Ammonia and total ammoniacal nitrogen concentration profiles at the MFC cathode.

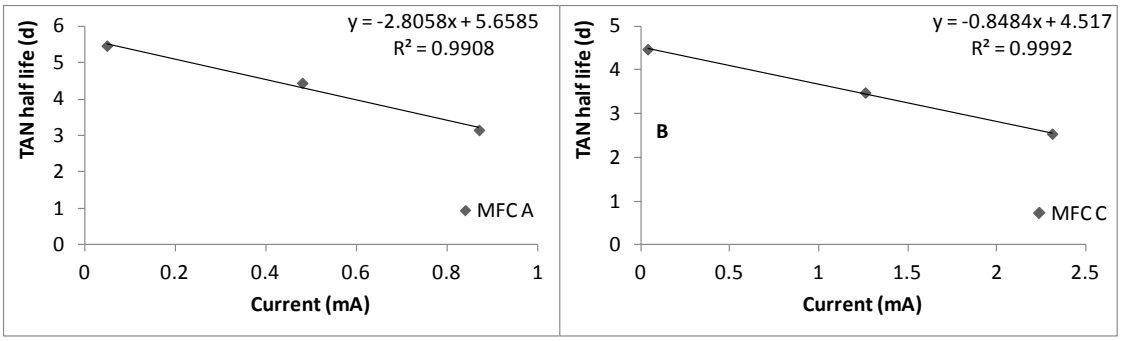

Figure 7-6. Half-life time for total ammoniacal nitrogen removal at different currents.

Experiment about the direct characterization of pH gradient at cathode was not conducted in this study, so the pH elevation remained a hypothesis. For further confirmation, the technique of three dimensional imaging by confocal scanning laser microscopy (CSLM) which was used to evaluate anode pH gradient can be adopted [213, 214]. In this quantitative CSLM method, a pH-sensitive fluoroprobe (a molecular probe) such as C-SNARF-4 (seminaphthorhodafluor-4F 5-(and-6) carboxylic acid) is chosen as a reliable pH indicator on cathode. After calibration for the suitable pH range, information from CSLM image can be analyzed to provide three-dimensional pH values at different distance to cathode at different operational conditions.

7.3.3 Effect of different cathodes on ammonium removal

MFCs of different cathode materials (MFC A, B, and C) were tested for power generation, and were further tested for their effects on ammonia removal at a high level of electrical currents (0.87, 1.52, and 2.31 mA for reactor A, B, and C, respectively) which was the optimal condition for ammonia removal according to the results and

discussion in previous section. The TAN removals of these MFCs were plotted in Figure 7-7.

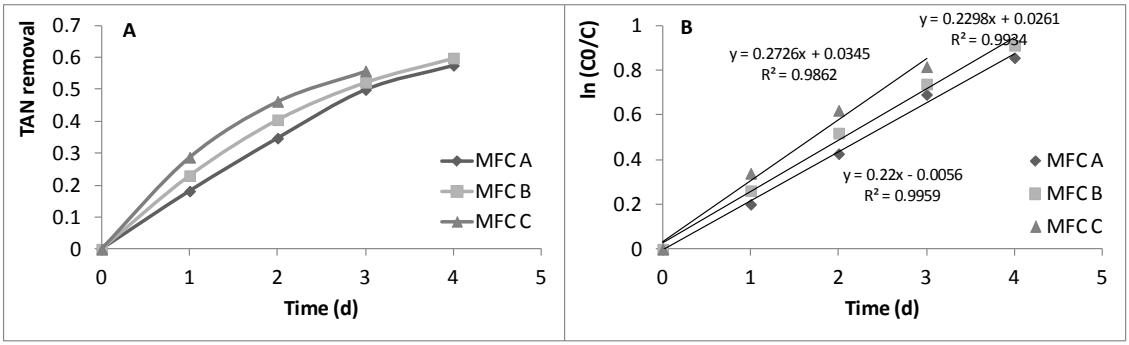

Figure 7-7. TAN removal in MFCs of different cathodes.

The MFC C, with 20% PTFE carbon cloth but no additional GDLs, removed TAN from the medium faster than the other two reactors, while the MFC A, with a cathode of 20% PTFE and GDLs, removed TAN the slowest among the three MFCs. The half-life times for the three reactors at the optimal current condition were 3.15, 3.01, and 2.54 d for reactor A, B, and C, respectively. There was a strong correlation between the half-life and electrical current with $R^2 = 0.9404$, shown in Figure 7-8. This correlation does not mean a causal relationship, but it is possible that the increased ammonia removal was a result of the increased electrical current which increased the local pH value around cathode. Another reason could be the reduced overall mass transfer coefficient of ammonia (Equation (7-9)) through cathode due to the reduced amount of PTFE as what happened in other types of membrane contactor, but our experimental data were not enough yet to confirm this possibility.

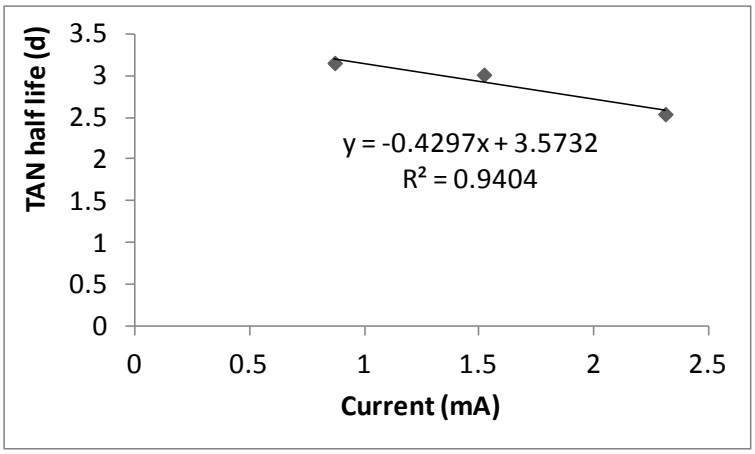

Figure 7-8. Half-life times of MFCs of different cathodes.

7.3.4 Ammonium removal in MFC-membrane contactor

A novel membrane contactor based on MFCs was made to improve the TAN removal. The TAN removal reached 64% from 87 to 31 mg-N/L after one day operation, while the normal MFC (MFC C) removed 29% TAN from 87 to 62 mg-N/L (Figure 7-9). After an operation of two days, the MFC-membrane contactor removed 87% TAN, which exceeds the removal in normal MFC by 41%. The half-life time of the TAN reduced from 2.54 to 0.67 d. After operation of two days, 68% of the initial ammonium, or 78% of the removed ammonium was recovered in the sulfuric acid solution. The substantial reduced half-life time can be attributed to the increased ratio of cathode surface area to reactor volume in this reactor (by 6.8-fold) and improved electrochemical performance (maximum current by 1.8-fold). These comparisons demonstrated the potential application of MFC-membrane contactor for ammonium recover from wastewater and the substantially improved ammonia removal efficiency.

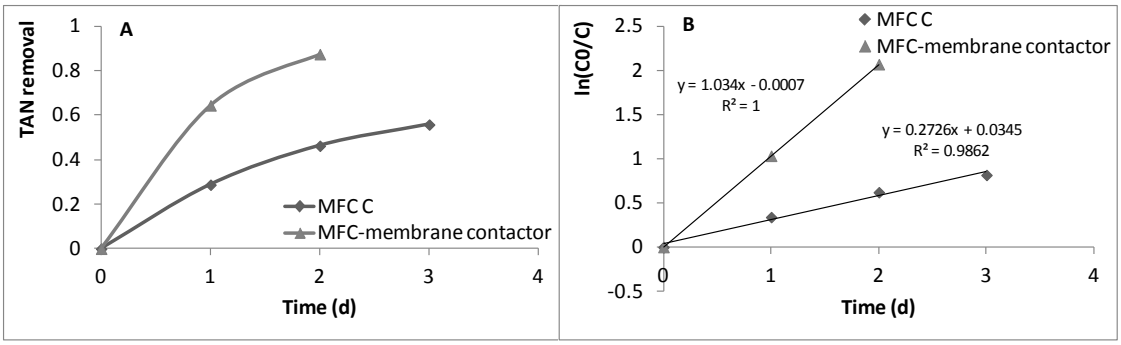

Figure 7-9. TAN removal in an MFC-membrane contactor and in a normal MFC.

7.4 Conclusions

Different MFC air-cathode structures were compared in this study to evaluate their ammonia removal efficiency. The 5% PTFE-treated cathode had the problem of water leak. The other cathodes, including the 20% PTFE+GDLs, 5% PTFE+GDLs, and 20% PTFE, did not have the problem of water leak, and the last one performed best both in power generation and ammonia removal. Tests in MFC A and C revealed that the half-life time of the total ammonium was proportional to electrical current, a strong evident demonstrating that the oxygen reduction reaction at cathode promoted ammonia volatilization by elevating pH nearby. On average, an increase of 1 mA in electrical current would reduce the half-life time by 2.8 d and 0.85 d for MFC A and C, respectively. Modifying regular MFCs to membrane contactor mode improved ammonia removal, because the surface area of hydrophobic membrane was increased. This improvement was indicated by the substantially reduced half-life time from the best case of 2.54 d of the best performed regular MFCs to only 0.67 d. The modification also allowed ammonia recovery from wastewater, and 78% of the removed ammonia was captured in sulfuric acid solution. This study demonstrated a novel way of ammonium

removal and recovery from wastewater by MFC based on membrane contactor mode, and better performance is still expected through optimizing the gas-diffusion materials and reactor structure.

Chapter 8. Conclusions and Future Work

8.1 Introduction

Wastewater from swine farms contains high concentrations of organic matters, nitrogen and phosphorus, which may lead to severe environmental issues to soil, water, and air. Developing effective treatment approaches for swine wastewater is urgent and crucial to sustain the hog industry. Microbial fuel cell (MFC) is a promising technology that shows a potential use in swine wastewater treatment because it can degrade organic substrate in wastewater biologically and electrochemically, and remove ammonium by volatilization at air cathode. MFC technology is also sustainable because it converts waste to electricity besides its function for wastewater treatment. This study developed effective MFCs for treating synthetic and swine wastewater to generate electrical energy and to achieve efficient removal of COD and total ammonium nitrogen.

8.2 Summary of the dissertation

Lab-scale single-chamber MFCs were developed in this study. MFCs were inoculated with different sludge/sediment and subject to electric stimulation (+2 V), and impact of inoculum type and electric stimulation on anodic biofilm, the internal resistances, and power generation were compared. Activated (AC) and anaerobic (AN) sludge showed faster enrichment of MFC anodic biofilm by 2 to 3 d than river sediment (RS), while AN-MFC presented highest VFA degradation rate. RS-MFC anode surface was covered with well-developed layers of biomass and had a much larger power output (195 μW or 98 mW m^{-2}) than AC- and AN-MFC after one month operation. For mature MFCs that

were under long-time operation, a transient application of negative voltages (-3 V) improved the cathode activity and maximum power output by 37%, due to the bactericidal effect of the electrode potential higher than +1.5 V *vs.* SHE.

The electrochemical and biological properties of MFC were modeled in this study. Current models in the literature did not provide tools to simulate or predict the change of overpotentials and other electrochemical properties on the assumption that the anodic biofilm catalyzes organic oxidation. Inclusion of activation overpotential and exchange current density in the model successfully described the performance of MFCs with regard to electricity generation and organic matter removal, suggesting a smaller external resistor accelerates organic matter removal and reduces sludge generation.

The removals of VFA and TAN in swine wastewater by MFCs had the half-life times of 4.99 and 7.84 d, respectively. But MFCs fed with raw swine wastewater generated relatively small power (28.2 μW), energy efficiency (0.37%) and Coulombic efficiency (0.15%). As the high strength of contaminants (e.g., ammonium and VFAs) swine wastewater showed inhibitory to electricity generation bacterial activity, zeolite/GAC were tested for their effects in controlling the contaminant levels, and further tested for MFCs performance with the indicators of power generation, energy recovery, and Coulombic efficiency. All of these indicators were substantially improved a lot by selective adsorption of contaminants, clearly showing the reduction of inhibitory effect of swine wastewater on MFC performance: power generation by over 80%, energy efficiency by up to 78%, and Coulombic efficiency by up to 37%.

To improve the ammonium removal, different cathode structures and hydrophobic treatment on cathode were designed, and the electricity generation in MFCs was found to promote ammonia removal as a result of improved volatilization at cathode. The use of 20% PTFE treated carbon cloth showed the best performance with a half-life time of 2.54 d for ammonium removal, while modification of the MFC to membrane contactor mode further reduced the half-life time to 0.67 d and recovered 78% of the removed ammonium.

8.3 Future work

Several obstacles must be overcome before MFCs can be theoretically better understood and practically used for wastewater treatment as a cost-effective technology. These obstacles include the energy loss, reactor scale-up, and specific issues related to swine wastewater treatment.

First, energy losses through overpotentials and other ways need be reduced. Open circuit potential of an MFC is usually observed much less than its electron motive force as the theoretical value at equilibrium. This phenomenon means that part of electrical energy generated by exoelectrogenic bacteria is lost. Activation overpotential, a term describing the electron transfer limit, causes substantial part of energy loss. Applying effective anode or cathode catalyst, cultivating and genetically modifying the electrochemically active bacterial consortia, and increasing the surface area of electrodes for microbial attachment and redox reactions may reduce this overpotential. Coulombic and cathodic losses, two types of energy loss rather than overpotentials, widely exist in MFCs.

Coulombic loss is caused when attached or suspended bacteria use substrate for metabolism but not for exoelectrogenesis, e.g., biomass growth which is almost unavoidable. Similarly, it is also possible that certain bacteria utilize cathode electrons as reducing power, which competes with oxygen reduction reaction. Therefore, effective electricity generation in MFCs should further reduce the overpotentials, Coulombic loss, and cathode loss.

Second, reducing costs of MFC reactors is critical when MFCs are up-scaled for real application. The cost of catalyst is among the most urgent ones: Pt/carbon black is used as catalyst for oxygen reduction in most MFC studies, while Pt is non-abundant and previous metal which has a high price. Catalysts that do not contain Pt and are of lower prices, such as Pd, Fe and Co based materials, are attracting attention over the years. Studies on CoTMPP, FePC, biocathodes, and activated carbon revealed that they may serve as Pt replacement with lower cost and of more sustainable, but more work is needed to optimize results and overcome the technical difficulties.

Finally, there are several issues related to swine wastewater as substrate in MFCs and related to its organic matters and nutrients removal. First, the inhibition of swine wastewater in electrochemical performance was evident, and selective adsorption substantially improved the performance; however, it was not yet clear which component played the critical role in the inhibition and how. Second, the ammonium removal was substantially improved by designing the MFC-membrane contactor, but the effects of operational parameters, such as flow rate, pH, and initial COD and ammonium concentration have not yet been evaluated by experiment or by simulation. The use of

other gas-diffusion materials rather than PTFE may further improve ammonium removal efficiency, and is worthwhile as future studies. Third, phosphorus removal in MFCs was not effective as the operation of 42 d only removed only 39%, so subsequent treatment is needed or the struvite precipitate from cathode needs further optimization. And fourth, the MFC model suggested that electricity generation consumed part of the organic substrate and reduced biomass production. As the sludge handling is costly in wastewater treatment, the sludge reduction is beneficial and is worthwhile for further confirmation.

References

[1] S.D. Carter, H. Kim, Technologies to reduce environmental impact of animal wastes associated with feeding for maximum productivity, Animal Frontiers, 3 (2013) 42-47.

[2] X. Wu, H. Lin, J. Zhu, Optimization of continuous hydrogen production from co-fermenting molasses with liquid swine manure in an anaerobic sequencing batch reactor, Bioresource Technol, (2013).

[3] N. Key, W.D. McBride, M. Ribaudo, S. Sneeringer, Trends and Developments in Hog Manure Management: 1998-2009, (2011).

[4] NASS, USDA, US Census of Agriculture 2002, in: US Department of Agriculture, National Agricultural Statistics Service, Washington, DC, 2004.

[5] NASS, USDA, US Census of Agriculture 2007, in: US Department of Agriculture, National Agricultural Statistics Service, Washington, DC, 2009.

[6] J. Martinez, P. Dabert, S. Barrington, C. Burton, Livestock waste treatment systems for environmental quality, food safety, and sustainability, Bioresource Technol, 100 (2009) 5527-5536.

[7] M. Poach, P. Hunt, G. Reddy, K. Stone, T. Matheny, M. Johnson, E. Sadler, Ammonia volatilization from marsh-pond-marsh constructed wetlands treating swine wastewater, (2004).

[8] OECD, Environmental indicators for agriculture, in: Methods and Results, Paris, France, 2001.

[9] R. Steffen, O. Szolar, R. Braun, Feedstocks for anaerobic digestion, Institute for Agrobiotechnology Tulln University of Agricultural Sciences, Viences, (1998).

[10] M.G.M. Girard, J.N.J. Nikiema, R.B.R. Brzezinski, G.B.G. Buelna, M.H.M. Heitz, A review of the environmental pollution originating from the piggery industry and of the available mitigation technologies: towards the simultaneous biofiltration of swine slurry and methane, Canadian Journal of Civil Engineering, 36 (2009) 1946-1957.

[11] R.L. Kellogg, C.H. Lander, D.C. Moffitt, N. Gollehon, Manure nutrients relative to the capacity of cropland and pastureland to assimilate nutrients: Spatial and temporal trends for the United States, Proceedings of the Water Environment Federation, 2000 (2000) 18-157.

[12] S. Sakar, K. Yetilmezsoy, E. Kocak, Anaerobic digestion technology in poultry and livestock waste treatment—a literature review, Waste management & research, 27 (2009) 3.

[13] B.E. Logan, D. Call, S. Cheng, H.V.M. Hamelers, T.H.J.A. Sleutels, A.W. Jeremiasse, R.A. Rozendal, Microbial Electrolysis Cells for High Yield

Hydrogen Gas Production from Organic Matter, Environ Sci Technol, 42 (2008) 8630-8640.

[14] B.E. Logan, Microbial Fuel Cells, 1st ed., Wiley-Interscience, Hoboken, New Jersey, 2008.

[15] J.Y. Nam, H.W. Kim, H.S. Shin, Ammonia inhibition of electricity generation in single-chambered microbial fuel cells, J Power Sources, 195 (2010) 6428-6433.

[16] D.R. Lovley, Microbial fuel cells: novel microbial physiologies and engineering approaches, Curr Opin Biotech, 17 (2006) 327-332.

[17] H. Liu, H. Hu, J. Chignell, Y. Fan, Microbial electrolysis: novel technology for hydrogen production from biomass, Biofuels, 1 (2010) 13.

[18] M.T. Madigan, J.M. Martinko, P.V. Dunlap, D.P. Clark, Biology of Microorganisms, Pearson Benjamin Cummings, San Francisco, 2009.

[19] J.S. Geelhoed, H.V.M. Hamelers, A.J.M. Stams, Electricity-mediated biological hydrogen production, Curr Opin Microbiol, 13 (2010) 307-315.

[20] D.R. Bond, D.R. Lovley, Evidence for involvement of an electron shuttle in electricity generation by Geothrix fermentans, Appl Environ Microb, 71 (2005) 2186.

[21] E. Marsili, D.B. Baron, I.D. Shikhare, D. Coursolle, J.A. Gralnick, D.R. Bond, Shewanella secretes flavins that mediate extracellular electron transfer, Proceedings of the National Academy of Sciences, 105 (2008) 3968.

[22] Y.A. Gorby, S. Yanina, J.S. McLean, K.M. Rosso, D. Moyles, A. Dohnalkova, T.J. Beveridge, I.S. Chang, B.H. Kim, K.S. Kim, Electrically conductive bacterial nanowires produced by Shewanella oneidensis strain MR-1 and other microorganisms, Proceedings of the National Academy of Sciences, 103 (2006) 11358.

[23] D.R. Bond, D.R. Lovley, Electricity production by Geobacter sulfurreducens attached to electrodes, Appl Environ Microb, 69 (2003) 1548-1555.

[24] B.E. Logan, Exoelectrogenic bacteria that power microbial fuel cells, Nat Rev Microbiol, 7 (2009) 375-381.

[25] E. Marsili, D.B. Baron, I.D. Shikhare, D. Coursolle, J.A. Gralnick, D.R. Bond, Shewanella Secretes flavins that mediate extracellular electron transfer, P Natl Acad Sci USA, 105 (2008) 3968-3973.

[26] M.E. Nielsen, D.M. Wu, P.R. Girguis, C.E. Reimers, Influence of Substrate on Electron Transfer Mechanisms in Chambered Benthic Microbial Fuel Cells, Environ Sci Technol, 43 (2009) 8671-8677.

[27] Y.A. Gorby, S. Yanina, J.S. McLean, K.M. Rosso, D. Moyles, A. Dohnalkova, T.J. Beveridge, I.S. Chang, B.H. Kim, K.S. Kim, D.E. Culley, S.B. Reed, M.F. Romine, D.A. Saffarini, E.A. Hill, L. Shi, D.A. Elias, D.W. Kennedy, G.

Pinchuk, K. Watanabe, S. Ishii, B. Logan, K.H. Nealson, J.K. Fredrickson, Electrically conductive bacterial nanowires produced by Shewanella oneidensis strain MR-1 and other microorganisms, P Natl Acad Sci USA, 103 (2006) 11358-11363.

[28] M.Y. El-Naggar, G. Wanger, K.M. Leung, T.D. Yuzvinsky, G. Southam, J. Yang, W.M. Lau, K.H. Nealson, Y.A. Gorby, Electrical transport along bacterial nanowires from Shewanella oneidensis MR-1, P Natl Acad Sci USA, 107 (2010) 18127-18131.

[29] D. Prasad, S. Arun, A. Murugesan, S. Padmanaban, R.S. Satyanarayanan, S. Berchmans, V. Yegnaraman, Direct electron transfer with yeast cells and construction of a mediatorless microbial fuel cell, Biosens Bioelectron, 22 (2007) 2604-2610.

[30] J. Sun, Y. Hu, Z. Bi, Y. Cao, Improved performance of air-cathode single-chamber microbial fuel cell for wastewater treatment using microfiltration membranes and multiple sludge inoculation, J Power Sources, 187 (2009) 471-479.

[31] J.R. Kim, B. Min, B.E. Logan, Evaluation of procedures to acclimate a microbial fuel cell for electricity production, Appl Microbiol Biot, 68 (2005) 23-30.

[32] B. Tartakovsky, M.F. Manuel, H. Wang, S.R. Guiot, High rate membrane-less microbial electrolysis cell for continuous hydrogen production, Int J Hydrogen Energ, 34 (2009) 672-677.

[33] P.D. Kiely, R. Cusick, D.F. Call, P.A. Selembo, J.M. Regan, B.E. Logan, Anode microbial communities produced by changing from microbial fuel cell to microbial electrolysis cell operation using two different wastewaters, Bioresource Technol, 102 (2011) 388-394.

[34] L. Barton, M. Mandl, A. Loy, Geomicrobiology: Molecular and Environmental Perspective, in, Springer, Dordrecht, the Netherlands, 2010, pp. 435.

[35] Y. Fan, E. Sharbrough, H. Liu, Quantification of the internal resistance distribution of microbial fuel cells, Environ Sci Technol, 42 (2008) 8101-8107.

[36] C.I. Torres, A.K. Marcus, B.E. Rittmann, Proton transport inside the biofilm limits electrical current generation by anode-respiring bacteria, Biotechnol Bioeng, 100 (2008) 872-881.

[37] G. Liu, M.D. Yates, S. Cheng, D.F. Call, D. Sun, B.E. Logan, Examination of microbial fuel cell start-up times with domestic wastewater and additional amendments, Bioresource Technol, (2011).

[38] X. Wang, Y. Feng, N. Ren, H. Wang, H. Lee, N. Li, Q. Zhao, Accelerated start-up of two-chambered microbial fuel cells: effect of anodic positive poised potential, Electrochim Acta, 54 (2009) 1109-1114.

[39] M. Sun, Z.X. Mu, G.P. Sheng, X.W. Liu, L. Zhang, C.R. Xia, H.L. Wang, Z.H. Tong, H.Q. Yu, Effects of a transient external voltage application on the

bioanode performance of microbial fuel cells, Electrochim Acta, 55 (2010) 3048-3054.

[40] D.A. Finkelstein, M. Leonard, J.G. Zeikus, Effect of electrode potential on electrode-reducing microbiota, Environ Sci Technol, 40 (2006) 6990-6995.

[41] P. Aelterman, S. Freguia, J. Keller, W. Verstraete, K. Rabaey, The anode potential regulates bacterial activity in microbial fuel cells, Appl Microbiol Biot, 78 (2008) 409-418.

[42] J.S. McLean, G. Wanger, Y.A. Gorby, M. Wainstein, J. McQuaid, S.I. Ishii, O. Bretschger, H. Beyenal, K.H. Nealson, Quantification of Electron Transfer Rates to a Solid Phase Electron Acceptor through the Stages of Biofilm Formation from Single Cells to Multicellular Communities, Environ Sci Technol, 44 (2010) 2721-2727.

[43] J.B. Rollefson, C.S. Stephen, M. Tien, D.R. Bond, Identification of an extracellular polysaccharide network essential for cytochrome anchoring and biofilm formation in Geobacter sulfurreducens, Journal of bacteriology, 193 (2011) 1023.

[44] A.J. Wang, W.Z. Liu, N.Q. Ren, J.Z. Zhou, S.A. Cheng, Key factors affecting microbial anode potential in a microbial electrolysis cell for H-2 production, Int J Hydrogen Energ, 35 (2010) 13481-13487.

[45] C. Picioreanu, K. Katuri, I. Head, M. Van Loosdrecht, K. Scott, Mathematical model for microbial fuel cells with anodic biofilms and anaerobic digestion, Water Science & Technology, 57 (2008) 965-971.

[46] S. Xie, P. Liang, Y. Chen, X. Xia, X. Huang, Simultaneous carbon and nitrogen removal using an oxic/anoxic-biocathode microbial fuel cells coupled system, Bioresource Technol, 102 (2011) 348-354.

[47] J. Ditzig, H. Liu, B.E. Logan, Production of hydrogen from domestic wastewater using a bioelectrochemically assisted microbial reactor (BEAMR), Int J Hydrogen Energ, 32 (2007) 2296-2304.

[48] Y.H. Jia, J.Y. Choi, J.H. Ryu, C.H. Kim, W.K. Lee, T.T. Hung, R.H. Zhang, D.H. Ahn, Hydrogen production from wastewater using a microbial electrolysis cell, Korean J Chem Eng, 27 (2010) 1854-1859.

[49] R.C. Wagner, J.M. Regan, S.E. Oh, Y. Zuo, B.E. Logan, Hydrogen and methane production from swine wastewater using microbial electrolysis cells, Water Res, 43 (2009) 1480-1488.

[50] H.Q. Yu, Z.H. Zhu, W.R. Hu, H.S. Zhang, Hydrogen production from rice winery wastewater in an upflow anaerobic reactor by using mixed anaerobic cultures, Int J Hydrogen Energ, 27 (2002) 1359-1365.

[51] R.D. Cusick, B. Bryan, D.S. Parker, M.D. Merrill, M. Mehanna, P.D. Kiely, G.L. Liu, B.E. Logan, Performance of a pilot-scale continuous flow microbial

electrolysis cell fed winery wastewater, Appl Microbiol Biot, 89 (2011) 2053-2063.

[52] P.A. Selembo, J.M. Perez, W.A. Lloyd, B.E. Logan, High hydrogen production from glycerol or glucose by electrohydrogenesis using microbial electrolysis cells, Int J Hydrogen Energ, 34 (2009) 5373-5381.

[53] T. Raghareutai, O. Chavalparit, M. Ongwandee, Development of environmental sustainability for the biodiesel industry in Thailand, Int J Sust Dev World, 17 (2010) 363-369.

[54] H. Yan, T. Saito, J.M. Regan, Nitrogen removal in a single-chamber microbial fuel cell with nitrifying biofilm enriched at the air cathode, Water Res, 46 (2012) 2215-2224.

[55] S.J. You, J.N. Zhang, Y.X. Yuan, N.Q. Ren, X.H. Wang, Development of microbial fuel cell with anoxic/oxic design for treatment of saline seafood wastewater and biological electricity generation, J Chem Technol Biot, 85 (2010) 1077-1083.

[56] Z. He, J. Kan, Y. Wang, Y. Huang, F. Mansfeld, K.H. Nealson, Electricity production coupled to ammonium in a microbial fuel cell, Environ Sci Technol, 43 (2009) 3391-3397.

[57] S. Ghafari, M. Hasan, M.K. Aroua, Bio-electrochemical removal of nitrate from water and wastewater—a review, Bioresource Technol, 99 (2008) 3965-3974.

[58] K.B. Gregory, D.R. Bond, D.R. Lovley, Graphite electrodes as electron donors for anaerobic respiration, Environmental Microbiology, 6 (2004) 596-604.

[59] Z. He, L.T. Angenent, Application of bacterial biocathodes in microbial fuel cells, Electroanal, 18 (2006) 2009-2015.

[60] P. Clauwaert, K. Rabaey, P. Aelterman, L. De Schamphelaire, T.H. Pham, P. Boeckx, N. Boon, W. Verstraete, Biological denitrification in microbial fuel cells, Environ Sci Technol, 41 (2007) 3354-3360.

[61] B. Virdis, K. Rabaey, Z. Yuan, J. Keller, Microbial fuel cells for simultaneous carbon and nitrogen removal, Water Res, 42 (2008) 3013-3024.

[62] B. Virdis, S.T. Read, K. Rabaey, R.A. Rozendal, Z. Yuan, J. Keller, Biofilm stratification during simultaneous nitrification and denitrification (SND) at a biocathode, Bioresource Technol, 102 (2011) 334-341.

[63] F. Fischer, C. Bastian, M. Happe, E. Mabillard, N. Schmidt, Microbial fuel cell enables phosphate recovery from digested sewage sludge as struvite, Bioresource Technol, 102 (2011) 5824-5830.

[64] O. Ichihashi, K. Hirooka, Removal and recovery of phosphorus as struvite from swine wastewater using microbial fuel cell, Bioresource Technol, (2012).

[65] S.B. Moussa, G. Maurin, C. Gabrielli, M.B. Amor, Electrochemical precipitation of struvite, Electrochemical and solid-state letters, 9 (2006) C97-C101.

[66] H. Liu, B.E. Logan, Electricity generation using an air-cathode single chamber microbial fuel cell in the presence and absence of a proton exchange membrane, Environ Sci Technol, 38 (2004) 4040-4046.

[67] K. Rabaey, L. Angenent, U. Schroder, J. Keller, Bioelectrochemical Systems: From Extracellular Electron Transfer to Biotechnologycal Application, in, IWA Publishing, London, 2010.

[68] O. Lefebvre, A. Uzabiaga, I.S. Chang, B.H. Kim, H.Y. Ng, Microbial fuel cells for energy self-sufficient domestic wastewater treatment—a review and discussion from energetic consideration, Appl Microbiol Biot, (2011) 1-12.

[69] J.J. Fornero, M. Rosenbaum, L.T. Angenent, Electric power generation from municipal, food, and animal wastewaters using microbial fuel cells, Electroanal, 22 (2010) 832-843.

[70] C. Donovan, A. Dewan, D. Heo, H. Beyenal, Batteryless, wireless sensor powered by a sediment microbial fuel cell, Environ Sci Technol, 42 (2008) 8591-8596.

[71] A. Shantaram, H. Beyenal, R.R.A. Veluchamy, Z. Lewandowski, Wireless sensors powered by microbial fuel cells, Environ Sci Technol, 39 (2005) 5037-5042.

[72] Y. Ahn, B.E. Logan, Effectiveness of domestic wastewater treatment using microbial fuel cells at ambient and mesophilic temperatures, Bioresource Technol, 101 (2010) 469-475.

[73] J.R. Kim, G.C. Premier, F.R. Hawkes, J. Rodríguez, R.M. Dinsdale, A.J. Guwy, Modular tubular microbial fuel cells for energy recovery during sucrose wastewater treatment at low organic loading rate, Bioresource Technol, 101 (2010) 1190-1198.

[74] B. Min, J.R. Kim, S.E. Oh, J.M. Regan, B.E. Logan, Electricity generation from swine wastewater using microbial fuel cells, Water Res, 39 (2005) 4961-4968.

[75] J.R. Kim, J. Dec, M.A. Bruns, B.E. Logan, Removal of odors from swine wastewater by using microbial fuel cells, Appl Environ Microb, 74 (2008) 2540-2543.

[76] NA, Teaching Notes, in, Cambridge, UK, pp. Department of Chemical Engineering and Biotechnology, University of Cambridge.

[77] Y.M. Zhang, M.D. Merrill, B.E. Logan, The use and optimization of stainless steel mesh cathodes in microbial electrolysis cells, Int J Hydrogen Energ, 35 (2010) 12020-12028.

[78] Z. He, S.D. Minteer, L.T. Angenent, Electricity generation from artificial wastewater using an upflow microbial fuel cell, Environ Sci Technol, 39 (2005) 5262-5267.

[79] Y. Yuan, B. Zhao, S. Zhou, S. Zhong, L. Zhuang, Electrocatalytic activity of anodic biofilm responses to pH changes in microbial fuel cells, Bioresource Technol, In Press, Accepted Manuscript.

[80] P.A. Selembo, M.D. Merrill, B.E. Logan, Hydrogen production with nickel powder cathode catalysts in microbial electrolysis cells, Int J Hydrogen Energ, 35 (2010) 428-437.

[81] S.A. Cheng, B.E. Logan, Evaluation of catalysts and membranes for high yield biohydrogen production via electrohydrogenesis in microbial electrolysis cells (MECs), Water Sci Technol, 58 (2008) 853-857.

[82] S.A. Cheng, D.F. Xing, D.F. Call, B.E. Logan, Direct Biological Conversion of Electrical Current into Methane by Electromethanogenesis, Environ Sci Technol, 43 (2009) 3953-3958.

[83] P.A. Selembo, Microbial electrolysis cells: Hydrogen production from glycerol and alternative cathode materials, in: Chemical Engineering, The Pennsylvania State University, University Park, PA, 2010, pp. 196.

[84] C.I. Torres, A.K. Marcus, P. Parameswaran, B.E. Rittmann, Kinetic experiments for evaluating the Nernst-Monod model for anode-respiring bacteria (ARB) in a biofilm anode, Environ Sci Technol, 42 (2008) 6593-6597.

[85] T.H.J.A. Sleutels, Microbial electrolysis: Kinetics and cell design, in: Department of Environmental Technology, Wageningen University, Wageningen, The Netherlands, 2010, pp. 127.

[86] A.K. Manohar, O. Bretschger, K.H. Nealson, F. Mansfeld, The use of electrochemical impedance spectroscopy (EIS) in the evaluation of the electrochemical properties of a microbial fuel cell, Bioelectrochemistry, 72 (2008) 149-154.

[87] Z. He, F. Mansfeld, Exploring the use of electrochemical impedance spectroscopy (EIS) in microbial fuel cell studies, Energy & Environmental Science, 2 (2009) 215-219.

[88] F. Zhao, R.C.T. Slade, J.R. Varcoe, Techniques for the study and development of microbial fuel cells: an electrochemical perspective, Chem Soc Rev, 38 (2009) 1926-1939.

[89] P.A. Selembo, M.D. Merrill, B.E. Logan, The use of stainless steel and nickel alloys as low-cost cathodes in microbial electrolysis cells, J Power Sources, 190 (2009) 271-278.

[90] L. Lu, N. Ren, X. Zhao, H. Wang, D. Wu, D. Xing, Hydrogen production, methanogen inhibition and microbial community structures in psychrophilic single-chamber microbial electrolysis cells, Energy & Environmental Science, 4 (2011) 1329-1336.

[91] L. Wang, J. Zhu, C. Miller, The Stability of Accumulating Nitrite from Swine Wastewater in a Sequencing Batch Reactor, Applied biochemistry and biotechnology, (2011) 1-11.

[92] T. Yamamoto, K. Takaki, T. Koyama, K. Furukawa, Long-term stability of partial nitritation of swine wastewater digester liquor and its subsequent treatment by Anammox, Bioresource Technol, 99 (2008) 6419-6425.

[93] M. Kithome, J. Paul, L. Lavkulich, A. Bomke, Kinetics of ammonium adsorption and desorption by the natural zeolite clinoptilolite, Soil Science Society of America Journal, 62 (1998) 622-629.

[94] S. Wang, Y. Peng, Natural zeolites as effective adsorbents in water and wastewater treatment, Chemical Engineering Journal, 156 (2010) 11-24.

[95] N. Widiastuti, H. Wu, H.M. Ang, D. Zhang, Removal of ammonium from greywater using natural zeolite, Desalination, 277 (2011) 15-23.

[96] J.S. Cyrus, G. Reddy, Sorption and desorption of ammonium by zeolite: Batch and column studies, Journal of Environmental Science and Health Part A, 46 (2011) 408-414.

[97] L. Qiu, S. Zhang, G. Wang, M. Du, Performances and nitrification properties of biological aerated filters with zeolite, ceramic particle and carbonate media, Bioresource Technol, 101 (2010) 7245-7251.

[98] A.A. Zorpas, V.J. Inglezakis, M. Stylianou, V. Irene, Sustainable Treatment Method of a High Concentrated NH 3 Wastewater by Using Natural Zeolite in Closed-Loop Fixed Bed Systems, Open Environmental Sciences, 4 (2010) 1-7.

[99] J.Y. Jung, Y.C. Chung, H.S. Shin, D.H. Son, Enhanced ammonia nitrogen removal using consistent biological regeneration and ammonium exchange of zeolite in modified SBR process, Water Res, 38 (2004) 347-354.

[100] J.R. Kim, Y. Zuo, J.M. Regan, B.E. Logan, Analysis of ammonia loss mechanisms in microbial fuel cells treating animal wastewater, Biotechnol Bioeng, 99 (2008) 1120-1127.

[101] B. Virdis, K. Rabaey, R.A. Rozendal, Z. Yuan, J. Keller, Simultaneous nitrification, denitrification and carbon removal in microbial fuel cells, Water Res, 44 (2010) 2970-2980.

[102] M. Paidar, K. Bouzek, H. Bergmann, Influence of cell construction on the electrochemical reduction of nitrate, Chemical Engineering Journal, 85 (2002) 99-109.

[103] W. Mook, M. Chakrabarti, M. Aroua, G. Khan, B. Ali, M. Islam, M. Abu Hassan, Removal of total ammonia nitrogen (TAN), nitrate and total organic carbon (TOC) from aquaculture wastewater using electrochemical technology: A review, Desalination, (2011).

[104] Y. Sakakibara, M. Kuroda, Electric prompting and control of denitrification, Biotechnol Bioeng, 42 (1993) 535-537.

[105] I. Vasiliadou, S. Pavlou, D. Vayenas, A kinetic study of hydrogenotrophic denitrification, Process biochemistry, 41 (2006) 1401-1408.

[106] S. Islam, M.T. Suidan, Electrolytic denitrification: long term performance and effect of current intensity, Water Res, 32 (1998) 528-536.

[107] H.I. Park, Y.J. Choi, D. Pak, Nitrate reduction using an electrode as direct electron donor in a biofilm-electrode reactor, Process biochemistry, 40 (2005) 3383-3388.

[108] H.S. Joo, M. Hirai, M. Shoda, Piggery wastewater treatment using Alcaligenes faecalis strain No. 4 with heterotrophic nitrification and aerobic denitrification, Water Res, 40 (2006) 3029-3036.

[109] Y.C. Chiu, L.L. Lee, C.N. Chang, A.C. Chao, Control of carbon and ammonium ratio for simultaneous nitrification and denitrification in a sequencing batch bioreactor, International biodeterioration & biodegradation, 59 (2007) 1-7.

[110] P. Clauwaert, J. Desloover, C. Shea, R. Nerenberg, N. Boon, W. Verstraete, Enhanced nitrogen removal in bio-electrochemical systems by pH control, Biotechnol Lett, 31 (2009) 1537-1543.

[111] Y.H. Jia, H.T. Tran, D.H. Kim, S.J. Oh, D.H. Park, R.H. Zhang, D.H. Ahn, Simultaneous organics removal and bio-electrochemical denitrification in microbial fuel cells, Bioprocess and biosystems engineering, 31 (2008) 315-321.

[112] B. Virdis, K. Rabaey, Z. Yuan, R.A. Rozendal, J. Keller, Electron fluxes in a microbial fuel cell performing carbon and nitrogen removal, Environ Sci Technol, 43 (2009) 5144-5149.

[113] C. Sukkasem, S. Xu, S. Park, P. Boonsawang, H. Liu, Effect of nitrate on the performance of single chamber air cathode microbial fuel cells, Water Res, 42 (2008) 4743-4750.

[114] C. Spiegel, PEM Fuel Cell Modeling and Simulation Using Matlab, Academic Press, Burlington, MA, 2008.

[115] A.W. Jeremiasse, H.V.M. Hamelers, J.M. Kleijn, C.J.N. Buisman, Use of Biocompatible Buffers to Reduce the Concentration Overpotential for Hydrogen Evolution, Environ Sci Technol, 43 (2009) 6882-6887.

[116] C. Picioreanu, I.M. Head, K.P. Katuri, M.C.M. van Loosdrecht, K. Scott, A computational model for biofilm-based microbial fuel cells, Water Res, 41 (2007) 2921-2940.

[117] R.P. Pinto, B. Srinivasan, A. Escapa, B. Tartakovsky, Multi-Population Model of a Microbial Electrolysis Cell, Environ Sci Technol, (2011) null-null.

[118] X.C. Zhang, A. Halme, Modelling of a microbial fuel cell process, Biotechnol Lett, 17 (1995) 809-814.

[119] R. Pinto, B. Srinivasan, M.F. Manuel, B. Tartakovsky, A two-population bio-electrochemical model of a microbial fuel cell, Bioresource Technol, 101 (2010) 5256-5265.

[120] Y. Zeng, Y.F. Choo, B.H. Kim, P. Wu, Modelling and simulation of two-chamber microbial fuel cell, J Power Sources, 195 (2010) 79-89.

[121] Z. Ren, T.E. Ward, J.M. Regan, Electricity production from cellulose in a microbial fuel cell using a defined binary culture, Environ Sci Technol, 41 (2007) 4781-4786.

[122] F. Rezaei, D. Xing, R. Wagner, J.M. Regan, T.L. Richard, B.E. Logan, Simultaneous cellulose degradation and electricity production by Enterobacter cloacae in a microbial fuel cell, Appl Environ Microb, 75 (2009) 3673-3678.

[123] D. Jiang, B. Li, W. Jia, Y. Lei, Effect of inoculum types on bacterial adhesion and power production in microbial fuel cells, Applied biochemistry and biotechnology, 160 (2010) 182-196.

[124] O. Kroukamp, R.G. Dumitrache, G.M. Wolfaardt, Pronounced Effect of the Nature of the Inoculum on Biofilm Development in Flow Systems, Appl Environ Microb, 76 (2010) 6025-6031.

[125] Z. Du, H. Li, T. Gu, A state of the art review on microbial fuel cells: a promising technology for wastewater treatment and bioenergy, Biotechnology advances, 25 (2007) 464-482.

[126] K. Nevin, H. Richter, S. Covalla, J. Johnson, T. Woodard, A. Orloff, H. Jia, M. Zhang, D. Lovley, Power output and columbic efficiencies from biofilms of Geobacter sulfurreducens comparable to mixed community microbial fuel cells, Environmental Microbiology, 10 (2008) 2505-2514.

[127] Z. He, H. Shao, L.T. Angenent, Increased power production from a sediment microbial fuel cell with a rotating cathode, Biosensors and Bioelectronics, 22 (2007) 3252-3255.

[128] D. Holmes, D. Bond, R. O'neil, C. Reimers, L. Tender, D. Lovley, Microbial communities associated with electrodes harvesting electricity from a variety of aquatic sediments, Microbial ecology, 48 (2004) 178-190.

[129] I. Castro, C. Oliveira, L. Domingues, J.A. Teixeira, A.A. Vicente, The Effect of the Electric Field on Lag Phase, β-Galactosidase Production and Plasmid Stability of a Recombinant Saccharomyces cerevisiae Strain Growing on Lactose, Food and Bioprocess Technology, (2011) 1-7.

[130] L. Loghavi, S. Sastry, A. Yousef, Effect of moderate electric field on the metabolic activity and growth kinetics of Lactobacillus acidophilus, Biotechnol Bioeng, 98 (2007) 872-881.

[131] S. Oh, J. Kim, J. Joo, B. Logan, Effects of applied voltages and dissolved oxygen on sustained power generation by microbial fuel cells, Water Science & Technology, 60 (2009) 1311-1317.

[132] K. Chung, I. Fujiki, S. Okabe, Effect of formation of biofilms and chemical scale on the cathode electrode on the performance of a continuous two-chamber microbial fuel cell, Bioresource Technol, 102 (2011) 355-360.

[133] D.R. Lovley, E.J.P. Phillips, Novel mode of microbial energy metabolism: organic carbon oxidation coupled to dissimilatory reduction of iron or manganese, Appl Environ Microb, 54 (1988) 1472-1480.

[134] L.S. Clesceri, A.E. Greenberg, A.D. Eaton, Standard Methods for the Examination of Water and Wastewater, in, 1998.

[135] X. Yang, M. Du, D.J. Lee, C. Wan, L. Zheng, G. Li, J.S. Chang, Enhanced production of volatile fatty acids (VFAs) from sewage sludge by β-cyclodextrin, Bioresource Technol, (2011).

[136] R.D. Cook, S. Weisberg, Applied Regression Including Computing and Graphics, John Wiley & Sons, 1999.

[137] P.T. Ha, H. Moon, B.H. Kim, H.Y. Ng, I.S. Chang, Determination of charge transfer resistance and capacitance of microbial fuel cell through a transient response analysis of cell voltage, Biosensors and Bioelectronics, 25 (2010) 1629-1634.

[138] P. She, B. Song, X.H. Xing, M. Loosdrecht, Z. Liu, Electrolytic stimulation of bacteria Enterobacter dissolvens by a direct current, Biochem Eng J, 28 (2006) 23-29.

[139] T. Matsunaga, S. Nakasono, T. Takamuku, J.G. Burgess, N. Nakamura, K. Sode, Disinfection of drinking water by using a novel electrochemical reactor employing carbon-cloth electrodes, Appl Environ Microb, 58 (1992) 686-689.

[140] H. Diao, X. Li, J. Gu, H. Shi, Z. Xie, Electron microscopic investigation of the bactericidal action of electrochemical disinfection in comparison with chlorination, ozonation and Fenton reaction, Process biochemistry, 39 (2004) 1421-1426.

[141] H.C. Flemming, J. Wingender, The biofilm matrix, Nat Rev Microbiol, 8 (2010) 623-633.

[142] H. Liu, S. Cheng, B.E. Logan, Production of electricity from acetate or butyrate using a single-chamber microbial fuel cell, Environ Sci Technol, 39 (2005) 658-662.

[143] A.K. Manohar, O. Bretschger, K.H. Nealson, F. Mansfeld, The polarization behavior of the anode in a microbial fuel cell, Electrochim Acta, 53 (2008) 3508-3513.

[144] N.S. Malvankar, T. Mester, M.T. Tuominen, D.R. Lovley, Supercapacitors Based on c‐Type Cytochromes Using Conductive Nanostructured Networks of Living Bacteria, Chemphyschem, 13 (2012) 463-468.

[145] A. Deeke, T.H. Sleutels, H.V.M. Hamelers, C.J.N. Buisman, Capacitive Bio-anodes enable renewable energy storage in Microbial Fuel Cells, Environ Sci Technol, 46 (2012) 3554-3560.

[146] S.V. Mohan, G. Mohanakrishna, P. Sarma, Effect of anodic metabolic function on bioelectricity generation and substrate degradation in single chambered microbial fuel cell, Environ Sci Technol, 42 (2008) 8088-8094.

[147] L. Liu, J. Liu, B. Gao, F. Yang, Minute electric field reduced membrane fouling and improved performance of membrane bioreactor, Separation and Purification Technology, (2011).

[148] H.B. Cao, X.G. Li, J.C. Wu, K.T. Yu, Y. Zhang, Simulation of the effects of direct electric current on multispecies biofilms, Process biochemistry, 38 (2003) 1139-1145.

[149] H.V.M. Hamelers, A. Ter Heijne, N. Stein, R.A. Rozendal, C.J.N. Buisman, Butler-Volmer-Monod model for describing bio-anode polarization curves, Bioresource Technol, 102 (2011) 381-387.

[150] Z. Ren, R.P. Ramasamy, S.R. Cloud-Owen, H. Yan, M.M. Mench, J.M. Regan, Time-course correlation of biofilm properties and electrochemical performance in single-chamber microbial fuel cells, Bioresource Technol, 102 (2011) 416-421.

[151] R. Freter, H. Brickner, J. Fekete, M.M. Vickerman, K.E. Carey, Survival and implantation of Escherichia coli in the intestinal tract, Infection and Immunity, 39 (1983) 686-703.

[152] A. Mašić, H.J. Eberl, Persistence in a Single Species CSTR Model with Suspended Flocs and Wall Attached Biofilms, Bulletin of mathematical biology, (2012) 1-26.

[153] W. Schecher, D. McAvoy, MINEQL+ Version 4.5, Environ. Res. Software, Hallowell, ME, (1998).

[154] U. Schröder, Anodic electron transfer mechanisms in microbial fuel cells and their energy efficiency, Physical Chemistry Chemical Physics, 9 (2007) 2619-2629.

[155] K. Neyerlin, W. Gu, J. Jorne, H.A. Gasteiger, Study of the exchange current density for the hydrogen oxidation and evolution reactions, J Electrochem Soc, 154 (2007) B631-B635.

[156] D.J. Batstone, J. Keller, I. Angelidaki, S. Kalyuzhnyi, S. Pavlostathis, A. Rozzi, W. Sanders, H. Siegrist, V. Vavilin, The IWA Anaerobic Digestion Model No 1(ADM 1), Water Science & Technology, 45 (2002) 65-73.

[157] J. Liu, D. Lowy, R. Baumann, L. Tender, Influence of anode pretreatment on its microbial colonization, Journal of applied microbiology, 102 (2007) 177-183.

[158] S. Freguia, K. Rabaey, Z. Yuan, J. Keller, Non-catalyzed cathodic oxygen reduction at graphite granules in microbial fuel cells, Electrochim Acta, 53 (2007) 598-603.

[159] S. Freguia, K. Rabaey, Z. Yuan, J. Keller, Sequential anode-cathode configuration improves cathodic oxygen reduction and effluent quality of microbial fuel cells, Water Res, 42 (2008) 1387-1396.

[160] B. Wang, J.-I. Han, A single chamber stackable microbial fuel cell with air cathode, Biotechnol Lett, 31 (2009) 387-393.

[161] K.P. Katuri, K. Scott, I.M. Head, C. Picioreanu, T.P. Curtis, Microbial fuel cells meet with external resistance, Bioresource Technol, 102 (2011) 2758-2766.

[162] M.M. Mench, Fuel Cell Engines, Wiley Online Library, 2008.

[163] X. Wu, W. Yao, J. Zhu, Effect of pH on continuous biohydrogen production from liquid swine manure with glucose supplement using an anaerobic sequencing batch reactor, Int J Hydrogen Energ, 35 (2010) 6592-6599.

[164] S. Jung, J.M. Regan, Comparison of anode bacterial communities and performance in microbial fuel cells with different electron donors, Appl Microbiol Biot, 77 (2007) 393-402.

[165] H. Liu, S. Cheng, B.E. Logan, Power generation in fed-batch microbial fuel cells as a function of ionic strength, temperature, and reactor configuration, Environ Sci Technol, 39 (2005) 5488-5493.

[166] Z. He, N. Wagner, S.D. Minteer, L.T. Angenent, An upflow microbial fuel cell with an interior cathode: assessment of the internal resistance by impedance spectroscopy, Environ Sci Technol, 40 (2006) 5212-5217.

[167] K.S. Ro, K. Cantrell, D. Elliott, P.G. Hunt, Catalytic wet gasification of municipal and animal wastes, Ind Eng Chem Res, 46 (2007) 8839-8845.

[168] A. Hinz, P.-O. Larsson, B. Skårman, A. Andersson, Platinum on alumina, titania, and magnesia supports for the combustion of methanol in a waste gas with trace amount of ammonia, Applied Catalysis B: Environmental, 34 (2001) 161-178.

[169] A. Hinz, P.-O. Larsson, A. Andersson, Influence of Pt loading on Al2O3 for the low temperature combustion of methanol with and without a trace amount of ammonia, Catalysis letters, 78 (2002) 177-183.

[170] R. Halseid, P.J. Vie, R. Tunold, Effect of ammonia on the performance of polymer electrolyte membrane fuel cells, J Power Sources, 154 (2006) 343-350.

[171] S.J. You, Q.L. Zhao, J.Q. Jiang, J.N. Zhang, S.Q. Zhao, Sustainable approach for leachate treatment: electricity generation in microbial fuel cell, Journal of Environmental Science and Health Part A, 41 (2006) 2721-2734.

[172] M. Rodrigo, P. Canizares, J. Lobato, R. Paz, C. Sáez, J. Linares, Production of electricity from the treatment of urban waste water using a microbial fuel cell, J Power Sources, 169 (2007) 198-204.

[173] S.C. Popat, D. Ki, B.E. Rittmann, C.I. Torres, Importance of OH− Transport from Cathodes in Microbial Fuel Cells, ChemSusChem, 5 (2012) 1071-1079.

[174] M. Rothrock Jr, A. Szogi, M. Vanotti, Recovery of ammonia from poultry litter using gas-permeable membranes, Transactions of the ASABE, 53 (2010) 1267-1275.

[175] M.B. Vanotti, A.A. Szogi, Use of gas-permeable membranes for the removal and recovery of ammonia from high strength livestock wastewater, Proceedings of the Water Environment Federation, 2011 (2011) 659-667.

[176] K. Hirooka, O. Ichihashi, Phosphorus recovery from artificial wastewater by microbial fuel cell and its effect on power generation, Bioresource Technol, (2013).

[177] X. Yuan, X. Shi, D. Zhang, Y. Qiu, R. Guo, L. Wang, Biogas production and microcystin biodegradation in anaerobic digestion of blue algae, Energy & Environmental Science, 4 (2011) 1511-1515.

[178] Y. Chen, J.J. Cheng, K.S. Creamer, Inhibition of anaerobic digestion process: A review, Bioresource Technol, 99 (2008) 4044-4064.

[179] M.B. Salerno, W. Park, Y. Zuo, B.E. Logan, Inhibition of biohydrogen production by ammonia, Water Res, 40 (2006) 1167-1172.

[180] H.-W. Kim, J.-Y. Nam, H.-S. Shin, Ammonia inhibition and microbial adaptation in continuous single-chamber microbial fuel cells, J Power Sources, 196 (2011) 6210-6213.

[181] C.J. Penn, J.G. Warren, S. Smith, Maximizing ammonium nitrogen removal from solution using different zeolites, Journal of environmental quality, 39 (2010) 1478-1485.

[182] S. Lagergren, About the theory of so-called adsorption of soluble substances, Kungliga Svenska Vetenskapsakademiens Handlingar, 24 (1898) 1-39.

[183] Y. Ho, G. McKay, Pseudo-second order model for sorption processes, Process biochemistry, 34 (1999) 451-465.

[184] H. Qiu, L. Lv, B.-c. Pan, Q.-j. Zhang, W.-m. Zhang, Q.-x. Zhang, Critical review in adsorption kinetic models, Journal of Zhejiang University-Science A, 10 (2009) 716-724.

[185] H. Freundlich, Over the adsorption in solution, J. Phys. Chem, 57 (1906) 385-470.

[186] I. Langmuir, The Constitution and Fundamental Properties of Solids and Liquids. Part I. Solids Journal of the American Chemical Society, 38 (1916) 2221-2295.

[187] O. Redlich, D.L. Peterson, A useful adsorption isotherm, J Phys Chem-Us, 63 (1959) 1024-1024.

[188] B. Boulinguiez, P. Le Cloirec, D. Wolbert, Revisiting the Determination of Langmuir Parameters Application to Tetrahydrothiophene Adsorption onto Activated Carbon, Langmuir, 24 (2008) 6420-6424.

[189] R. Han, J. Zhang, P. Han, Y. Wang, Z. Zhao, M. Tang, Study of equilibrium, kinetic and thermodynamic parameters about methylene blue adsorption onto natural zeolite, Chemical Engineering Journal, 145 (2009) 496-504.

[190] P. Senthil Kumar, S. Ramalingam, C. Senthamarai, M. Niranjanaa, P. Vijayalakshmi, S. Sivanesan, Adsorption of dye from aqueous solution by cashew nut shell: Studies on equilibrium isotherm, kinetics and thermodynamics of interactions, Desalination, 261 (2010) 52-60.

[191] K.V. Kumar, Linear and non-linear regression analysis for the sorption kinetics of methylene blue onto activated carbon, Journal of hazardous materials, 137 (2006) 1538-1544.

[192] Y.-S. Ho, Second-order kinetic model for the sorption of cadmium onto tree fern: a comparison of linear and non-linear methods, Water Res, 40 (2006) 119-125.

[193] I. Tan, B. Hameed, A. Ahmad, Equilibrium and kinetic studies on basic dye adsorption by oil palm fibre activated carbon, Chemical Engineering Journal, 127 (2007) 111-119.

[194] K. Saltalı, A. Sarı, M. Aydın, Removal of ammonium ion from aqueous solution by natural Turkish (Yıldızeli) zeolite for environmental quality, Journal of hazardous materials, 141 (2007) 258-263.

[195] H. Zheng, L. Han, H. Ma, Y. Zheng, H. Zhang, D. Liu, S. Liang, Adsorption characteristics of ammonium ion by zeolite 13X, Journal of hazardous materials, 158 (2008) 577-584.

[196] H. Huo, H. Lin, Y. Dong, H. Cheng, H. Wang, L. Cao, Ammonia-nitrogen and phosphates sorption from simulated reclaimed waters by modified clinoptilolite, Journal of hazardous materials, (2012).

[197] Q. Li, L. Chai, Z. Yang, Q. Wang, Kinetics and thermodynamics of Pb (II) adsorption onto modified spent grain from aqueous solutions, Appl Surf Sci, 255 (2009) 4298-4303.

[198] Y. Yu, Y.-Y. Zhuang, Z.-H. Wang, Adsorption of water-soluble dye onto functionalized resin, Journal of colloid and interface science, 242 (2001) 288-293.

[199] T. Kotsopoulos, X. Karamanlis, D. Dotas, G. Martzopoulos, The impact of different natural zeolite concentrations on the methane production in thermophilic anaerobic digestion of pig waste, Biosystems Engineering, 99 (2008) 105-111.

[200] R. Borja, E. Sánchez, M. Duran, Effect of the clay mineral zeolite on ammonia inhibition of anaerobic thermophilic reactors treating cattle manure, Journal of Environmental Science & Health Part A, 31 (1996) 479-500.

[201] Z. Milán, E. Sánchez, P. Weiland, R. Borja, A. Martín, K. Ilangovan, Influence of different natural zeolite concentrations on the anaerobic digestion of piggery waste, Bioresource Technol, 80 (2001) 37-43.

[202] NRC, Air emissions from animal feeding operations: current knowledge, future needs, National Academy Press, 2003.

[203] P. Ndegwa, A. Hristov, J. Arogo, R. Sheffield, A review of ammonia emission mitigation techniques for concentrated animal feeding operations, Biosystems engineering, 100 (2008) 453-469.

[204] M. Doorn, D. Natschke, S. Thorneloe, J. Southerland, Development of an emission factor for ammonia emissions from US swine farms based on field tests and application of a mass balance method, Atmospheric Environment, 36 (2002) 5619-5625.

[205] H. ApSimon, M. Kruse, J. Bell, Ammonia emissions and their role in acid deposition, Atmospheric Environment (1967), 21 (1987) 1939-1946.

[206] S. Eggleston, L. Buendia, K. Miwa, T. Ngara, K. Tanabe, IPCC guidelines for national greenhouse gas inventories, Institute for Global Environmental Strategies, Hayama, Japan, (2006).

[207] S. Lopez-Ridaura, H. Werf, J.M. Paillat, B. Le Bris, Environmental evaluation of transfer and treatment of excess pig slurry by life cycle assessment, J Environ Manage, 90 (2009) 1296-1304.

[208] R. Manuzon, L. Zhao, H. Keener, M. Darr, A Prototype Acid Spray Scrubber for Absorbing Ammonia Emissions From Exhaust Fans of Animal Buildings Transactions of the ASABE, 50 (2007) 1395-1407.

[209] H. Lin, X. Wu, C. Miller, J. Zhu, Improved performance of microbial fuel cells enriched with natural microbial inocula and treated by electrical current, Biomass and Bioenergy, 54 (2013) 170-180.

[210] A. Mandowara, P.K. Bhattacharya, Membrane contactor as degasser operated under vacuum for ammonia removal from water: A numerical simulation of mass transfer under laminar flow conditions, Computers & Chemical Engineering, 33 (2009) 1123-1131.

[211] J. Ni, Mechanistic models of ammonia release from liquid manure: a review, Journal of Agricultural Engineering Research, 72 (1999) 1-17.

[212] F. Zhao, F. Harnisch, U. Schröder, F. Scholz, P. Bogdanoff, I. Herrmann, Challenges and constraints of using oxygen cathodes in microbial fuel cells, Environ Sci Technol, 40 (2006) 5193-5199.

[213] A.E. Franks, K.P. Nevin, H. Jia, M. Izallalen, T.L. Woodard, D.R. Lovley, Novel strategy for three-dimensional real-time imaging of microbial fuel cell communities: monitoring the inhibitory effects of proton accumulation within the anode biofilm, Energy & Environmental Science, 2 (2009) 113-119.

[214] R.C. Hunter, T.J. Beveridge, Application of a pH-sensitive fluoroprobe (C-SNARF-4) for pH microenvironment analysis in Pseudomonas aeruginosa biofilms, Appl Environ Microb, 71 (2005) 2501-2510.